

The Effect of Overhang on Wind-Driven Rain Wetting for a Mid-Rise Building

Vincent Chiu

A Thesis

in

The Department

of

Building, Civil and Environmental Engineering

Presented in Partial Fulfillment of the Requirements

For the Degree of Master of Applied Science (Building Engineering) at

Concordia University

Montreal, Quebec, Canada

March 2016

© Vincent Chiu, 2016

CONCORDIA UNIVERSITY
School of Graduate Studies

This is to certify that the thesis prepared

By: Vincent Chiu

Entitled: The Effect of Overhang on Wind-Driven Rain Wetting for a Mid-Rise Building

and submitted in partial fulfillment of the requirements for the degree of

Master of Applied Science (Building Engineering)

complies with the regulations of the University and meets the accepted standards with respect to originality and quality.

Signed by the final Examining Committee:

_____	Chair
<i>Dr. R. Zmeaureanu</i>	
_____	Examiner
<i>Dr. P. Pillay</i>	
_____	Examiner
<i>Dr. C. Alecsandru</i>	
_____	Supervisor
<i>Dr. H. Ge</i>	
_____	Supervisor
<i>Dr. T. Stathopoulos</i>	

Approved by _____
Chair or Department of Graduate Program Director

Dean of Faculty

Date _____

Abstract

The Effect of Overhang on Wind-Driven Rain Wetting for a Mid-Rise Building

Vincent Chiu

Wind-driven rain (WDR) is one of the main sources of water causing moisture related damage in buildings. Rainwater that is absorbed and that penetrates through the cladding may lead to failures of building materials and components. Roof overhangs are a common feature that can be used to reduce the amount of WDR on building facades. Experimental studies and CFD modeling have shown that roof overhangs shelter the building facade from WDR. However, there is limited quantitative evaluation of the effectiveness of overhangs in protecting the building facade from WDR. A six-storey mid-rise building with a flat roof located in Vancouver, British Columbia has been equipped with a retractable overhang along with a rooftop weather station and thirty-one WDR gauges that have been strategically mounted on the building facades. The spatial distribution of WDR on the building facades has been studied without and with overhang (0.6 m and 1.2 m overhangs). The effectiveness of the roof overhang under real-life conditions with respect to the most important meteorological parameters of wind speed and wind direction has been assessed using two methods: similarity and symmetry. The overhangs reduce the WDR deposition on the facade, especially the areas right below the overhangs. The effectiveness of the overhangs is highly dependent on the wind speed and direction - the effectiveness decreases with increasing wind speed and increases for oblique winds. In addition, a model of the test building and its surroundings has been placed in Concordia's atmospheric boundary layer wind tunnel to verify the exposure and wind flow near the facades.

Acknowledgements

I would like to thank my supervisors, Dr. H. Ge and Dr. T. Stathopoulos for their invaluable support and guidance throughout this research project.

I would like to acknowledge the financial support received from NSERC Strategic Research Network for Engineered Wood-Based Building Systems (NEWBuildS), the Homeowner Protection Office Branch of BC Housing, and the Faculty of Engineering and Computer Science of Concordia University. I would also like to thank the British Columbia Housing Management Commission for allowing us to use their building for this study.

Table of Contents

List of Figures	viii
List of Tables	xvi
List of Symbols	xviii
CHAPTER 1: INTRODUCTION	1
1.1. Problem Statement	1
1.2. Scope	2
1.3. Aim & Methodology	2
1.4. Outline of the Thesis	3
CHAPTER 2: LITERATURE REVIEW	4
2.1. Wind	4
2.2. Rain	8
2.3. Wind-Driven Rain on Buildings	9
2.3.1. Experimental Methods	12
2.3.2. Semi-Empirical Methods	13
2.3.3. Numerical Methods	14
2.4. Effectiveness of Overhangs	15
2.5. Errors Associated with WDR Measurements	17
CHAPTER 3: EXPERIMENTAL SETUP & METHODOLOGY	21
3.1. Field Measurements	21
3.1.1. The Location and Description of the Building	21

3.1.2. Instrumentation and Sensor Location	23
3.2. Wind Tunnel Measurements	31
3.2.1. Description of the Atmospheric Boundary Wind Tunnel.....	31
3.2.2. Model and Exposure	31
3.2.3. Velocity Measurements	35
3.3. Data Analysis	36
3.3.1. On-Site Weather Comparisons	36
3.3.2. On-Site Weather Conditions.....	47
3.3.3. Airfield Driving Rain Index	48
3.3.4. Spatial Distribution of Wind-Driven Rain on the Building Facade	49
3.3.5. Wall Index	57
3.4. Effectiveness of Overhang	59
3.4.1. Similarity	59
3.4.2. Symmetry.....	59
CHAPTER 4: RESULTS AND DISCUSSION.....	61
4.1. On-Site Weather Comparisons.....	61
4.1.1. Surrounding Weather Stations.....	61
4.1.2. Wind Tunnel Measurements.....	61
4.2. On-site Weather Conditions	68
4.2.1. Entire Monitoring Period.....	68
4.2.2. Weather Conditions for Different Monitoring Periods.....	70

4.3. Airfield Driving Rain Index	72
4.4. Spatial Distribution of Wind-Driven Rain on the Building Facade	76
4.4.1. Catch Ratio	76
4.4.2. Wall Factor	85
4.5. Wall Index	90
4.6. The Effectiveness of Overhang	94
4.6.1. Similarity	94
4.6.2. Symmetry	99
4.6.3. Similarity vs. Symmetry	100
4.6.4. Overhang Effectiveness	103
CHAPTER 5: CONCLUSION AND FUTURE WORK	112
5.1. Conclusions	112
5.2. Recommendations for Future Work	114
REFERENCES	115
APPENDIX A	A-1
APPENDIX B	B-1
APPENDIX C	C-1

List of Figures

Figure 2.1 – Mean wind speed profiles over terrain with different roughness characteristics for an assumed gradient wind speed of 10 m/s (from Wind Power Program, 2015).	5
Figure 2.2 – Power spectrum of the horizontal wind speed (Van der Hoven, 1957).	6
Figure 2.3 – Schematic representation of wind flow around a high-rise building (from Beranek & Van Koten, 1979).	7
Figure 2.4 – Contours of the streamwise horizontal velocity component (dimensionless: U/U_{10}) in a vertical plane through the center of the building for (a) mid-rise building slab and (b) high-rise building slab and their corresponding raindrop trajectories shown in (c) and (d), respectively (from Blocken & Carmeliet, 2006c).	10
Figure 2.5 – Top view of the wind-flow pattern around a rectangular building with a flat roof in a horizontal plane 3 m above ground for $\theta_{10} =$ (a) 0° , (b) 22.5° , (c) 45° and (d) 67.5° (from Abuku et al., 2009).	11
Figure 2.6 – Top view of raindrop trajectories of 1 mm raindrops impacting the facade 3 m above ground for $\theta_{10} =$ (a) 0° , (b) 22.5° , (c) 45° and (d) 67.5° (from Abuku et al., 2009).	12
Figure 2.7 – Result of the numerical simulation of drop adhesion, coagulation and runoff on a acrylic glass surface. The “cumulative inflicted WDR” is the sum of adhesion water and measured WDR (from Blocken & Carmeliet 2006a).	18
Figure 3.1 – Aerial view of the building site (from Google Maps).	21
Figure 3.2 – Panoramic view of the test building’s surroundings (the north, east, south, and west sides of the building are marked in the photo).	22
Figure 3.3 – The east and north facades of the test building with the strategically placed WDR gauges and retractable overhang (drawn in SketchUp).	22

Figure 3.4 – The wind monitor and temperature/relative humidity probe mounted on the tripod cross arm and mast. The tripod sits atop the mechanical room roof which is located in the center of the main roof.....	24
Figure 3.5 – Horizontal rain gauge placed in the center of the main roof.	24
Figure 3.6 – Sketch of the wall-mounted wind-driven rain gauge (from Osorio 2013b).	25
Figure 3.7 – Plan view of the test building and the WDR gauge locations.	27
Figure 3.8 – Side view of the east facade and the WDR gauge locations.	28
Figure 3.9 – Side view of the west facade and the WDR gauge location.....	29
Figure 3.10 – Side view of the (a) North facade and (b) South facade and their WDR gauge location(s).	30
Figure 3.11 – The test building and surrounding buildings within a 200 meter radius.	32
Figure 3.12 – Top view of the test building model. The measurement points near the east and north facade are shown in addition to the wind monitor location.....	33
Figure 3.13 – Side view of the east facade of the test building model with the location of wind monitor and facade measurement points.....	34
Figure 3.14 – Side view of the north facade of the test building model with the location of wind monitor and facade measurement points.....	35
Figure 3.15 – Location of Pitt Meadows Regional Airport and Vancouver International Airport with respect to the test building (from Google Maps).	37
Figure 3.16 – Frequency of hourly wind direction (°) at the test building, Vancouver Sea Island and Pitt Meadows (Period from August 16, 2013 to June 30, 2015).....	38
Figure 3.17 – Hourly wind speed between the test building, Vancouver Sea Island and Pitt Meadows.	40

Figure 3.18 – Wind speed at the test building corrected to Vancouver Sea Island. (February 5th, 2014 from 14:00 to 18:00)	41
Figure 3.19 – Monthly horizontal rainfall for the test building, Vancouver Sea Island and Pitt Meadows.	42
Figure 3.20 – Total horizontal rainfall at the test building and surrounding stations in the Greater Vancouver region.	42
Figure 3.21 – Normalized mean velocity and turbulence intensity for a suburban exposure measured in the boundary layer wind tunnel.	44
Figure 3.22 – Five-minute data record for 1-hour.	45
Figure 3.23 – Comparison of the normalized velocity at the wind monitor location in the wind tunnel vs. in the field (Stand-alone test building); for the directions: $\theta=0^\circ$ (East) and $\theta=135^\circ$ (South-east).	46
Figure 3.24 – Comparison of the normalized velocity at the wind monitor location in the wind tunnel vs. in the field (Test building with surroundings); for the directions: $\theta=0^\circ$ (East) and $\theta=135^\circ$ (South-east).	47
Figure 3.25 – Sketch of the tipping bucket mechanism used to measure the collected rainwater by the WDR gauges (from Osorio, 2013a).	51
Figure 4.1 – Normalized velocities on the (a) East facade, (b) North facade Stand-alone test building, $\theta = 0^\circ$	63
Figure 4.2 – Normalized velocities on the (a) East facade, (b) North facade Stand-alone test building, $\theta = 45^\circ$ (from north-east).	64
Figure 4.3 – Normalized velocities on the (a) East facade, (b) North facade Test building with surrounding buildings, $\theta = 0^\circ$	65
Figure 4.4 – Normalized velocities on the (a) East facade, (b) North facade Test building with surrounding buildings, $\theta = 45^\circ$ (from north-east).	66

Figure 4.5 – Normalized velocities on the (a) East facade, (b) North facade Test building with surrounding buildings, $\theta = 45^\circ$ (from north-east)	67
Figure 4.6 – (a) Wind direction frequency; (b) Wind speed frequency; and (c) Rainfall intensity cumulative frequency at the test building for the entire monitoring period (from August 16, 2013 to July 13, 2015).	69
Figure 4.7 – Wind direction frequency at the test building.	70
Figure 4.8 – Wind speed frequency at the test building.	71
Figure 4.9 – Rainfall intensity cumulative frequency at the test building.	72
Figure 4.10 – Airfield driving rain index and measured WDR on the east facade. No overhang. DRI height refers to the distance from the roofline. (Data collected from August 16, 2013 to December 2, 2014).....	73
Figure 4.11 – Airfield driving rain index and measured WDR on the east facade. With a 0.6 m overhang. DRI height refers to the distance from the roofline. (Data collected from March 2, 2015 to July 13, 2015)	74
Figure 4.12 – Airfield driving rain index and measured WDR on the east facade. With a 1.2 m overhang. DRI height refers to the distance from the roofline. (Data collected from December 2, 2014 to March 2, 2015).....	74
Figure 4.13 – Airfield driving rain index and measured WDR on the north facade. No overhang. DRI height refers to the distance from the roofline. (Data collected from August 16, 2013 to December 2, 2014).....	75
Figure 4.14 – Airfield driving rain index and measured WDR on the north facade. With a 0.6 m overhang. DRI height refers to the distance from the roofline. (Data collected from March 2, 2015 to July 13, 2015)	75
Figure 4.15 – Airfield driving rain index and measured WDR on the north facade. With a 1.2 m overhang. DRI height refers to the distance from the roofline. (Data collected from December 2, 2014 to March 2, 2015).....	76

Figure 4.16 – Catch ratios on the (a) East facade and (b) North facade. No overhang. (Data collected from August 16, 2013 to December 2, 2014)	79
Figure 4.17 – Catch ratios on the (a) East facade and (b) North facade. With a 0.6 m overhang. (Data collected from March 2, 2015 to December 2, 2015)	80
Figure 4.18 – Catch ratios on the (a) East facade and (b) North facade. With a 1.2 m overhang. (Data collected from December 2, 2014 to March 2, 2015)	81
Figure 4.19 – Wind angle, θ (Plan View).	82
Figure 4.20 – Catch ratio vs. wind speed for four approaching wind angles on gauge ES1. (a) $\theta = 0 \pm 15^\circ$; (b) $\theta = 30 \pm 15^\circ$; (c) $\theta = 60 \pm 15^\circ$; (d) $\theta = 90 - 15^\circ$	83
Figure 4.21 – Catch ratio vs. wind speed when $\theta = 0 \pm 15^\circ$ for gauges ES1 to ES4. (a) ES1, (b) ES2; (c) ES3 and (d) ES4.....	84
Figure 4.22 – Wall Factors on the (a) East facade and (b) North facade. No overhang. (Data collected from August 16, 2013 to December 2, 2014)	87
Figure 4.23 – Wall Factors on the (a) East facade and (b) North facade. With a 0.6 m overhang. (Data collected from March 2, 2015 to December 2, 2015)	88
Figure 4.24 – Wall Factors on the (a) East facade and (b) North facade. With a 1.2 m overhang. (Data collected from December 2, 2014 to March 2, 2015)	89
Figure 4.25 – Comparison between measured WDR and calculated WDR using (1) measured wall factors and (2) ISO suggested wall factors (a) east facade and (b) north facade No overhang	91
Figure 4.26 – Comparison between measured WDR and calculated WDR using (1) measured wall factors and (2) ISO suggested wall factors (a) east facade and (b) north facade With a 0.6 m overhang.....	92
Figure 4.27 – Comparison between measured WDR and calculated WDR using (1) measured wall factors and (2) ISO suggested wall factors (a) east facade and (b) north facade With a 1.2 m overhang.....	93

Figure 4.28 – Rainfall intensity (R_h), wind speed (U_{ref}), and wind direction (θ) for rain event 16. (February 10 to February 25, 2014).....	95
Figure 4.29 – Rainfall intensity (R_h), wind speed (U_{ref}), and wind direction (θ) for rain event 16. (December 4, 2014 to December 11, 2014).....	95
Figure 4.30 – Relative error of WDR measurements as a function of the number of tips.	97
Figure 4.31 – Percent reduction in catch ratios. (Average of similar rain events vs. average using symmetry) East facade with a 0.6 m overhang.	101
Figure 4.32 – Percent reduction in catch ratios. (Average of similar rain events vs. average using symmetry) East facade with a 1.2 m overhang.	101
Figure 4.33 – Percent reduction in catch ratios using the similarity approach. (Average of similar rain events vs. average of the entire monitoring period) North facade with a 0.6 m overhang..	102
Figure 4.34 – Percent reduction in catch ratios using the similarity approach. (Average of similar rain events vs. average of the entire monitoring period) North facade with a 1.2 m overhang..	102
Figure 4.35 – Percent reduction in catch ratios. East facade with (a) 0.6 m overhang and (b) 1.2 m overhang. The percentage reduction in catch ratio is displayed (average of similar rain events). The wind speeds are predominantly in the range of 0 to 4 m/s. The wind direction is approximately normal to the east facade.	104
Figure 4.36 – Percent reduction in catch ratios. North facade with (a) 0.6 m overhang and (b) 1.2 m overhang. The percentage reduction in catch ratio is displayed (average of similar rain events). The wind speeds are predominantly in the range of 0 to 4 m/s. The wind direction is approximately normal to the east facade.	105
Figure 4.37 – Percent reduction in catch ratio with respect to wind speed, $\theta = 0 \pm 15^\circ$. East facade with a 0.6 m overhang.	108
Figure 4.38 – Percent reduction in catch ratio with respect to wind speed, $\theta = 0 \pm 15^\circ$. East facade with a 1.2 m overhang.	108
Figure 4.39 – Plan view of approaching wind angles towards the east facade.....	109

Figure 4.40 – Percent reduction in catch ratios with respect to wind direction; all wind speeds. East facade with a 0.6 m overhang.	1100
Figure 4.41 – Percent reduction in catch ratios with respect to wind direction; all wind speeds. East facade with a 1.2 m overhang.	1100
Figure A.1 – Concordia University’s atmospheric boundary layer wind tunnel (from Stathopoulos 1984).	A-2
Figure A.2 – Hourly values of temperature between the test building, Vancouver Sea Island and Pitt Meadows.	A-5
Figure A.3 – Hourly values of relative humidity between the test building, Vancouver Sea Island and Pitt Meadows.	A-6
Figure B.1 – Normalized velocities on the (a) East facade, (b) North facade Stand-alone test building, $\theta = 0^\circ$	B-1
Figure B.2 – Normalized velocities on the (a) East facade, (b) North facade Stand-alone test building, $\theta = 45^\circ$ (from north-east).	B-2
Figure B.3 – Normalized velocities on the (a) East facade, (b) North facade Test building with surrounding buildings, $\theta = 0^\circ$	B-3
Figure B.4 – Normalized velocities on the (a) East facade, (b) North facade Test building with surrounding buildings, $\theta = 45^\circ$ (from north-east).	B-4
Figure B.5 – Normalized velocities on the (a) East facade, (b) North facade Test building with surrounding buildings, $\theta = 45^\circ$ (from south-east).	B-5
Figure C.1 – Rain event 7. (a) Hourly horizontal rainfall intensity (R_h), wind speed (U_{ref}), and wind direction (θ); (b) Wind direction frequency; (c) Wind speed frequency; and (d) Rainfall intensity cumulative frequency.	C-1
Figure C.2 - Rain event 16. (a) Hourly horizontal rainfall intensity (R_h), wind speed (U_{ref}), and wind direction (θ); (b) Wind direction frequency; (c) Wind speed frequency; and (d) Rainfall intensity cumulative frequency.	C-2

Figure C.3 - Rain event 13. (a) Hourly horizontal rainfall intensity (R_h), wind speed (U_{ref}), and wind direction (θ); (b) Wind direction frequency; (c) Wind speed frequency; and (d) Rainfall intensity cumulative frequency.	C-3
Figure C.4 - Rain event 17. (a) Hourly horizontal rainfall intensity (R_h), wind speed (U_{ref}), and wind direction (θ); (b) Wind direction frequency; (c) Wind speed frequency; and (d) Rainfall intensity cumulative frequency.	C-4
Figure C.5 - Rain event 11. (a) Hourly horizontal rainfall intensity (R_h), wind speed (U_{ref}), and wind direction (θ); (b) Wind direction frequency; (c) Wind speed frequency; and (d) Rainfall intensity cumulative frequency.	C-5
Figure C.6 - Rain event 18. (a) Hourly horizontal rainfall intensity (R_h), wind speed (U_{ref}), and wind direction (θ); (b) Wind direction frequency; (c) Wind speed frequency; and (d) Rainfall intensity cumulative frequency.	C-6
Figure C.7 - Rain event 9. (a) Hourly horizontal rainfall intensity (R_h), wind speed (U_{ref}), and wind direction (θ); (b) Wind direction frequency; (c) Wind speed frequency; and (d) Rainfall intensity cumulative frequency.	C-7
Figure C.8 - Rain event 19. (a) Hourly horizontal rainfall intensity (R_h), wind speed (U_{ref}), and wind direction (θ); (b) Wind direction frequency; (c) Wind speed frequency; and (d) Rainfall intensity cumulative frequency.	C-8
Figure C.9 - Rain event 20. (a) Hourly horizontal rainfall intensity (R_h), wind speed (U_{ref}), and wind direction (θ); (b) Wind direction frequency; (c) Wind speed frequency; and (d) Rainfall intensity cumulative frequency.	C-9
Figure C.10 - Rain event 21. (a) Hourly horizontal rainfall intensity (R_h), wind speed (U_{ref}), and wind direction (θ); (b) Wind direction frequency; (c) Wind speed frequency; and (d) Rainfall intensity cumulative frequency.	C-10

List of Tables

Table 2.1 – Wind profile values of gradient height and mean speed exponents for different terrain categories (Aynsley et al, 1977).....	6
Table 2.2 – The intensity of rain. (Environment Canada, 2015).	8
Table 3.1 – Exposure type, elevation, reference height, gradient height, and mean speed exponent for Pitt Meadows, Vancouver Sea Island, and the test building.	38
Table 3.2 – Wall Factor, W provided by the International Organization for Standardization to take into account different building configurations (height, type of roof, roof overhangs) (from ISO 15927-3 2009).	56
Table 4.1 – Error estimates for the accumulated WDR measured on the east facade for rain event 7.....	96
Table 4.2 – Catch ratios on the east facade for rain events 7 and 16.	97
Table 4.3 – Percent reduction in catch ratios when comparing similar rain events. East facade with a 0.6 m overhang.....	98
Table 4.4 – Percent reduction in catch ratios when comparing similar rain events. East facade with a 1.2 m overhang.....	98
Table 4.5 – Percent reduction in catch ratios when using symmetry. East facade with a 0.6 m overhang.....	99
Table 4.6 – Percent reduction in catch ratios when using symmetry. East facade with a 1.2 m overhang.....	99
Table A.1 – Instrumentation technical specifications.	A-1
Table A.2 – Repeatability test for the wind profile velocities measured above the mechanical room roof in the wind tunnel.	A-3

Table A.3 – Repeatability test for the velocities measured near the east facade in the wind tunnel.	A-4
Table A.4 – Rain events.	A-7
Table A.5 – Relative error (e_{TOT}) associated with the WDR measured by the gauges on the east facade.	A-8
Table A.6 – Relative error (e_{TOT}) associated with the WDR measured by the gauges on the north facade.	A-9
Table B.1 – Summary of On-Site Weather Conditions for the Different Monitoring Periods.	B-6
Table B.2 – Catch ratios for each monitoring period.	B-7
Table B.3 – Comparison of measured wall factors with ISO suggested wall factors.	B-8
Table B.4 – Catch ratios for rain events used to assess the effectiveness of overhang.	B-9
Table C.1 – Rain event 7 summary.	C-1
Table C.2 – Rain event 16 summary.	C-2
Table C.3 – Rain event 13 summary.	C-3
Table C.4 – Rain event 17 summary.	C-4
Table C.5 – Rain event 11 summary.	C-5
Table C.6 – Rain event 18 summary.	C-6
Table C.7 – Rain event 9 summary.	C-7
Table C.8 – Rain event 19 summary.	C-8
Table C.9 – Rain event 20 summary.	C-9
Table C.10 – Rain event 21 summary.	C-10

List of Symbols

Roman Symbols

A_d	equivalent frontal area of a raindrop	m^2
C_D	drag coefficient	-
C_R	roughness coefficient	-
C_T	topography coefficient	-
D	drag force	N
E_{AW}	adhesion water evaporation	mm
E_{EVAP}	evaporation from reservoir or tipping bucket	mm
E_{RW}	rest water evaporation	g
E_{TIP}	loss of water during a tip	g/tip
E_{TOT}	total absolute error	mm
E_{UC}	undercooling condensation	mm
e_{TOT}	relative error	%
H	effective height of feature	m
I_{WS}	wall index	mm
K_R	terrain factor	-
L_u	effective length of the upwind slope	m
n	number of tips	-
O	obstruction factor	-
$R_{airfield}$	airfield driving rain index	mm
R_h	horizontal rainfall intensity	mm/hr
R_{wdr}	wind-driven rain intensity	mm/h
S_h	total accumulated horizontal rain	mm
S_{wdr}	total accumulated wind-driven rain	mm
s	factor for cliffs and escarpments	-
\bar{U}	mean wind speed	m/s
U	wind speed	m/s
U_{10}	wind speed at 10 m height	m/s

\bar{U}_g	mean gradient wind speed	m/s
U_g	gradient wind speed	m/s
U_{ref}	reference wind speed	m/s
U_{REL}	relative speed of the wind around a raindrop	m/s
U_z	wind speed at height z	m/s
U^*_{ABL}	friction velocity	m/s
V_{BOWL}	volume of bowls	g
W	wall factor	-
Z	height above grade	m
Z_0	aerodynamic roughness length	m
Z_g	gradient height	m
Z_{min}	minimum height	m
Z_{ref}	reference height	m

Greek Symbols

α	mean speed exponent	-
η	catch ratio	-
θ	wind direction	°
Θ	wall orientation	°
κ	Von Karman constant	-
μ	mean value	-
ρ	density of air	kg/m ³
σ	standard deviation	-
ϕ	upwind slope	-

Acronyms

ABL	Atmospheric Boundary Layer
BS	British Standard

CFD	Computational Fluid Dynamics
CLT	Cross Laminated Timber
DRI	Driving Rain Index
GIS	Geographical Information Systems
HAM	Heat-Air-Moisture
ISO	International Organization for Standardization
NBCC	National Building Code of Canada
OH	Overhang
RE	Rain Event

CHAPTER 1: INTRODUCTION

1.1. Problem Statement

Wind-driven rain (WDR) is caused by the co-occurrence of wind and rain. Raindrops falling towards the ground at their terminal velocity are given a horizontal velocity component as a result of the wind, causing the rain to be driven against building facades. WDR is an important research topic in building science because it is one of the most significant sources of moisture affecting the hygrothermal performance and the durability of building facades. Excessive moisture accumulation on porous materials may lead to water penetration, freeze-thaw damage, efflorescence, cracking, and facade soiling. Furthermore, water penetration may lead to the chemical breakdown of organic materials (such as wood), mold growth, reduce the effectiveness of insulating materials, and damage interior finishes and furniture (Straube & Schumacher, 2006; Blocken, 2004; Kerr, 2004; Ricketts & Lovatt, 1996; El-Shimi et al., 1980). Hence, knowledge on WDR is very important for the proper design of building enclosures. It is also an essential boundary condition for the study of the hygrothermal performance and durability of building facades with Heat-Air-Moisture (HAM) transfer models.

In spite of the importance of this environmental load, there is very limited data on the amount of WDR impacting multi-storey buildings. There exists a critical data gap for buildings six to eight storeys high with overhangs. Roof overhangs have been traditionally used for purposes including protection against rain. However, there is limited quantitative data regarding the effectiveness of roof overhangs. Previous studies show that the shapes of the roof and overhang have a significant impact on the amount of WDR deposited on the building facade. Pitched roofs and overhangs protect the wall below by shadowing and redirecting airflow.

In recent years, the need to reduce energy consumption and the environmental impact of buildings has led to opportunities for building mid-rise, and even high-rise, wood structures. Given that wood, as a structural element, is sensitive to moisture, it is critical to ensure long-term durability of wood structure buildings. Therefore, it is important to find solutions to reduce the WDR exposure and protect buildings from damages caused by moisture from WDR. Within this context, a research program supported by the NSERC NEWBuildS has been initiated to carry out a systematic evaluation and quantification of the effect of overhang on WDR loads of buildings

through full-scale field measurements and CFD modeling with the ultimate goal to provide recommendations on effective overhang designs for regions with high WDR exposure.

Given the level of skepticism in the construction community on the utility of overhangs on taller buildings, it is essential that data be generated to determine minimum effective overhang recommendations. The findings will be relevant to platform-frame, heavy timber, cross laminated timber (CLT) and hybrid construction. Such knowledge is critical in developing technical solutions and robust designs for ensuring durability performance of mid-rise wood construction, which can then be integrated into building design guidelines, codes and standards and also help advance building innovations.

1.2. Scope

This research is part of the Natural Sciences and Engineering Research Council of Canada's NEWBuildS network. NEWBuildS is a multi-disciplinary NSERC strategic research network for Engineered Wood-based Building Systems. NEWBuildS focuses its research on projects related to the use of wood-based products in mid-rise and non-residential construction. The projects address a range of building performance issues such as: structural, fire, durability, energy, and serviceability. The current research falls under Theme 4: Durability and Energy.

This thesis investigates the performance of overhangs in terms of protecting the facade from WDR. As mentioned earlier, although roof overhangs are known as an effective solution to the problems caused by WDR, their effects are not known in detail.

1.3. Aim & Methodology

The objective of this research is to quantify the effectiveness of roof overhang on reducing WDR loads on building facade under real life conditions through field measurements. The field data is being used to validate a CFD model under further development, which will be used for a systematic study of different overhang designs under various climatic conditions. Ultimately, these research efforts will lead to recommendations on effective roof overhang designs for various types of buildings.

The test building used in this study is a six-storey mid-rise building with a flat roof located in Vancouver, British Columbia. Field data has been collected over a period of two and a half years

in order to determine the effectiveness of varying widths of overhang in protecting the building from WDR. Data collected include on-site weather conditions (wind speed, wind direction, rainfall intensity, temperature, relative humidity) and WDR on the building facade at strategically selected locations with a sufficiently high spatial resolution on the east and north facades. The exposure of the building location has been verified in a boundary layer wind tunnel and the wind flow around the building is investigated. The spatial distribution of WDR on facades is determined using catch ratios and wall factors and is reported over the entire monitoring period and for each rain event defined according to the ISO standard. The effectiveness of overhangs is assessed using two methods: similarity and symmetry. The similarity approach compares the catch ratios determined over two similar rain events: one for the case with overhang and the other for the case without overhang. The symmetry approach takes advantage of the more or less symmetrical wetting pattern on the east facade due to the prevailing wind direction being from the east during rain hours. The retractable roof overhang is placed only on the right side of the east facade, while the WDR gauges are symmetrically placed on the left and right sides of the east facade. Therefore, the percentage reductions in catch ratios provided by the roof overhang may be determined by comparing the catch ratios on the right side of the east facade (beneath the overhang) to the catch ratios on the left side of the east facade (no overhang above it). Wind tunnel measurements on a building model were carried out in parallel.

1.4. Outline of the Thesis

In Chapter 2, a detailed literature review about WDR research and the effectiveness of overhangs is provided. In Chapter 3, the measurement set-up and methodology for the test building and the wind tunnel model is presented. In Chapter 4, the spatial distribution of WDR across the building facade is presented and the effectiveness of overhang is investigated. Finally, Chapter 5 will provide some conclusions and recommendations for future work.

CHAPTER 2: LITERATURE REVIEW

This chapter presents an overview of wind, rain and wind-driven rain (WDR) followed by a review of research attempting to quantify the WDR load on building facades. Section 2.1 contains information on wind, especially wind flow in the atmospheric boundary layer since this is relevant for the field study and the wind tunnel model. Section 2.2 contains information on rain. Section 2.3 elaborates on WDR and the three approaches used to quantify WDR on building facades. Section 2.4 presents a review of studies done to quantify WDR loads on building facades with a focus on those that have studied the effectiveness of overhangs and peaked roofs. Finally, in Section 2.5, the errors associated with WDR measurements are discussed.

2.1. Wind

In meteorology, wind is a two-dimensional vector quantity specified by the wind speed and the wind direction. Wind derives its energy from the sun; solar radiation is strongest at the equator and this produces temperature differences, which result in pressure differences causing atmospheric circulations. At high levels, the air is deflected to the right in the northern hemisphere and to the left in the southern hemisphere forming the so-called geostrophic winds generally occurring at heights of 500 m to 2 km. Additional variations are due to seasonal effects (the annual march of the sun north and south of the equator), geographical effects (uneven distribution of land and water), and the rotation of the earth (greater speed at the equator than near the poles).

Closer to the surface of the earth, the roughness of the terrain starts to influence the flow of wind due to friction. The layer where the wind is influenced by the earth's roughness is called atmospheric boundary layer. Two methods are used to determine the mean wind speed profile associated with a neutrally-stable (where thermal effects are negligible compared to turbulence caused by surface friction – this occurs during cloudy days and in strong winds), equilibrium boundary layer: (1) the log-law and (2) the power law. The log law is expressed as:

$$U_z = \frac{u_{ABL}^*}{\kappa} \ln \left(\frac{Z + Z_0}{Z_0} \right) \quad (2.1)$$

where U_z is the mean speed at height z , u_{ABL}^* is the friction velocity, κ is the Von Karman constant and Z_0 is the aerodynamic roughness length. The power law is expressed as:

$$\frac{U_z}{U_g} = \left(\frac{Z}{Z_g} \right)^\alpha \quad (2.2)$$

where U_g is the gradient mean wind speed at the gradient height Z_g above ground, at which ground roughness no longer has an effect. The mean speed exponent α varies with roughness, with values as low as 0.1 for open sea to 0.4 for city centres.

The difference between the logarithmic-law and the power law lies in the fact that the logarithmic law is theoretically derived whereas the power-law is empirical where the constant α is derived from measurements. The National Building Code of Canada uses the power-law. Figure 2.1 displays the mean wind speed profiles over terrain with different roughness characteristics for an assumed gradient wind speed of 10 m/s.

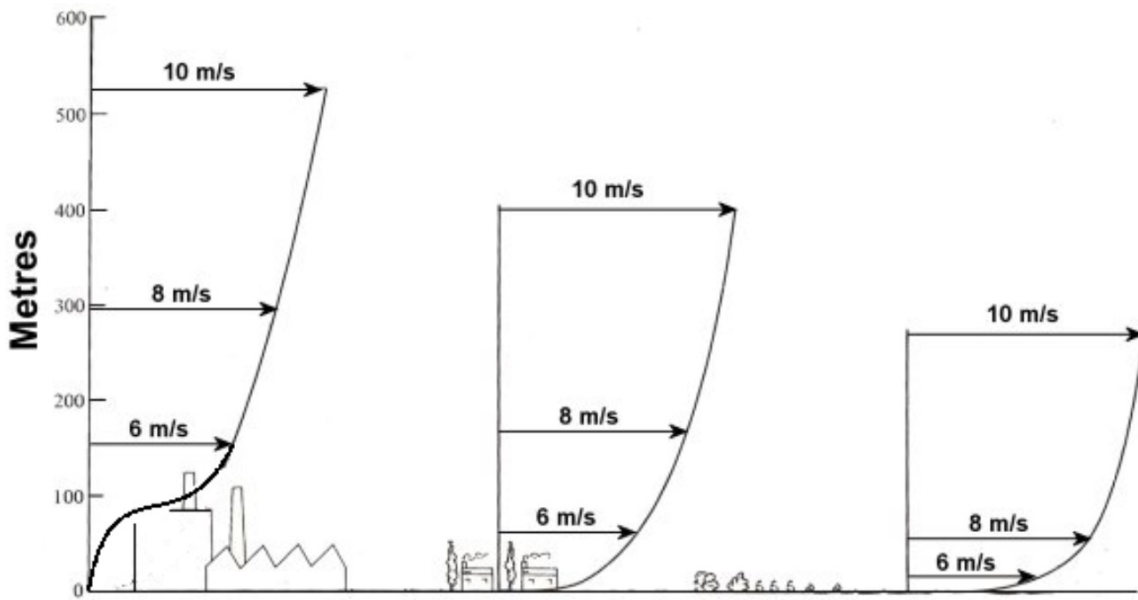


Figure 2.1 – Mean wind speed profiles over terrain with different roughness characteristics for an assumed gradient wind speed of 10 m/s (from Wind Power Program, 2015).

Table 2.1 – Wind profile values of gradient height and mean speed exponents for different terrain categories (Aynsley et al, 1977).

Terrain Category	Gradient Height, Z_g (m)	Mean Speed Exponent, α
1. Open sea, ice, tundra	250	0.11
2. Open country with low scrub or scattered trees	300	0.15
3. Suburban areas, small towns, well-wooded areas	400	0.25
4. Numerous tall buildings, city centres, well-developed industrial areas	500	0.36

When measuring the wind speed, the sampling time can range from 1 minute to less than a second. Typically, these samples are averaged to obtain the mean wind speed over a certain period of time. The choice of averaging period can be guided by the power spectrum of the horizontal wind speed (Van der Hoven, 1957) seen in Figure 2.2. The peaks reveal where much of the wind energy is situated – during periods of 4 days, 1 day, and 1 minute. These correspond to the passage of large-scale pressure systems, the diurnal frequency of wind, and gusts. The region with low energy in between peaks is called a “*spectral gap*.” Thus, averaging wind speed measurements within the range of 10 minutes to periods of over an hour provides relatively stable mean values (Blocken, 2004).

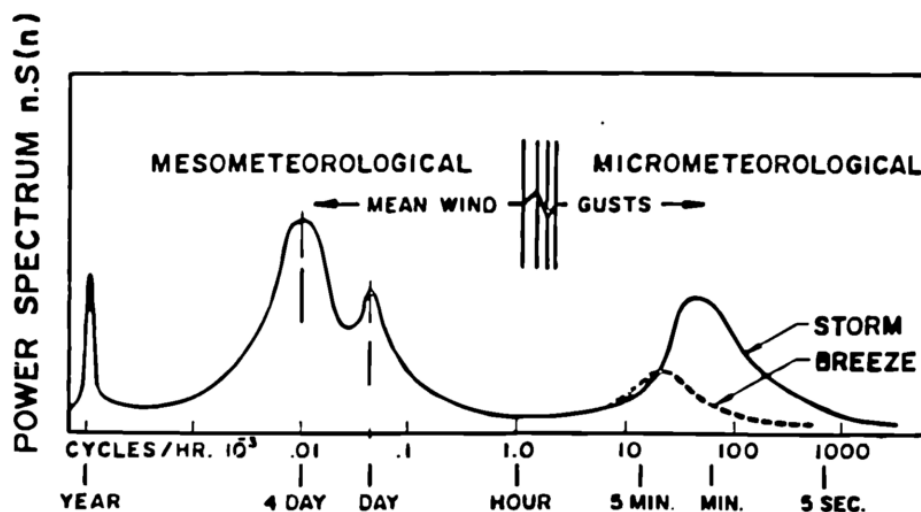


Figure 2.2 – Power spectrum of the horizontal wind speed (from Van der Hoven, 1957).

The spatial distribution of wind-driven rain on a building facade is highly dependent on the wind-building interaction. As wind approaches a building, the flow of the wind is disrupted by the building as seen in Figure 2.3. Further discussion about the wind-building interaction on the raindrop trajectories will be carried out in Section 2.3.

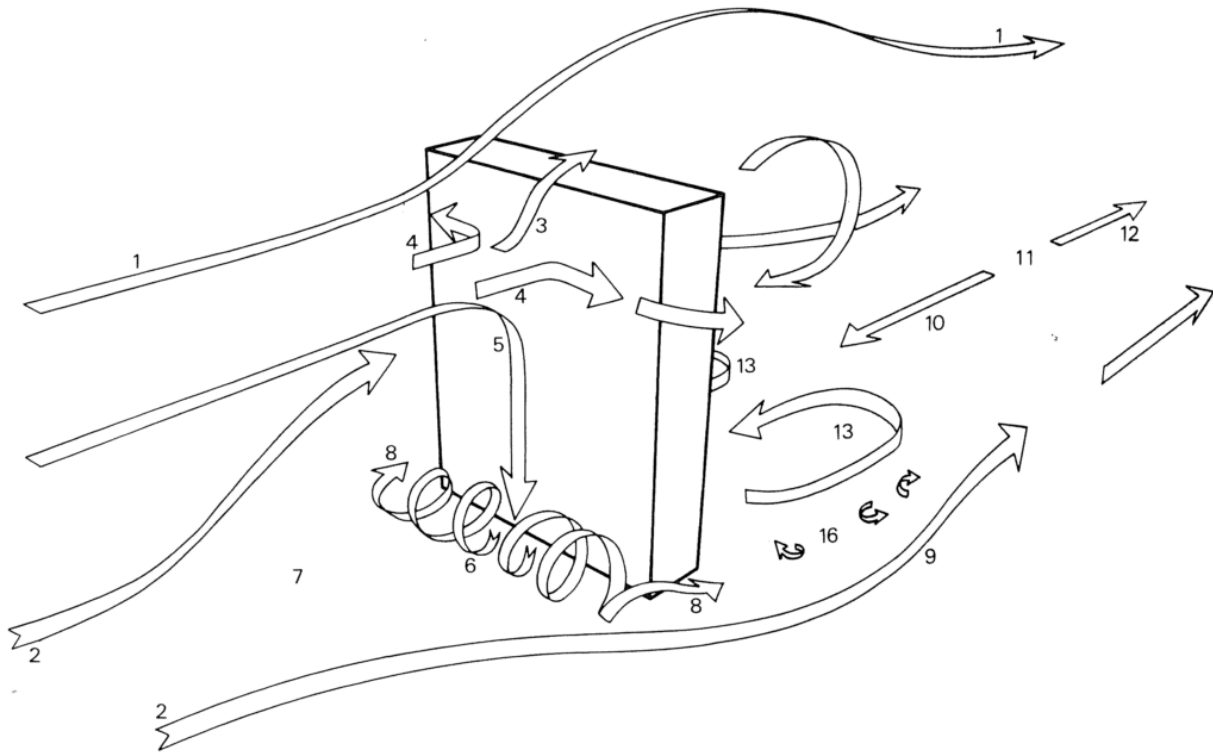


Figure 2.3 – Schematic representation of wind flow around a high-rise building (from Beranek & Van Koten, 1979).

The number in the diagram indicates a certain aspect of the air flow, as follows (Beranek & Van Koten, 1979):

- 1, 2:** Airflow over and around the building.
- 3, 4:** Airflow in front of the building is partly deflected above and aside.
- 5:** The larger part of the airflow in front of the building is deflected downwards.
- 6:** Vortices in front of the building; the main stream at ground level is away from the building.
- 7:** Stagnation point in front of the building.
- 8:** Significant increase in wind speed at the bottom corners of the building.
- 9:** Broad jet streams with increased velocity next to the building.

- 10:** Reversed airflow behind the building.
- 11:** Stagnation point behind the building where the flow directions are opposite.
- 12:** Air stream in the direction of the wind behind the rear stagnation point.
- 13:** The backflow is also responsible for the creation of rotating vortices behind the building.
- 16:** High velocity gradient area (the shear layer), is made up of small fast rotating vortices.

2.2. Rain

According to Environment Canada, rain is defined as precipitation in the form of liquid water droplets greater than 0.5 mm; if widely scattered, the drop size may be smaller. The intensity of rain is based on the rate of fall and is shown in Table 2.2.

Table 2.2 – The intensity of rain (Government of Canada (Environment Canada), 2013).

Intensity	Description
Very Light	Scattered drops that do not completely wet a surface
Light	Greater than a trace and up to 2.5 mm/hr
Moderate	2.6 mm/hr to 7.5 mm/hr
Heavy	7.6 mm/hr and greater

Rain is formed in the process of evaporation and condensation. As moist air rises to lower pressures, it expands and cools. Clouds are formed when part of the water vapour condenses on atmospheric aerosols from natural and anthropogenic sources. As the cloud droplets grow in size, their weight becomes greater and they fall due to gravity. There are two main types of rain clouds: (1) cumuliform and (2) stratiform. *Cumuliform* clouds form when the air becomes unstable due to small-scale air parcels rising spontaneously when disturbed because they become warmer than their immediate surroundings (buoyant lifting). As a result, these clouds are isolated with vertical depth. Precipitation from cumuliform clouds tends to suddenly start with large intensity, however, it tends to be of short duration. *Stratiform* clouds occur when large-scale layers of the atmosphere are forced upward in a stable atmosphere. As a result, these clouds are wide but with little vertical depth. Precipitation from stratiform clouds is generally steady and of small intensity lasting for many hours.

It has been observed that the fraction of large raindrops in rain increases as the rainfall intensity increases (Best, 1950). As the raindrop falls from the sky at its terminal velocity, it takes on a

specific shape that is dependent on its size. The terminal velocity of falling water droplets has been observed to increase rapidly for smaller drops, however, the curve flattens out as the drop diameter approaches 5 mm (Gunn & Kinzer, 1949). Smaller raindrops are spherical in shape, however, as the drops increase in size, the base of the falling drops starts to flatten due to drag force. The critical diameter at which the drops becomes unstable and break apart is in the range of 5 to 6 mm. The drag coefficient can be defined as:

$$C_d = \frac{D}{\rho A_d \frac{U_{REL}^2}{2}} \quad (2.3)$$

where D is the drag force on the raindrop, ρ is the air density, A_d is the equivalent frontal area of the raindrop, and U_{REL} is the relative speed of the wind around the drop.

2.3. Wind-Driven Rain on Buildings

The wind-driven rain load is difficult to quantify due to the complex interactions between the wind, rain and the buildings, which they affect. The quantity of WDR impinging on building facades is governed by several wind and rain characteristics, such as: wind speed, wind direction, rainfall intensity, and the duration and frequency of the rain event. In addition, building characteristics such as: environmental topology, building geometry, sheltering by surroundings, facade orientation and location on the facade further affect the WDR load (Blocken, 2004).

The building significantly modifies the flow of approaching wind upstream and downstream of the building, thus, the wind-building interaction is directly related to the spatial distribution of WDR on the building facade(s). CFD modeling of the wind-building interaction has given an understanding to the disturbance of the wind flow pattern around and near building facades. As wind approaches a building, the presence of the building causes a disturbance in the wind flow pattern resulting in a decrease of the upstream wind-velocity component near the building known as the “wind-blocking effect” (Blocken et al., 2009; Blocken & Carmeliet, 2006c). Contours of the streamwise horizontal wind-velocity component upstream of several stand-alone buildings have been modeled to investigate the wind blocking effect for different structures (Blocken & Carmeliet, 2006c), shown in Figure 2.4. Figure 2.4a-b show the contours of the streamwise

horizontal velocity components for a mid- and high-rise building slab with their corresponding raindrop trajectories in Figure 2.4c-d. The decrease of the upstream wind-velocity near the buildings result in raindrop trajectories with a downward curvature near the windward facade, leading to a decrease of rain deposition around these areas.

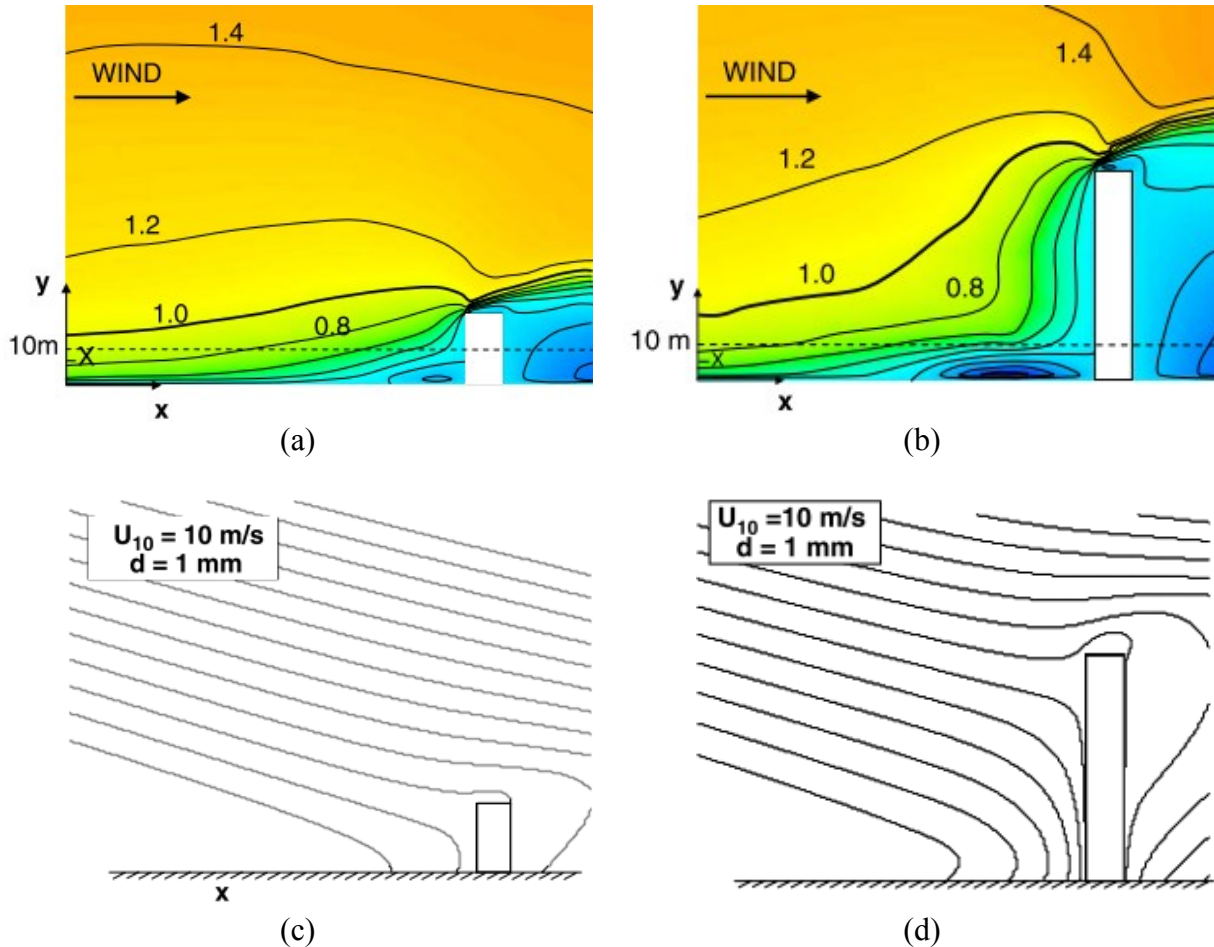


Figure 2.4 – Contours of the streamwise horizontal velocity component (dimensionless: U/U_{10}) in a vertical plane through the center of the building for (a) mid-rise building slab and (b) high-rise building slab and their corresponding raindrop trajectories shown in (c) and (d), respectively (from Blocken & Carmeliet, 2006c).

CFD modeling has also shed light on the possible behavior of wind flow near the building surface for various approaching wind angles (Sepehr et al., 2014; Sepehr, 2013; Abuku et al., 2009; Blocken et al., 2007; Blocken, 2004). As the angle between the approaching wind and the normal to the facade increases, the wind-flow pattern around the building changes, resulting in different wind characteristics encountered near the surface of the facade. CFD simulations on a simple rectangular building (Abuku et al., 2009) shows this in Figure 2.5a-d. For $\theta_{10} = 0^\circ$ (Figure

2.5a), the stagnation region in the center of the facade can be seen as low velocity vectors with an increase in wind speed towards the facade edges. For $\theta_{10} = 22.5^\circ$ (Figure 2.5b), the stagnation region shifts to the right (upwind) edge and the wind speed increases towards the downstream edge with the velocity vectors almost parallel to the facade. For $\theta_{10} = 45^\circ$ (Figure 2.5c), no obvious stagnation region can be seen and the wind flow is marked by high velocity vectors which are smaller at the upstream edge and increases towards downstream edge; the velocity vectors towards the downstream edge become increasingly parallel to the facade. For $\theta_{10} = 67.5^\circ$ (Figure 2.5d), the stagnation region can be seen on the narrower facade and the velocity vectors are almost parallel to the wider facade with constant length. The resulting raindrop trajectories for the oblique winds are seen in Figure 2.6a-d. The shape of the trajectories near the facade are highly influenced by the wind flow near that region; the trajectories near the stagnation regions are straight and start to deviate as the wind flow deviates.

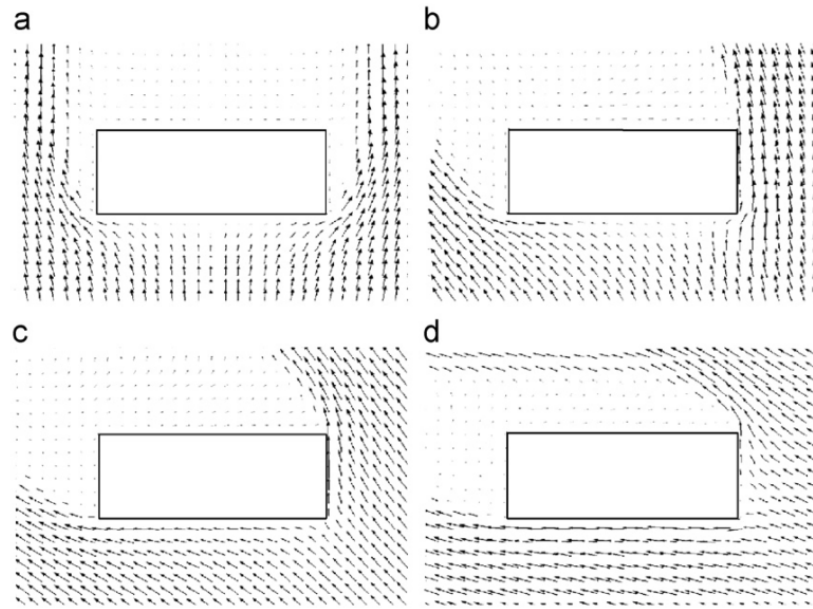


Figure 2.5 – Top view of the wind-flow pattern around a rectangular building with a flat roof in a horizontal plane 3 m above ground for $\theta_{10} =$ (a) 0° , (b) 22.5° , (c) 45° and (d) 67.5° (from Abuku et al., 2009).

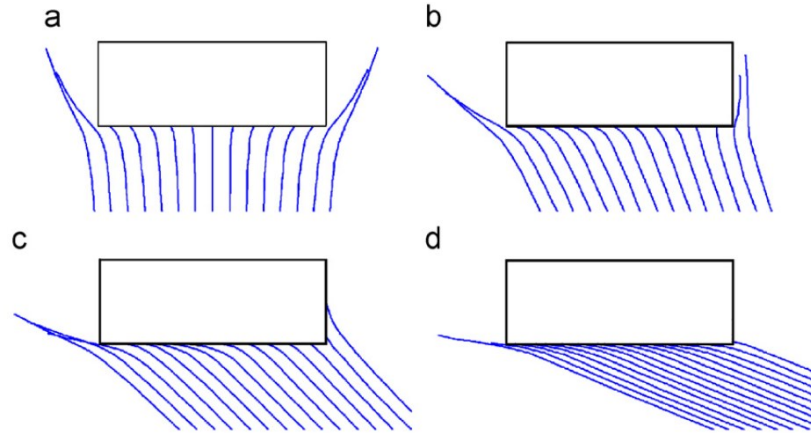


Figure 2.6 – Top view of raindrop trajectories of 1 mm raindrops impacting the facade 3 m above ground for $\theta_{10} =$ (a) 0° , (b) 22.5° , (c) 45° and (d) 67.5° (from Abuku et al., 2009).

Research efforts to quantify WDR loads can be separated into three categories: (1) experimental methods, (2) semi-empirical methods, and (3) numerical methods, and are briefly discussed below.

2.3.1. Experimental Methods

Experimental methods are the oldest method of quantification and have essentially remained unchanged since the first measurements in early twentieth century. Experimental methods consist of measuring WDR with gauges equipped with a vertical aperture to collect the WDR and a reservoir or a tipping bucket mechanism to collect or measure the quantity of rain water.

Although the method of measurement is simple, measurement errors are complex and unique. Experiments have yielded and validated the “classic” wetting pattern, whereby: (1) the windward facade receives the majority of wetting, (2) on the windward facade, wetting increases from the bottom of the facade to the top and from the middle of the facade to the sides; the top corners are the most wetted, followed by the top and side edges, (3) for high and wide buildings, the windward facade receives relatively little rain, except for the top corners and top and side edges, (4) The WDR intensity at a specific location increases proportionally with wind speed and horizontal rainfall intensity (Blocken & Carmeliet, 2004).

Experimental WDR measurements are the primary and only truly reliable approach for quantifying WDR, however, they are not practical because of the time and costs associated with them. Furthermore, limited spatial and temporal information and the fact that measurements at

one site have a limited application to another site, limit the application of experimental methods. However, field measurements serve as a basis for the development and validation of semi-empirical methods and for the validation of numerical methods. Moreover, experimental methods may examine the influence of complex building geometries and design details such as roof overhangs.

2.3.2. Semi-Empirical Methods

Semi-empirical methods correlate the WDR loads on building surfaces from data obtained from meteorological weather stations and are practical for design applications due to their simplicity. However, they provide only rough estimates of the WDR exposure. Two semi-empirical methods exist: (1) the *WDR index* and (2) the *WDR relationship*.

The *WDR index* is the product of the wind speed and the horizontal rainfall amount and is roughly proportional to the WDR amount; it is an indication of the wetness of a geographical location not the actual WDR amount on the any given building facade. The first WDR maps, based off the product of wind speed and horizontal rainfall amount, were constructed in Norway and the UK, followed by other European countries (Blocken & Carmeliet, 2004; Lacy, 1971; Avendano, 1966; Blociszewski, 1966; Jessing, 1966; Jonesen & Marcu, 1966; Lacy & Shellard, 1962). Over time, the WDR index evolved from a quantitative approach (comparing the WDR exposure from a particular location in respect to another) to a qualitative approach (actually determining free WDR amounts and WDR amounts on facades) (Blocken & Carmeliet, 2004). The WDR maps led to the development of the BSI Draft for Development 93 which took on several forms before becoming the ISO 15927 (International Standard Organization (ISO), 2009; CEN, 1997; British Standards Institution, 1984, 1992).

The *WDR relationship* is a method that relates WDR intensity to wind speed, wind direction and horizontal rainfall intensity using a WDR coefficient, which takes into account the interaction between wind, rain and buildings. The first WDR relationship was suggested by Hoppestad and later refined by Lacy (1965). Later, a WDR coefficient was introduced taking into account the local phenomena induced by the topography and the building itself, obtained through measurements and the angle between the approaching wind and the normal to the facade. The validity of using cosine projection has been investigated using CFD modeling, which has shown

that its use may give rise to significant errors (Blocken & Carmeliet, 2006b), however, no alternative is available.

The ISO 15927-3, 2009 mentioned above, prescribes a procedure that is constructed from both the *WDR index* and the *WDR relationship*. The procedure comprises of calculating the: (1) *airfield indices* and (2) *wall indices*. The airfield index is a relative indicator of the potential WDR exposure of a specific wall and is the amount that would be collected by a free standing WDR gauge (does not take into account topology, building geometry, design details, etc.). The wall index considers the interaction of the wind with the building and thus, the quantity of WDR that would fall onto a real building wall, by multiplying the airfield index with several factors.

Semi-empirical methods may provide a rough estimate of the WDR load on any given building and may be sufficient in some cases, however, it is not adequate when more detailed information is needed such as: the spatial distribution of WDR across a building facade and the effect of building details such as balconies, pitched roofs, overhangs, etc.

2.3.3. Numerical Methods

Numerical methods came into existence more recently. Researchers realized that the complexity of the WDR phenomenon may be further investigated using numerical methods. Computational Fluid Dynamics (CFD) uses numerical techniques to obtain the wind flow pattern. During the 1990's, Choi (2001, 1994a, 1994b, 1993) developed a numerical method where raindrop trajectories were calculated based on a steady-state 3D wind flow pattern. The flow pattern is obtained by solving the 3D Reynolds Averaged Navier-Stokes equations, the continuity equation, and the equations of the standard k- ϵ turbulence model. Based on the raindrop trajectories ending on the facade and the raindrop size distribution, the specific catch ratio and catch ratio may be calculated. Thus, the spatial distribution of WDR on buildings may be determined under steady-state conditions of wind and rain.

Blocken & Carmeliet (2000) extended Choi's method by adding: (1) the temporal component and (2) a weighted data averaging technique, to determine the spatial and temporal distribution of WDR. Numerical results show a general agreement with experimental observations where the catch ratio increases with wind speed and a "classic" wetting pattern is observed, where the top corners and top and side edges receives the majority of the WDR load. Despite the few

encouraging validation studies, further validation studies for different environmental topologies, building geometries, and building details, such as roof overhangs, are required.

2.4. Effectiveness of Overhangs

Roof overhangs have been traditionally used for purposes including protection against rain. However, there is limited quantitative data regarding the effectiveness of roof overhangs. Previous studies show that the shapes of the roof and overhang have a significant impact on the amount of WDR deposited on the building facade. Pitched roofs and overhangs protect the wall below it by shadowing and redirecting airflow.

Inculet & Surry (1995) studied the influence of building geometry and architectural details such as balconies, cornices, pitched roofs, and inset corners on the wetting pattern of scaled down building models placed in a boundary layer wind tunnel. They found that cornices may be successful in protecting the top of the building facade just below the cornice.

CMHC (Ricketts & Lovatt, 1996) published a survey of building envelope failures in the lower mainland of British Columbia due to the large number of envelope problems related to water penetration. Water penetration was largely due to the design and construction of the wall assemblies with respect to water management principles. The survey found that the lack of overhangs was a contributing factor to moisture damages in wood frame walls; as the width of the overhang decreased, the percentage of walls that had encountered problems increased. Hence, the size of a roof overhang correlated directly with the probability of rain related damages. CMHC (Surry & Hangan, 2000) also conducted CFD simulations on a six-storey building. The simulation found that a cornice reduced the amount of rain on the upper portion of the wall by about by up to 4 times. The cornice did increase the wetting in some areas, however, it was deemed acceptable in the context of the overall positive effect of the cornice. No mention of the cornice sizing was made in the study.

Blocken & Carmeliet (2005) performed WDR measurements on a low-rise building with a combination of a flat-roof and a sloped-roof with different overhang widths. Their study found that the flat roof with a smaller overhang width received significantly more rain than the sloped roof with a slightly larger overhang. It was also noticed that a 2 cm increase in overhang width significantly decreased the amount of WDR below it. The CFD-based simulations by Blocken

(2007, 2004) have shown that the shelter effect by roof overhang increases, for fixed wind speed and raindrop diameter, as the overhang width increases. The shelter effect, however, decreases as wind speed increases since the trajectories become more inclined and the “sweeping effect” becomes more important.

Ge & Krpan (2009) performed a large-scale experimental study on various buildings in the lower mainland of British Columbia. The field measurements showed that adding typical overhangs – 30 to 60 cm wide – to a low-rise building and a 90 cm overhang to a 12-storey high-rise building can significantly reduce the deposition of WDR on the building, by about four and one and a half times, respectively, especially at the upper portion of the facade. The protection area extends to about 2.4 m below the roofline for the studied high-rise building. This may be partly due to the lower wind speeds during rain events and the smaller size of rain droplets. Most of the driving rain impacting high-rise buildings occurs at the upper part of the building, within 2.4 m below the roofline (Inculet & Surry, 1995), due to the abrupt change in direction of wind over the edge of the roof and the inability of rain droplets to change direction so rapidly. The lower part receives very little amount of WDR due to the wind blocking effect (Blocken & Carmeliet, 2006c). Consequently, the provision of an overhang may be effective for high-rise buildings, particularly for the coastal climate of British Columbia. For regions with higher wind speeds and larger droplet sizes, the protection of overhang may not be so effective.

A comprehensive analysis of the effect of roof overhang on the WDR wetting of a low-rise cubic building was carried out by CFD modeling (Sepehr et al., 2014; Sepehr, 2013). The influence of wind speed, wind angle and rainfall intensity was investigated for various overhang sizes. The modeling results indicated that the introduction of the overhang changed both the magnitude and the pattern of the WDR deposition on the facade. The impact of the overhang on the WDR wetting of the facade varied locally. All the tested overhangs helped protect the upper half of the facade from WDR under all studied wind and rain conditions. The lower half of the facade, however, remained almost unaffected by the overhang. The protective effect of the overhang increased as its width increased, as well as when the building was subjected to lower wind speeds. It was also shown that, compared to rainfall intensity, wind speed and wind angle had greater impacts on the WDR load, as well as the performance of overhangs. An effectiveness

index was introduced to quantify the effects of the overhang. This index was shown to give a meaningful measure of the effects of overhangs.

2.5. Errors Associated with WDR Measurements

When dealing with a complex phenomenon such as WDR, one can imagine the complexities of collecting and measuring the amount of rainfall with measurement equipment. To further complicate things, no standard design for WDR gauges exist. Therefore, an adequate measurement of WDR should be accompanied by the associated error estimates as stated by several authors (Nore et al., 2007; Blocken & Carmeliet, 2006a; Blocken, 2004).

The errors normally associated with WDR measurements are: (1) adhesion water evaporation, (2) evaporative losses from the reservoir, (3) splashing of drops from the collection area, (4) condensation on the collection area and (5) wind error. The duration, intensity, type of rain event and the sampling frequency also affect the accuracy of the measurements.

Adhesion Water Evaporation

Adhesion water refers to the water that sticks to the WDR gauge collection area and does not run off into the reservoir. The amount of WDR impinged on a WDR gauge collection area can only be measured once surface runoff occurs. Surface runoff happens once the accumulated WDR exceeds a threshold value on the collection area. This threshold value is dependent on the design of the gauge and the material(s) used in its fabrication. Below this threshold value, the WDR adhered to the collection plate will eventually evaporate and is never measured. For instance, a numerical simulation of drop adhesion, coagulation and runoff found that for an acrylic glass surface: (1) less than 0.12 mm of cumulative inflicted WDR resulted in no runoff (all water is adhered to the collection area) and (2) above this threshold value, the amount of adhesion water decreases and then fluctuates around 0.05 to 0.08 mm, as seen in Figure 2.7 (Blocken & Carmeliet, 2006a).

Adhesion water is highly dependent on the type of surface of which the WDR gauge is made of. Comparative studies of different WDR gauges by Kragh (1998) and Högberg et al. (1999), indicated that gauges equipped to measure adhesion water (i.e. WDR gauge suspended from a load cell and WDR gauge equipped with an automated wiper) may collect up to twice the

amount of WDR measured from traditional WDR gauges. Adhesion water evaporation has been identified as the major source of error for WDR gauges in numerous studies (Osorio, 2013a; Nore et al., 2007; Blocken & Carmeliet, 2006a; Blocken, 2004; Högberg, 2002; Högberg et al., 1999). The relative error due to adhesion water decreases as the amount of WDR collected increases.

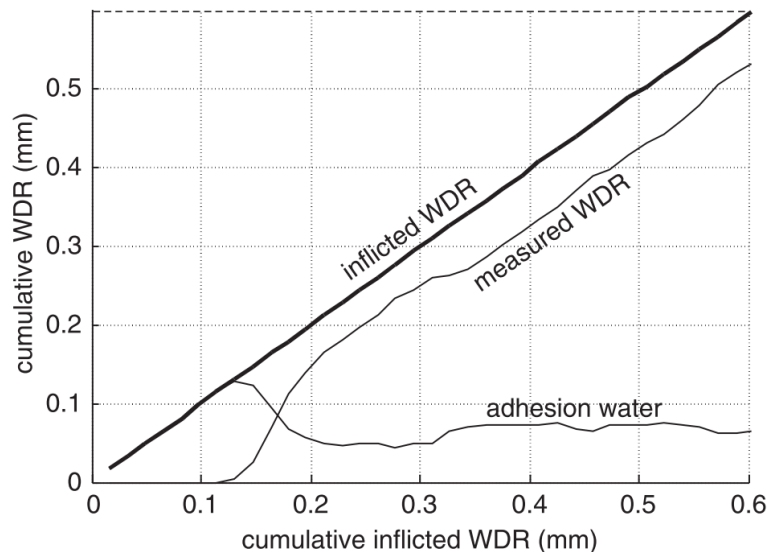


Figure 2.7 – Result of the numerical simulation of drop adhesion, coagulation and runoff on a acrylic glass surface. The “cumulative inflicted WDR” is the sum of adhesion water and measured WDR (from Blocken & Carmeliet 2006a).

Evaporative Losses from the Reservoir

Evaporative losses from the reservoir, of which the WDR is collected, can be measured and is small during rain given the high relative humidity. The addition of a few drops of light oil may slow down the evaporative losses in the reservoir.

The use of a tipping-bucket mechanism essentially eliminates evaporative losses from a reservoir but it introduces two additional errors which must be taken into account: (1) the error caused by the rest water that remains in the bucket at the end of a spell and (2) the error due to loss of incoming water running by and not collected by the bucket due to its brief vertical position during the tip.

The first is the error caused by the rest water that remains in the bucket at the end of the spell. Since a tip only occurs when the bucket is completely filled, the rest water is not registered for

the spell. If the rest water does not evaporate before the start of the next spell, it will be added to the new spell. Second, there is an error due to the loss of incoming water running by and not collected by the bucket due to its brief vertical position during the tip (Nore et al., 2007).

Splashing of Drops from the Collection Area

Splashing losses refers to the loss of water when the collision of a water drop onto a solid surface occurs and is considered to be an extremely complex phenomenon, which involves many factors. Recessed gauges have been experimented with by Högberg (2002); they performed better than the non-recessed gauges by reducing splashing for high wind speed and heavy rainfall intensities. The recessed gauges, however, had an increase of adhesion water evaporation because of their larger collection area, for light to moderate rainfall intensities. According to Blocken & Carmeliet (2006a), splashing becomes more important as the raindrop size, raindrop speed and hence, the raindrop kinetic energy increases. A wind tunnel test performed by Gandemer (2001) concluded that splashing does not occur for WDR conditions with a reference speed of less than 10 m/s and with drop sizes smaller than 1 mm.

Condensation on the Collection Area

Undercooling condensation on the WDR gauge collection area can be calculated based on the meteorological data and surface temperatures of the gauge collection area. Since thermocouples are not normally installed on WDR gauges, the temperature of the cladding is used with the assumption that the surface temperature of the gauge collection area is equal to the surface temperature of the cladding due to the large contact area of the WDR gauge (Nore et al., 2007). Estimates of condensation errors can also be obtained by a simulation with a heat-air-moisture transfer models (Blocken & Carmeliet, 2006a). Either way, condensation errors are considered to be small for all gauge types, the typical condensation with nocturnal infrared loss on a vertical surface on a clear night is on the order of a few tenths of a millimeter (Nore et al., 2007; Camuffo, 1998).

Wind Errors

Wind errors are caused by the disturbance of the wind-flow pattern and the raindrop trajectories near the gauge by the presence of the gauge itself (Blocken & Carmeliet, 2006a). Wind errors are

expected to be smaller for periods when the wind is blowing approximately perpendicular to the collection area of the WDR gauge because of the small wind speed that occurs on the surface. However, for sharp wind angles (e.g. 60° to 90° from the normal to the wall), higher wind speeds exist near the surface and the influence of the rim of the gauge significantly increases. These wind errors are difficult to quantify, however, they may be estimated using CFD simulations.

CHAPTER 3: EXPERIMENTAL SETUP & METHODOLOGY

3.1. Field Measurements

3.1.1. The Location and Description of the Building

The test building, known as the Cassiar Building, is a six-storey rectangular residential building with a flat roof located in Vancouver (near Burnaby) in British Columbia. The building is located within a suburban location; it is surrounded by two- to three-storey residential buildings to its North and West and a highway to its East and South (Figure 3.1). It is a fairly open site within a suburban setting making it an ideal building for wind-driven rain studies.



Figure 3.1 – Aerial view of the building site (from Google Maps).

The test building is 39.2 m long, 15.2 m wide, 19.8 m high and is oriented in such a way that the four facades of the building face the cardinal wind directions. A panoramic view of the building's surroundings is shown in Figure 3.2. The prevailing wind direction during rain is predominately from the east, therefore, special attention has been paid to the east facade. To

study the effectiveness of various overhang widths in reducing wind-driven rain wetting, sections of both the east and north facades are equipped with a retractable overhang (0 to 1.2 m), shown in Figure 3.3.



Figure 3.2 – Panoramic view of the test building's surroundings (the north, east, south and west sides of the building are marked in the photo).

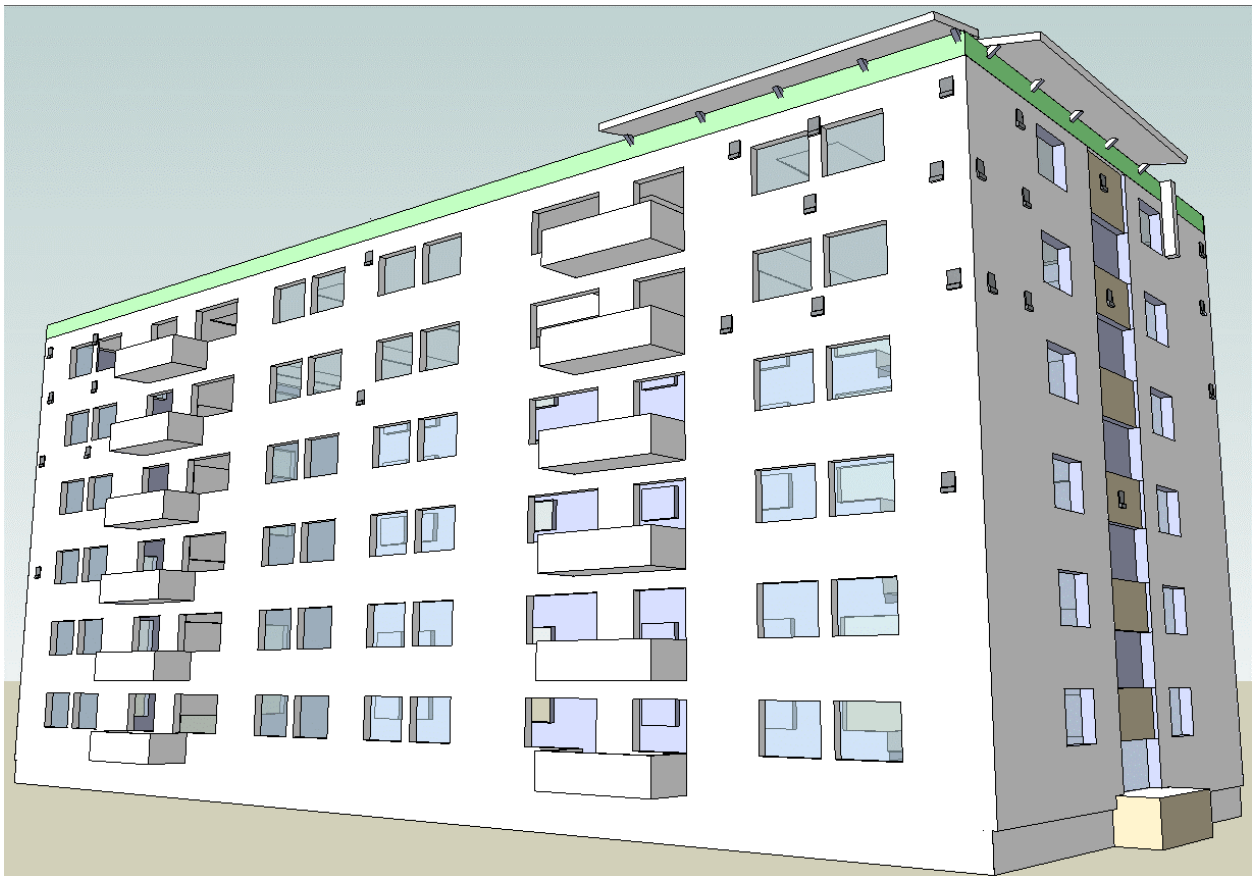


Figure 3.3 – The east and north facades of the test building with the strategically placed WDR gauges and retractable overhang (drawn in SketchUp).

3.1.2. Instrumentation and Sensor Location

The instruments used to collect wind speed, wind direction, horizontal rainfall, wind-driven rain, temperature, and relative humidity are discussed below. Technical specifications of the instruments are shown in Table A.1 in APPENDIX A.

Wind Monitor

The wind monitor measures the wind speed and the wind direction and is mounted on top of a tripod cross-arm (4.6 m) above the mechanical room in the center of the roof (Figure 3.4). This location helps minimize the local turbulence caused by the building and to distance the wind monitor from obstacles on the roof such as the solar heat collectors. The wind monitor can measure wind speed within a range of 0 to 50 m/s and has an accuracy of ± 0.2 m/s or 1% of the reading (Campbell Scientific, 2013b).

Temperature and Relative Humidity Probe

The temperature and relative humidity probe measures the ambient air temperature and its corresponding relative humidity. It is mounted on the tripod's mast (Figure 3.4) and is shielded from the sun and wind by use of a radiation shield. The temperature sensor has a measurement range of -50°C to $+50^{\circ}\text{C}$ with an accuracy of $\pm 0.1^{\circ}\text{C}$. The relative humidity sensor has a range of 0 to 100% non-condensing and an accuracy of 0.8% (Campbell Scientific, 2013a).

Horizontal Rain Gauge

The horizontal rain gauge is 29.2 cm high with a conical collection area (24.5 cm diameter) constructed of gold anodized spun aluminum. The resolution of the tipping bucket is 1 tip with a volume per tip of 4.73 mL/tip and a rainfall per tip of 0.1 mm/tip. The gauge has an accuracy of 1% up to 50 mm/hr. The gauge is placed close to the center of the main roof to distance itself from obstructions that may cause local turbulence and wind deformation (Figure 3.5).

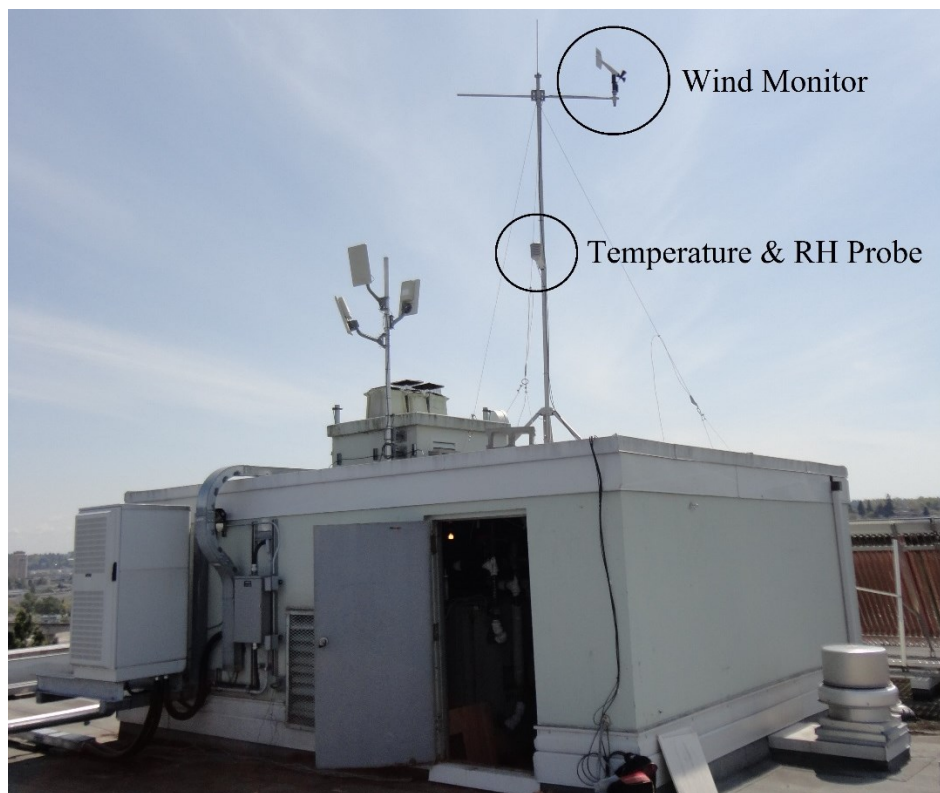


Figure 3.4 – The wind monitor and temperature/relative humidity probe mounted on the tripod cross arm and mast. The tripod sits atop the mechanical room roof which is located in the center of the main roof.



Figure 3.5 – Horizontal rain gauge placed in the center of the main roof.

Wind-driven Rain Gauges

The WDR gauges are a custom made aluminum plate-type gauge consisting of a square collection area, 30.5 cm by 30.5 cm, for a collection area of 930.3 cm² shown in Figure 3.6. Water runoff is directed to the bottom of the collection area, where a small funnel directs the water to a tipping bucket, which is housed in the lower portion of the gauge. The perimeter of the collection area is raised (25.4 mm), to prevent outside water from falling onto the collection area. The top of the rain gauge is sloped downwards towards the rear to direct runoff rainwater away from the collection area. The volume of the collected rainwater in the reservoir is automatically registered using a tipping bucket mechanism and the resolution of the tipping bucket is 0.06 mm per tip.

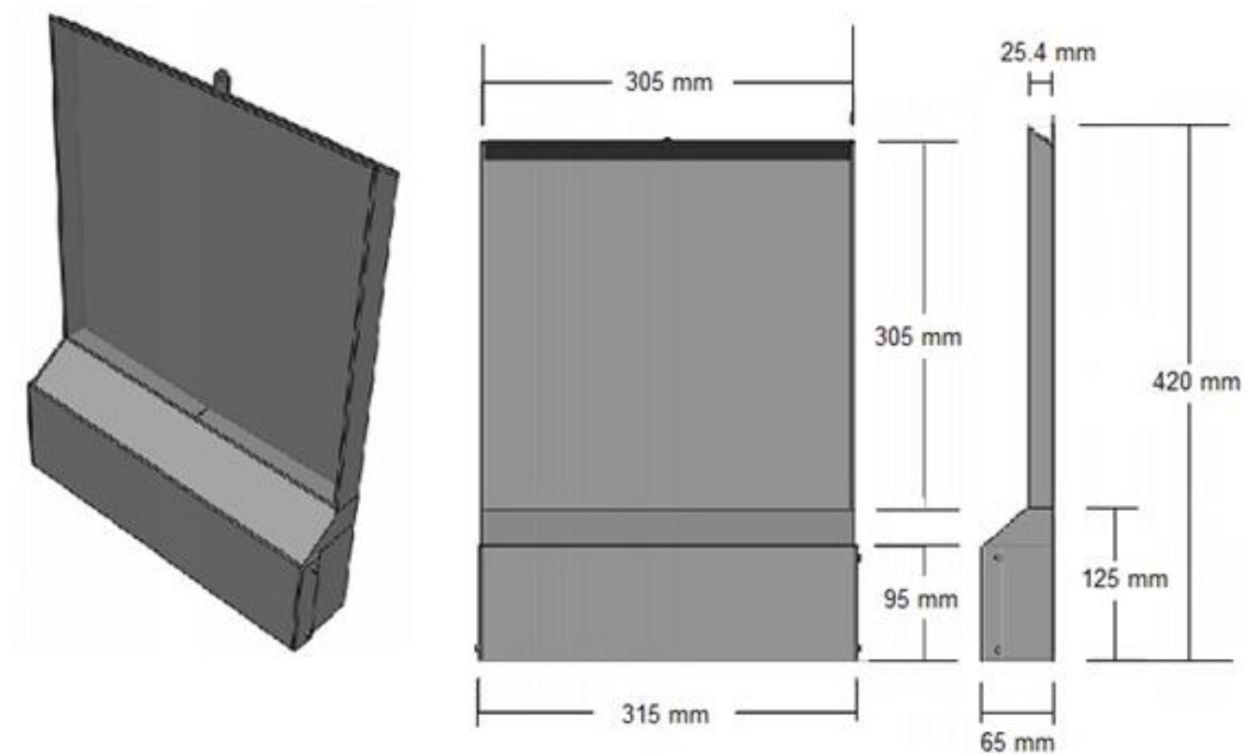


Figure 3.6 – Sketch of the wall-mounted wind-driven rain gauge (from Osorio 2013b).

A total of 31 WDR gauges have been installed on the test building: 18 on the east facade, 11 on the north facade, 1 on the west facade and 1 on the south facade. Figure 3.3 shows the WDR gauges on the east and north facades with respect to the overhang location in three dimensions. The gauges were installed with a vertical staggered formation to prevent water caught by the

gauge above from falling onto the gauge below. Figure 3.7 shows the plan view of the test building with the WDR gauge locations. Figure 3.8 to Figure 3.10 shows the location of the WDR gauges on the east, west, north and south facades, respectively.

Data Collection

The wind monitor, temperature and relative humidity probe, horizontal rain gauge and WDR gauges are all connected to a central data logger, which is programmed to collect and store raw data every 5 minutes. The wind data (wind speed and wind direction) is gathered at 1 Hz sampling frequency and averaged every 5 minutes. The temperature and relative humidity is also averaged every 5 minutes. The sum of tips is registered for the horizontal rain gauge and the driving rain gauges every 5 minutes. The data logger was connected to the internet via Ethernet which allowed the data to be collected remotely. The first recorded rain event began at 10:00 PM on August 16, 2013.

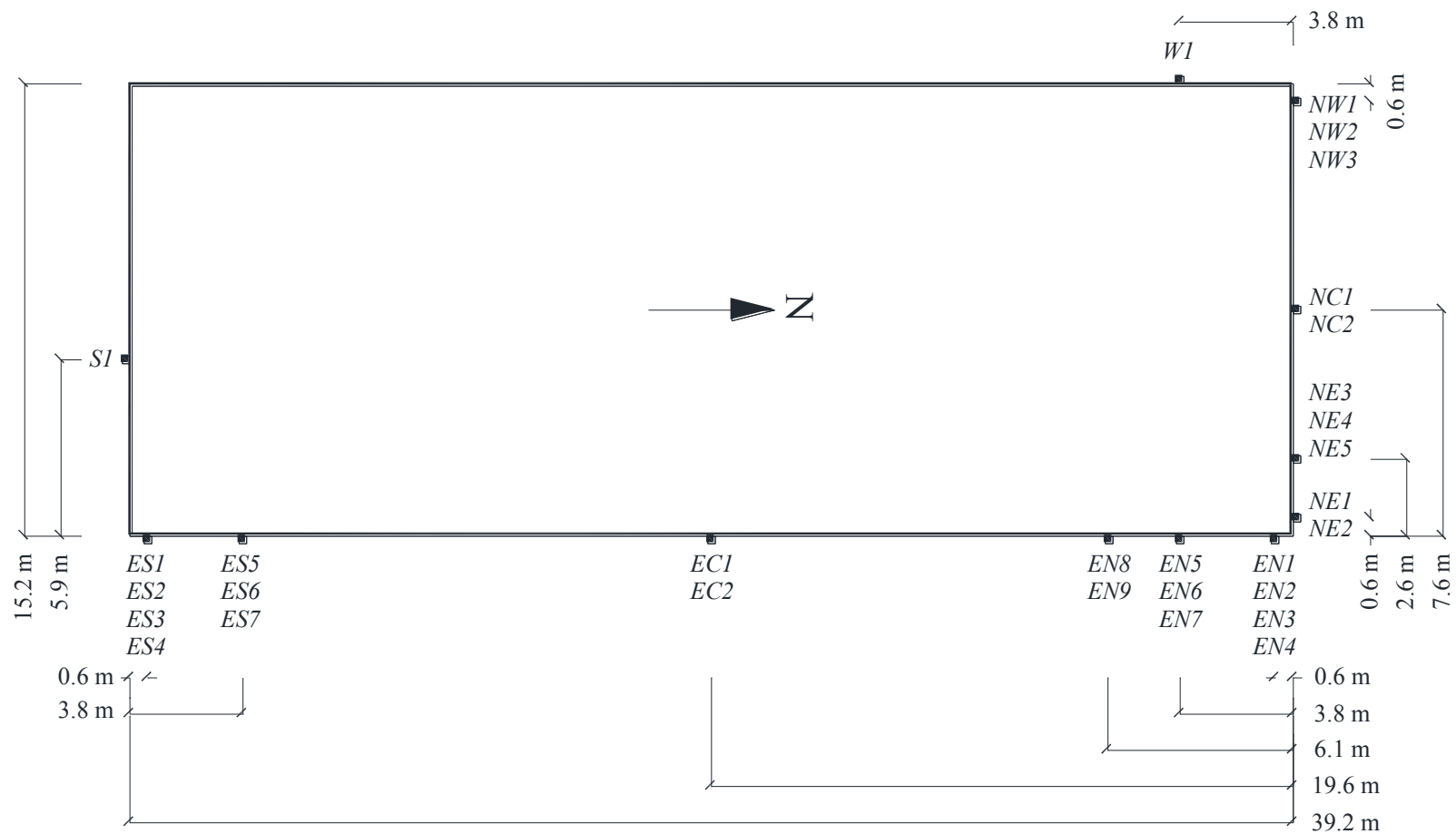


Figure 3.7 – Plan view of the test building and the WDR gauge locations.

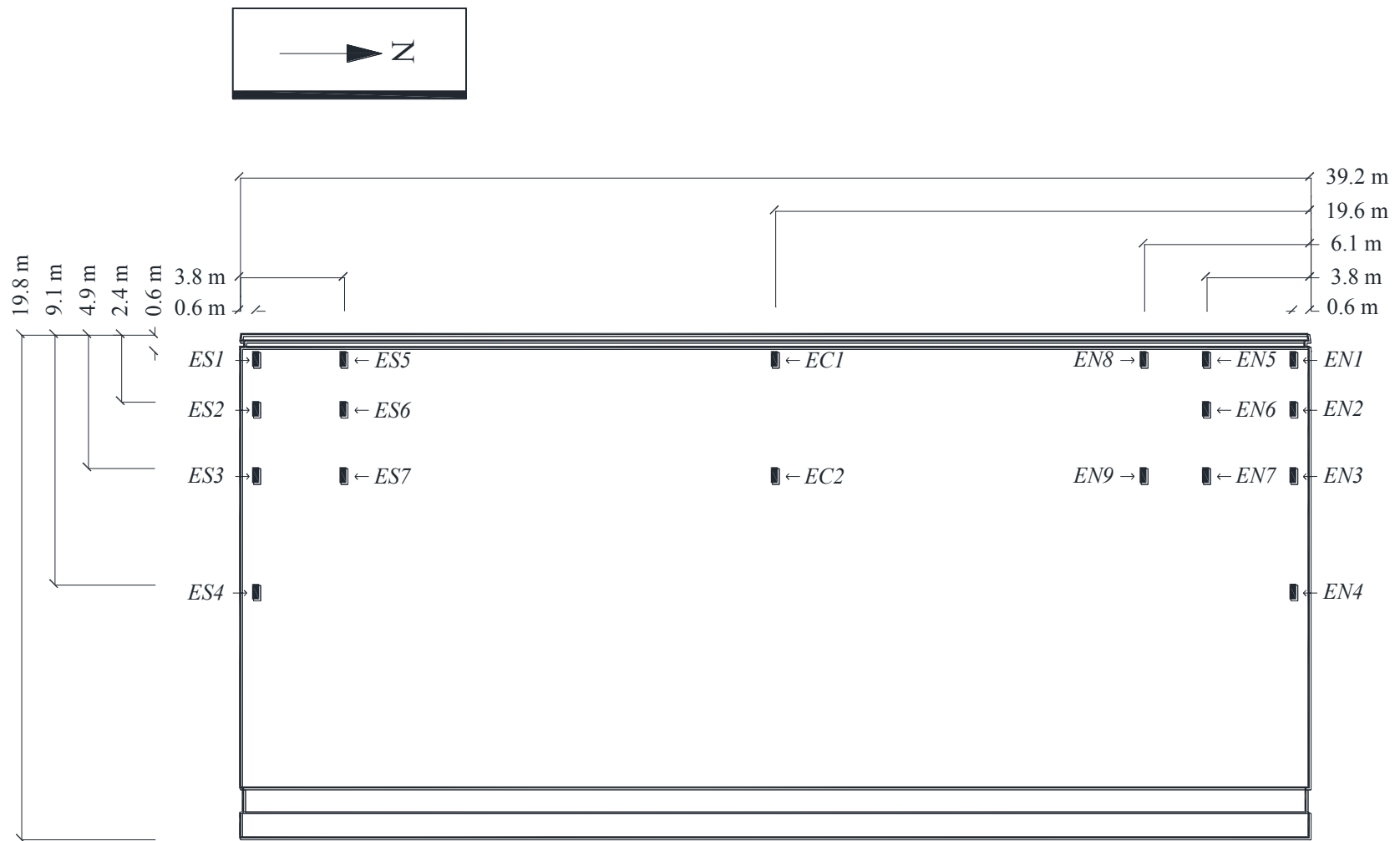


Figure 3.8 – Side view of the east facade and the WDR gauge locations.



Figure 3.9 – Side view of the west facade and the WDR gauge location.

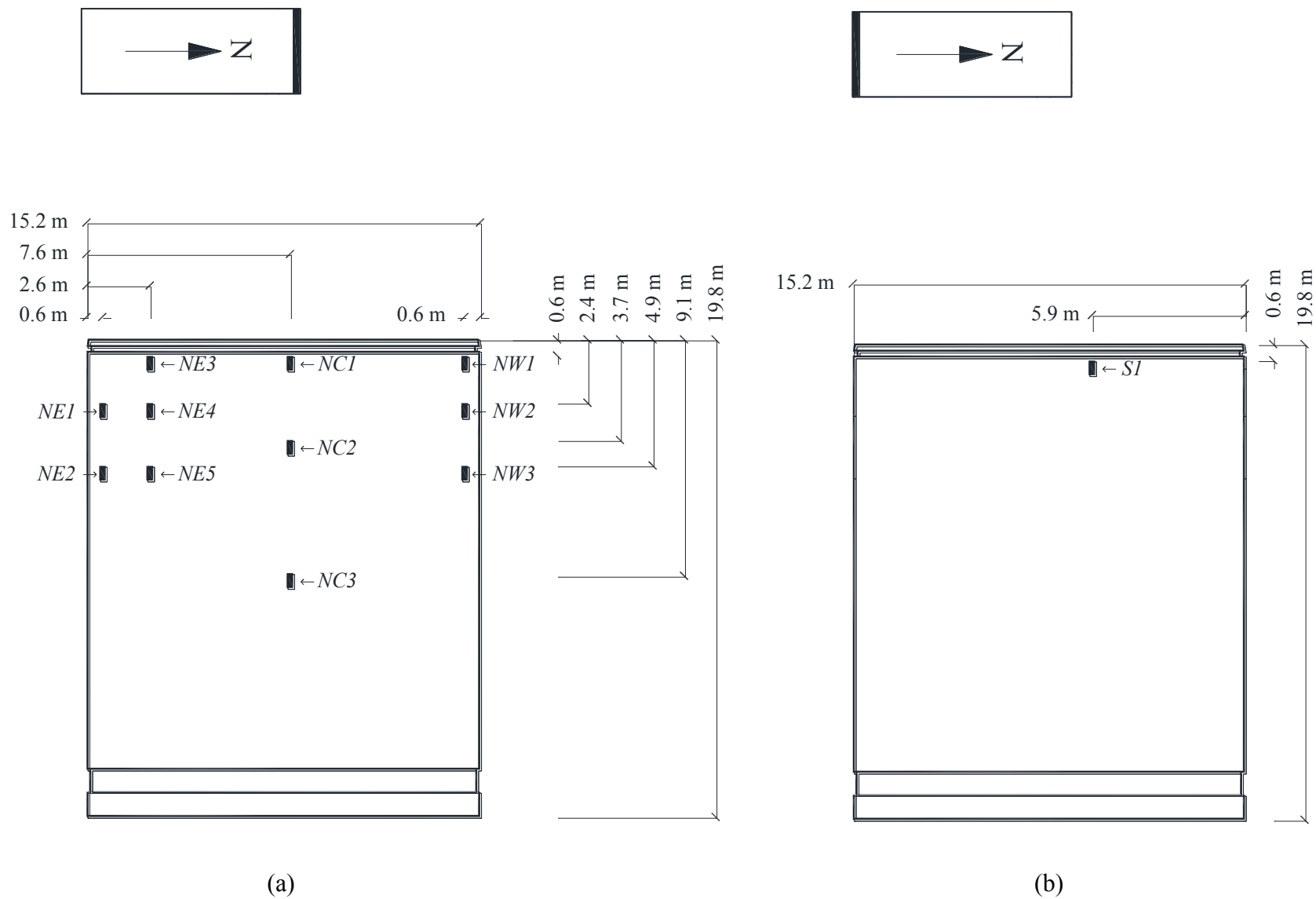


Figure 3.10 – Side view of the (a) North facade and (b) South facade and their WDR gauge location(s).

3.2. Wind Tunnel Measurements

3.2.1. Description of the Atmospheric Boundary Wind Tunnel

Concordia University's atmospheric boundary-layer wind tunnel is located in the Building Aerodynamics lab of the Engineering, Computer Science and Visual Arts Integrated Complex at the Sir George Williams campus. It is an open-circuit blowdown wind tunnel with a centrifugal blower and a rectangular cross-section. The tunnel has a test section 12.20 m long, 1.80 m wide and has an adjustable suspended roof with a minimum and maximum height of 1.40 m and 1.80 m, respectively. The wind tunnel is equipped with a 1.21 m diameter turntable downstream of the test section.

A MARK HOT double inlet centrifugal blower with a capacity of 40 m³/s at a static pressure of 4 cm of water is capable of producing a maximum wind velocity of 14 m/s. The velocity distribution in an empty tunnel is approximately symmetric with respect to the vertical axis passing through the center of the turntable – measurements show that there is a $\pm 4\%$ deviation from the mean velocity below 250 mm height (Stathopoulos, 1984). A schematic of the wind tunnel is shown in Figure A.1 in APPENDIX A.

3.2.2. Model and Exposure

Test Building and Surrounding Buildings

A 1:400 scale model of the test building and its surroundings within a 200 m radius have been fabricated and placed in an ABL wind tunnel. The 1:400 scale was selected based on the surroundings and successful simulations at this scale of the most important variables of the atmospheric boundary layer under strong wind conditions, carried out in this wind tunnel (Stathopoulos, 1984). The models are cut from extruded polystyrene foam insulation using a hot wire cutter and glued to a particle board base. The test building and its surroundings within a 200 m radius are shown in Figure 3.11.

The test building model is 98 mm long, 38 mm wide and 50 mm high. There is a mechanical room located on the center of the roof measuring 15 mm long, 13 mm wide and 6 mm high. The top view of the test building model is shown in Figure 3.12. The proximity of the measurements to the facades were limited due to the profile of the Cobra Probe. There are 23 measurement points on

the east facade and 15 measurement points on the north facade shown in Figure 3.13 and Figure 3.14, respectively. The circular points have WDR gauges associated with them in the field, whereas the triangular points do not.



Figure 3.11 – The test building and surrounding buildings within a 200 meter radius.

Exposure

The test building in the field is located within a suburban environment, therefore, a similar exposure is simulated in the wind tunnel. To obtain a suburban wind profile, a mixture of roughness elements have been placed along the length of the test section of the tunnel. The roof of the wind tunnel was adjusted along the length of the test section to satisfy the condition of zero longitudinal pressure gradient for a suburban exposure. The blower was set to maximum speed.

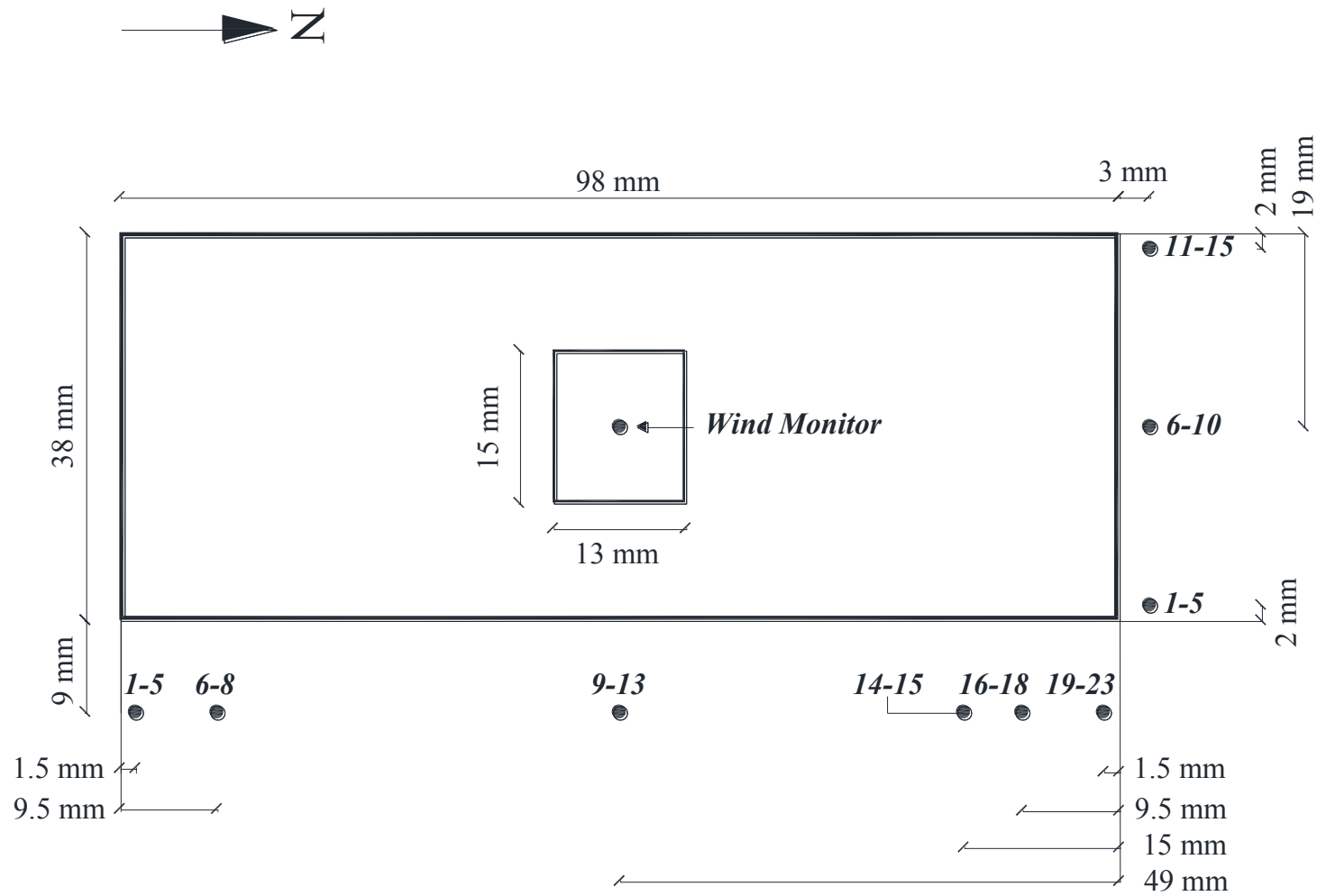


Figure 3.12 – Top view of the test building model. The measurement points near the east and north facade are shown in addition to the wind monitor location.

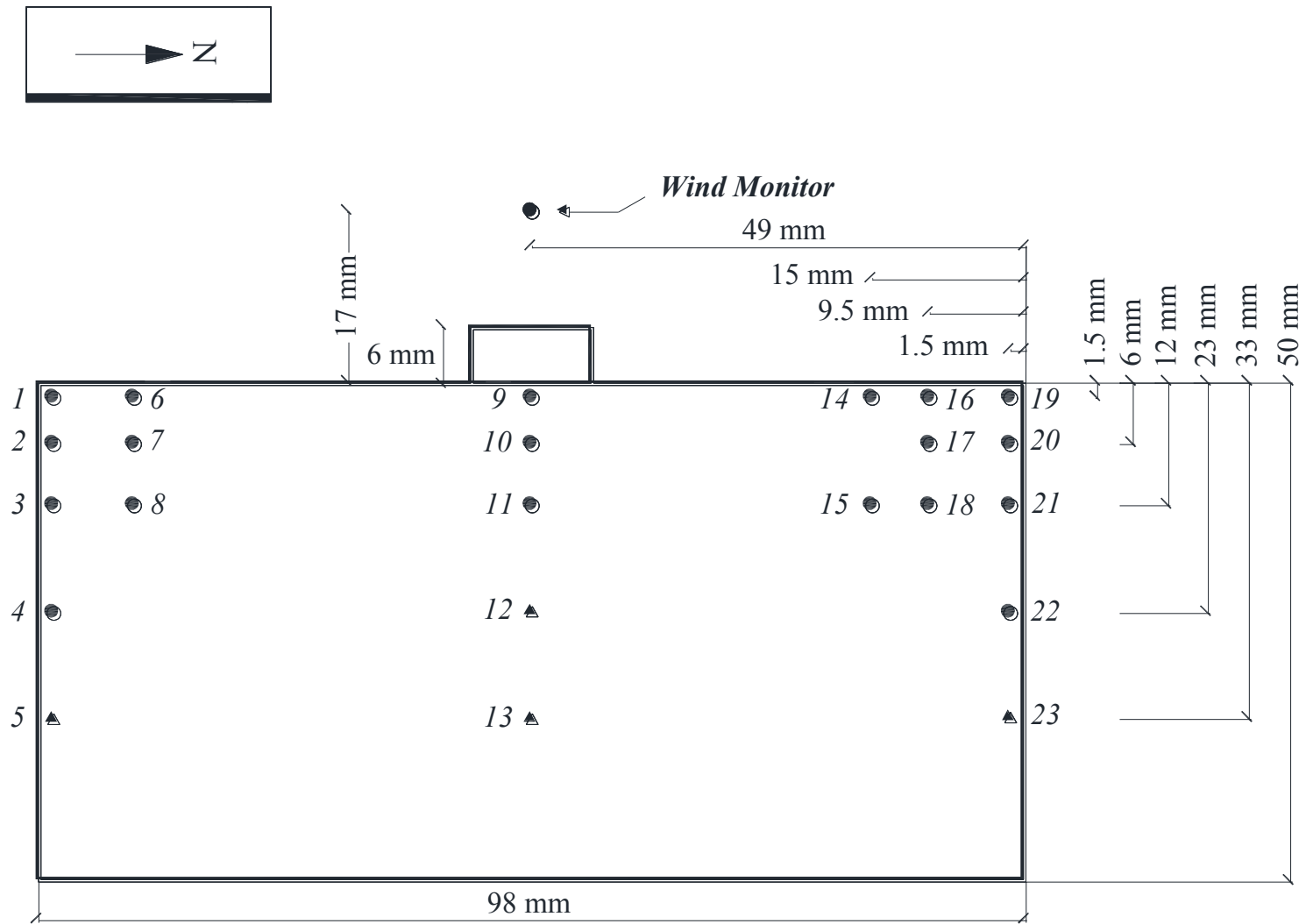


Figure 3.13 – Side view of the east facade of the test building model with the location of wind monitor and facade measurement points.

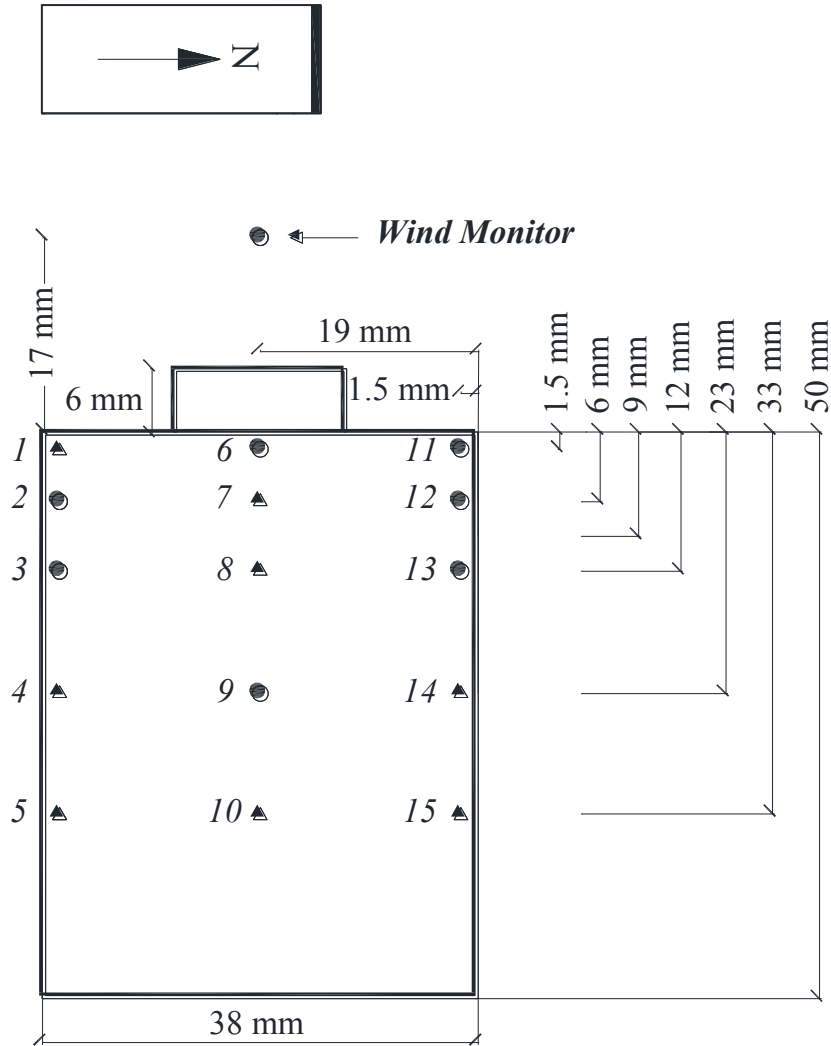


Figure 3.14 – Side view of the north facade of the test building model with the location of wind monitor and facade measurement points.

3.2.3. Velocity Measurements

To measure the velocities in the wind tunnel, a Series 100 Cobra Probe was used. The Cobra Probe is a multi-hole pressure probe that provides dynamic, 3-component velocity and local static pressure measurements in real-time. The Probe is capable of a linear frequency response from 0 Hz to more than 2 kHz and is available in various ranges for use between 2 m/s and 100 m/s (TurbulentFlow Instrumentation, 2011). Although the probe comes pre-configured, the accuracy was verified by comparing the mean values measured by the Cobra Probe with the measurements of a pitot static tube mounted at the same location. In addition, the measurements

were checked for repeatability for the wind profile above the mechanical room roof and in front of the east facade. The average percent difference between the two tests were 1% and 6% for the wind profile above the roof and the east facade, respectively. The results for repeatability are shown in Table A.2 and Table A.3 in APPENDIX A.

The methodology comparing the wind tunnel measurements to the field measurements are discussed in Section 3.3.1.2 and velocities measured near the facades in the wind tunnel are presented in Section 4.1.2.

3.3. Data Analysis

Field data collected from August 16th 2013 to December 2nd 2015 is used for analysis. The data analysis carried out include the: (1) on-site weather conditions (2) airfield driving rain index, (3) spatial distribution of WDR, (4) wall index and (5) effectiveness of overhang. The on-site wind data has been verified by comparison with data reported by Environment Canada from surrounding weather stations. The spatial distribution of WDR on the building facade has been investigated for three cases: (1) no overhang, (2) 0.6 m overhang and (3) 1.2 m overhang. The effectiveness of the roof overhang under real-life conditions with respect to the most important meteorological parameters of wind speed and wind direction has been assessed.

3.3.1. On-Site Weather Comparisons

To ensure that all of the equipment measuring the meteorological parameters are reliable, a comparison of the meteorological data measured on-site was made with nearby weather stations. As mentioned earlier, the local wind and rain measurements from local weather stations may deviate from the actual wind and rain experienced at the test site due to the local microclimate, however, a general comparison will be made nonetheless.

3.3.1.1. Surrounding Weather Stations

The meteorological parameters collected on-site have been compared to two nearby airport weather stations (Government of Canada (Environment Canada), 2013): (1) Vancouver Sea Island station, which is located next to Vancouver International Airport and (2) Pitts Meadows station, which is located at a regional airport east of the test building. The locations of the two airport stations with respect the test building are shown in Figure 3.15. The following

meteorological parameters are compared: (1) wind direction, (2) wind speed, (3) temperature, (4) relative humidity and (5) horizontal rainfall.

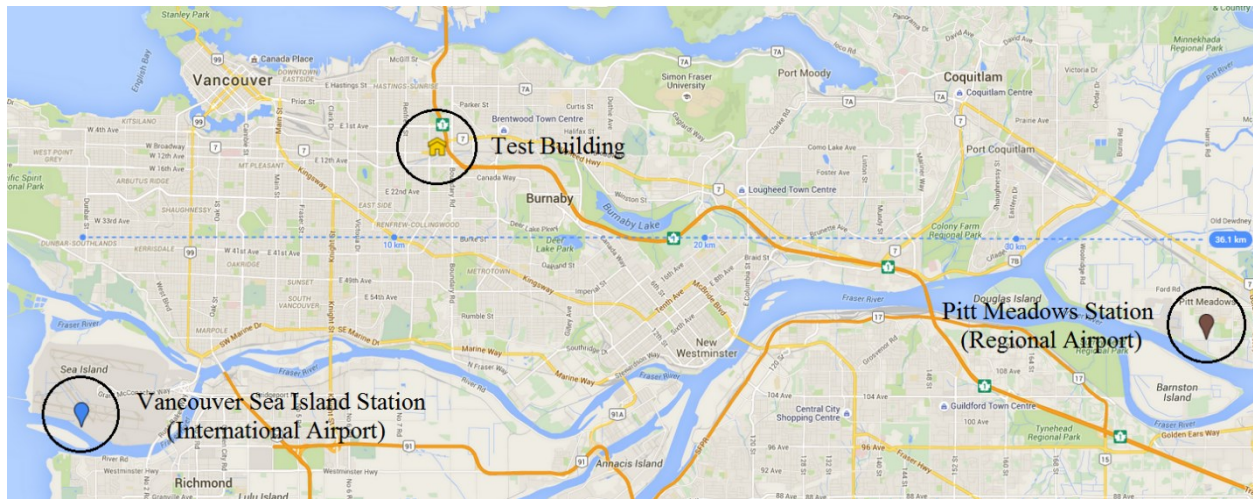


Figure 3.15 – Location of Pitt Meadows Regional Airport and Vancouver International Airport with respect to the test building (from Google Maps).

The exposure types assigned to Pitt Meadows, Vancouver Sea Island and the test building are shown in Table 3.1. The test building is primarily surrounded by two- to three-storey buildings, with no tall buildings in its immediate vicinity, therefore, is considered “suburban.” Vancouver Sea Island and Pitt Meadows stations are both situated at airports, within a generally flat area, so both are considered “open country.” Elevation refers to the elevation of the observing location above mean sea level. The elevations of Pitt Meadows and Vancouver Sea Island are obtained from Environment Canada (Government of Canada (Environment Canada), 2013) and are 5 m and 2.1 m, respectively. The elevation of the test building is approximately 34 m according to VanMap (City of Vancouver, 2014), a web-based application created by the City of Vancouver’s Geographical Information Systems (GIS) department. The reference height (Z_{ref}) is the height at which the wind data is being collected. The measurements at Pitt Meadows and Vancouver Sea Island are taken at 10 m according to Environment Canada (Government of Canada (Environment Canada), 2013). The reference height for the test building is 26.8 m as the wind monitor is mounted on a tripod cross-arm on top of the roof.

Table 3.1 – Exposure type, elevation, reference height, gradient height, and mean speed exponent for Pitt Meadows, Vancouver Sea Island, and the test building.

	Pitt Meadows	Vancouver Sea Island	Test Building
Exposure	Open country	Open country	Suburban
Elevation (m)	5	2.1	34
Reference Height, Z_{ref} (m)	10	10	26.8
Gradient Height, Z_g (m)	300	300	400
Mean Speed Exponent, α	0.15	0.15	0.25

Wind Direction

The frequency of hourly wind direction is shown in Figure 3.16 for the three stations. The predominant wind direction is from the east for all three stations. The wind rose for the test building is similar to that of Vancouver Sea Island, however, there is a higher frequency of east-south-east winds present at the test building. Pitt Meadows receives a relatively higher frequency of northerly and southerly winds, which may be attributed to the valley leading to Pitt Lake to the north and the Fraser River to its south.

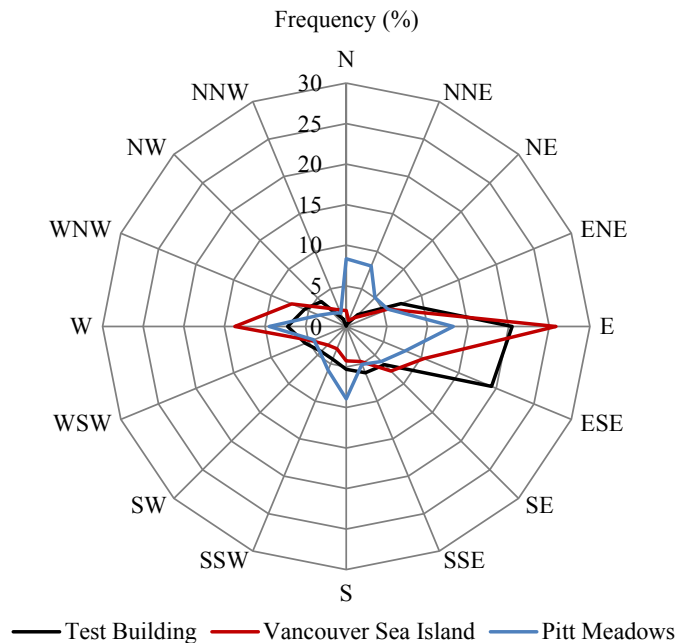


Figure 3.16 – Frequency of hourly wind direction ($^{\circ}$) at the test building, Vancouver Sea Island and Pitt Meadows (Period from August 16, 2013 to June 30, 2015).

Wind Speed

The hourly wind speeds for the test building, Vancouver Sea Island and Pitt Meadows are shown in Figure 3.17 for a period of a month. The wind speed at the test building has been converted to an “open country” exposure so that a direct comparison can be made with the two other “open country” exposures. There is a general agreement between the three stations; however, the influence of local microclimates is evident. The wind speed measured at the test building is similar to the wind speed measured at Vancouver Sea Island; both have a mean hourly wind speed of approximately 2.0 to 2.2 m/s, whereas the mean hourly wind speed at Pitt Meadows is approximately 1.4 m/s. The standard deviation is almost the same for both the test building and Vancouver Sea Island at approximately 1.0 m/s.

The wind speed and direction is of particular importance to WDR studies, therefore, a closer comparison of the on-site measured wind data is conducted. The comparison is composed of converting consecutive hours of high wind speeds with similar wind directions, from one station to another, using the power law (equation 2.2). The power law is considered a good representation of the variation of mean wind speed with height for strong winds over smooth terrain, and with the appropriate exponents, also applicable to cases of rough terrain (Hutcheon & Handegord, 1995). Thus, the wind data used for this analysis has been filtered, using only reference wind speeds greater than 5 m/s from the reference weather station. This wind speed category generally corresponds to a neutral or slightly unstable atmosphere (Turner, 1994) giving a more reliable comparison between stations.

Since the wind direction is predominantly from east to west in the region, the wind speed measured at the test building has been converted to Vancouver Sea Island. Consecutive hours of high wind speeds measured at the test building ($U_{\text{ref}} > 5 \text{ m/s}$) have been considered and the wind direction between the two stations had to be approximately the same. Figure 3.18 shows the wind speed measured at the test building converted to the exposure and elevation experienced at the airport for almost identical wind directions (107° to 120° from the north). The corrected wind speed at the test building is in general agreement with the wind speed measured at Vancouver Sea Island for the same time period. This confirms that a suburban exposure exists at the test building site, at least for the area upstream of the east facade.

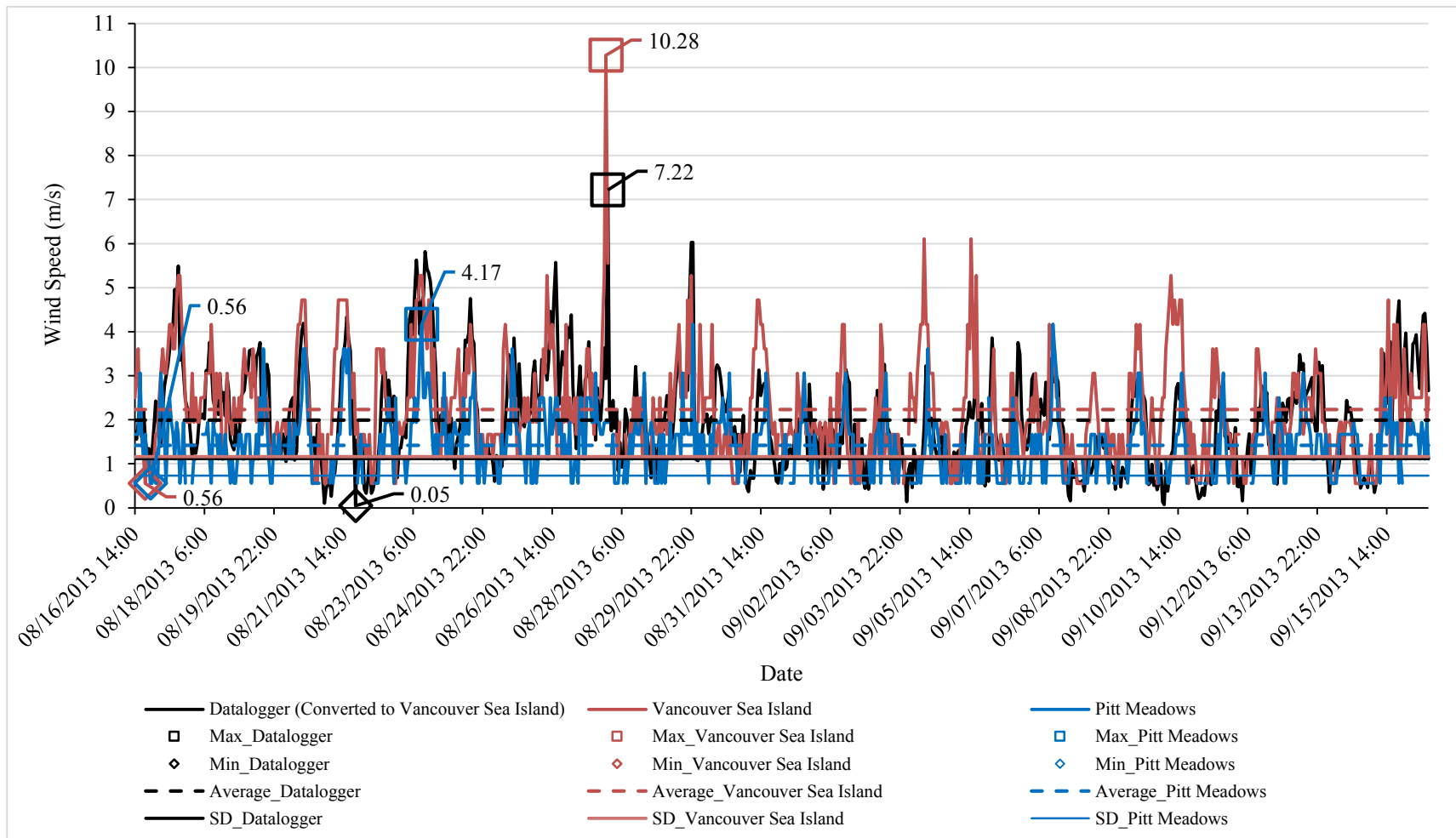


Figure 3.17 – Hourly wind speed between the test building, Vancouver Sea Island and Pitt Meadows.

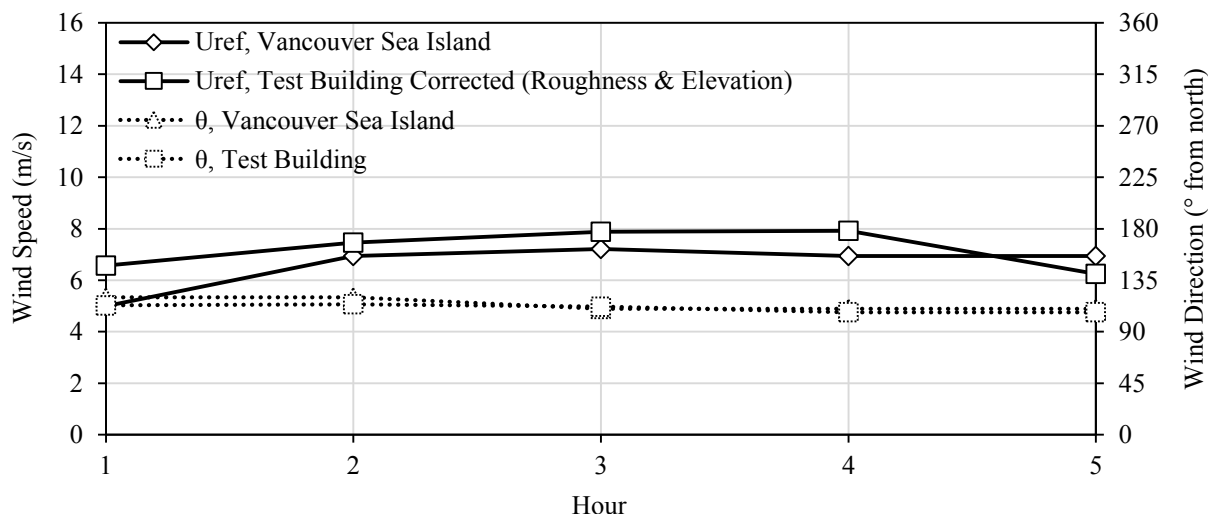


Figure 3.18 – Wind speed at the test building corrected to Vancouver Sea Island.
(February 5th, 2014 from 14:00 to 18:00)

Horizontal Rainfall, Temperature, and Relative Humidity

Figure 3.19 shows the monthly horizontal rainfall measured at the test building, Vancouver Sea Island and Pitt Meadows. Generally in Vancouver, the majority of precipitation occurs during the winter months with a relatively small amount of rain during the summer months, as is the case for the monitoring period in this study. The rainy season normally starts to pick up around October-November and lasts until March-April. There is also significantly less rain measured at Vancouver Sea Island compared to those measured at the test building and Pitt Meadows. This may be attributable to the sea breezes and mountainous terrain which makes Greater Vancouver a region of microclimates. For instance, in North Vancouver, about 20 km away from Vancouver Sea Island, the amount of rain received doubles per year as measured at the base of Grouse Mountain (Government of Canada (Environment Canada), 2013). Figure 3.20 shows the total horizontal amount received for the entire monitoring period at the test building and surrounding stations.

The hourly values of temperature and relative humidity for the test building, Vancouver Sea Island and Pitt Meadows are shown in Figure A.2 and Figure A.3, respectively, in APPENDIX A for a period of a month. The temperature fluctuations for the three stations are in general agreement with each other, with an average temperature ranging from 18 to 20°C for the period.

Vancouver Sea Island has the lowest highs and the highest lows due its proximity to the coast, which moderates it temperature. The hourly values of relative humidity among the three stations are also similar, however, the measurements taken at the test building are more in line with the measurements taken at Pitt Meadows.

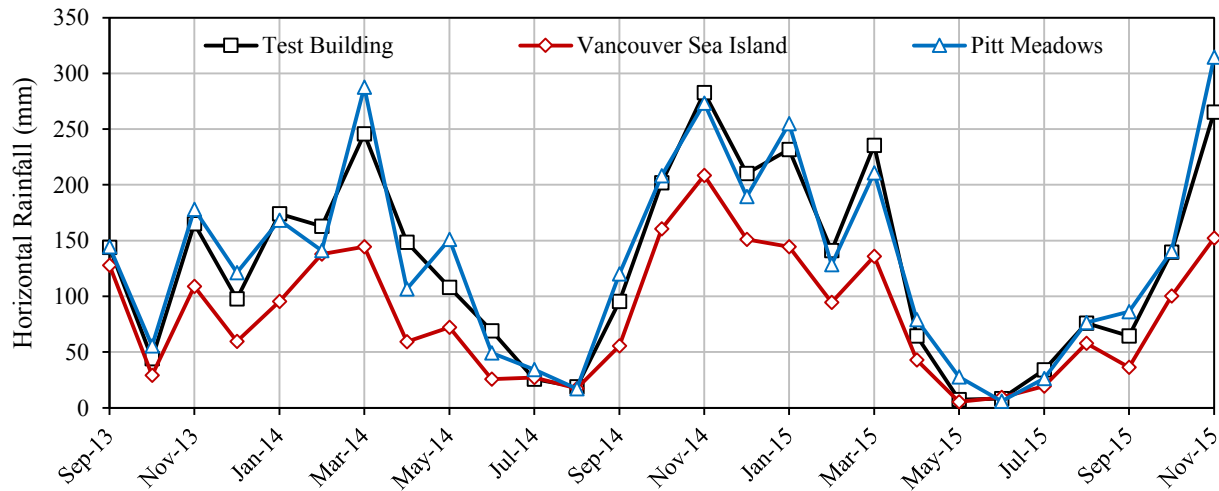


Figure 3.19 – Monthly horizontal rainfall for the test building, Vancouver Sea Island and Pitt Meadows.

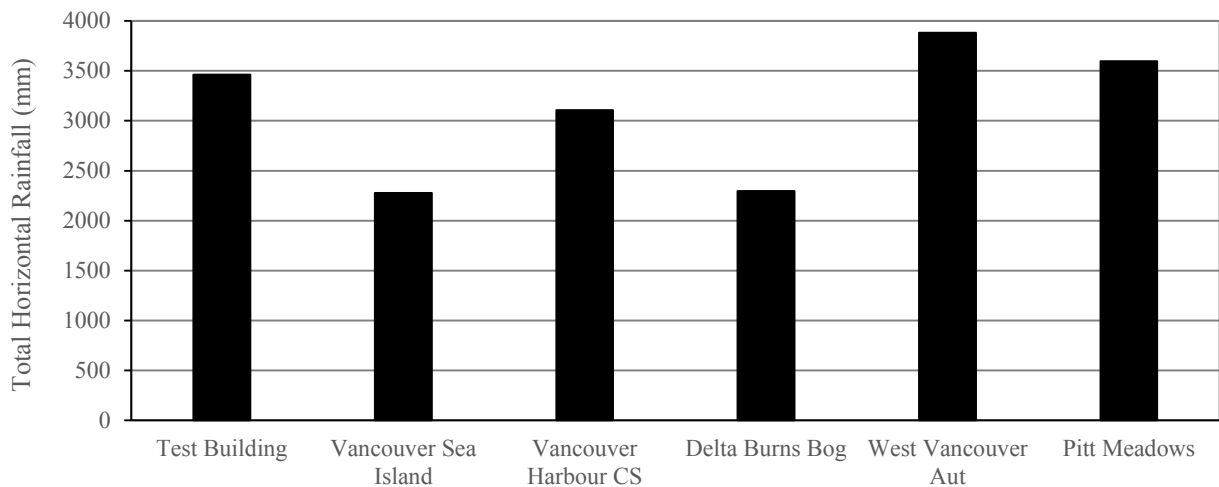


Figure 3.20 – Total horizontal rainfall at the test building and surrounding stations in the Greater Vancouver region.

3.3.1.2. Wind Tunnel Measurements

Wind tunnel measurements have been conducted in Concordia's atmospheric boundary layer (ABL) wind tunnel. To model the field, a suburban exposure has been created using roughness elements and a scaled down test building and its surrounding buildings have been placed in the wind tunnel. The purpose of the wind tunnel measurements is to: (1) verify the wind profile, (2) verify the terrain roughness, (3) confirm that the wind speed measured at the test building roof top can be accurately converted using the power law and (4) provide additional data useful for validation of CFD modeling.

To investigate the influence of the test building's surroundings on the wind flow near the test building, measurements have been conducted for a stand-alone test building and for a test building with surroundings. For both cases, velocity measurements have been carried out for the following approaching wind angles: (1) 0° (normal to the facade), (2) 45° (from the north-east and south-east).

3.3.1.2.1. Wind Profile

The characteristics of the wind profile were determined by taking measurements along the vertical axis in the center of the turntable with no model(s) present. The velocities were normalized by simply dividing the mean velocities measured (\bar{U}) by the mean gradient velocity (\bar{U}_g) measured, as follows:

$$\text{Normalized Velocity} = \frac{\bar{U}}{\bar{U}_g} \quad (3.1)$$

The following suburban wind profile characteristics were generated in the wind tunnel:

- 1) Gradient height (Z_g) = 80 cm
- 2) Gradient wind speed (U_g) = 14.4 m/s
- 3) Mean speed exponent (α) = 0.22

The normalized mean velocities and turbulence intensities measured in the wind tunnel for the suburban configuration are shown in Figure 3.21. The mean speed exponent of 0.22 obtained in the wind tunnel is very close to the 0.25 value assigned to the field building and is used.

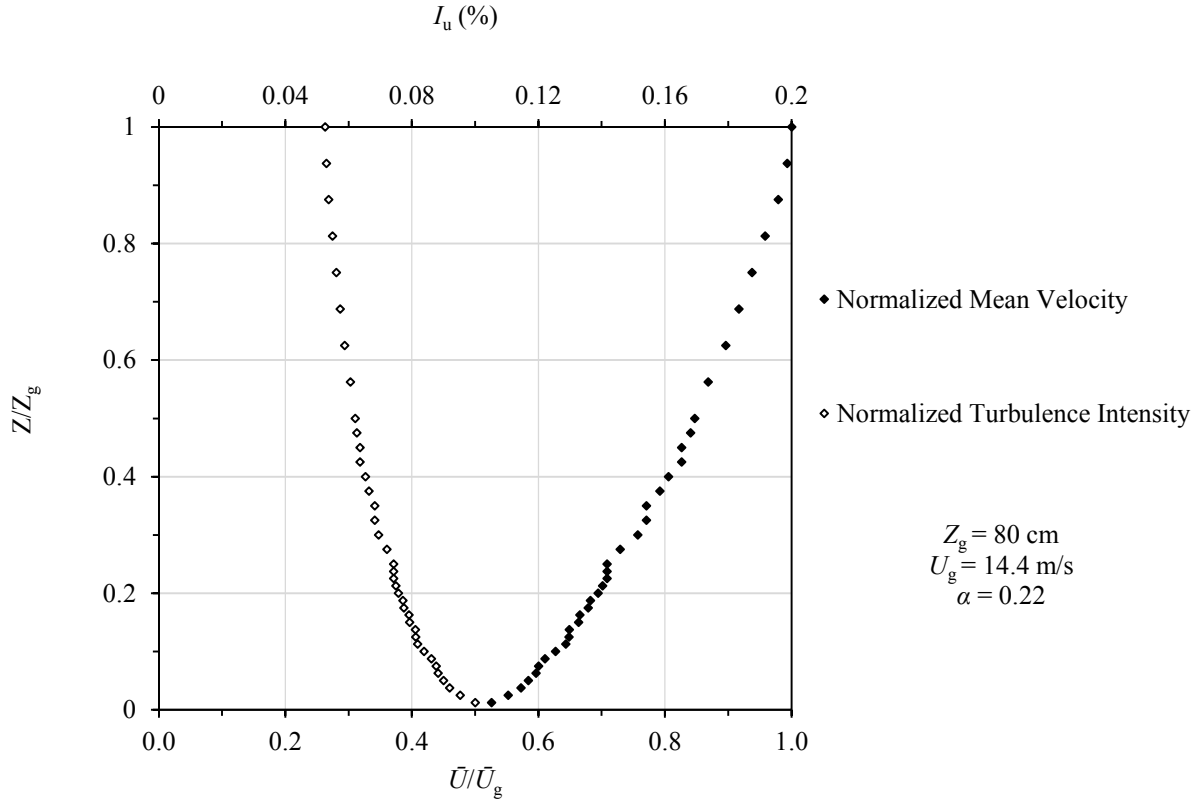


Figure 3.21 – Normalized mean velocity and turbulence intensity for a suburban exposure measured in the boundary layer wind tunnel.

3.3.1.2.2. Wind Monitor

Once a suburban wind profile was successfully modeled in the wind tunnel, the building model(s) were placed in the wind tunnel and tested. To verify the wind profile and the terrain roughness, the wind tunnel measurements were compared to the field measurements. In order to do this, the normalized velocities measured by the wind monitor in the field were compared to the normalized velocities measured at the wind monitor location in the wind tunnel. This is simply the average velocity measured at the wind monitor location divided by the mean gradient velocity using equation 3.1.

In the field, the velocities measured by wind monitor were divided by gradient velocities obtained from two nearby airport weather stations: Pitt Meadows and Vancouver Sea Island. Hourly records with the highest wind speeds and the most similar wind directions between the test building and the airport stations were selected. Since the prevailing wind direction at the test building is from the east and south-east, it was possible to find records that fit the following hourly wind parameters:

- 1) $U_{\text{ref}} > 5 \text{ m/s}$ and $\theta = 90 \pm 10^\circ$ for winds coming from the *east* (90°).
- 2) $U_{\text{ref}} > 5 \text{ m/s}$ and $\theta = 135 \pm 10^\circ$ for winds coming from the *south-east* (135°).

The hourly data meeting the above criteria were verified to have relatively stable wind with small fluctuations of wind speed and direction within the hour by analyzing the five-minute data. Figure 3.22 shows a five-minute data record measured at the test building. The wind speed fluctuates from just over 4 m/s to just under 8 m/s within the hour with a mean wind speed of 5.8 m/s. The wind direction is fairly constant with an average of 97° and a standard deviation of only 6° .

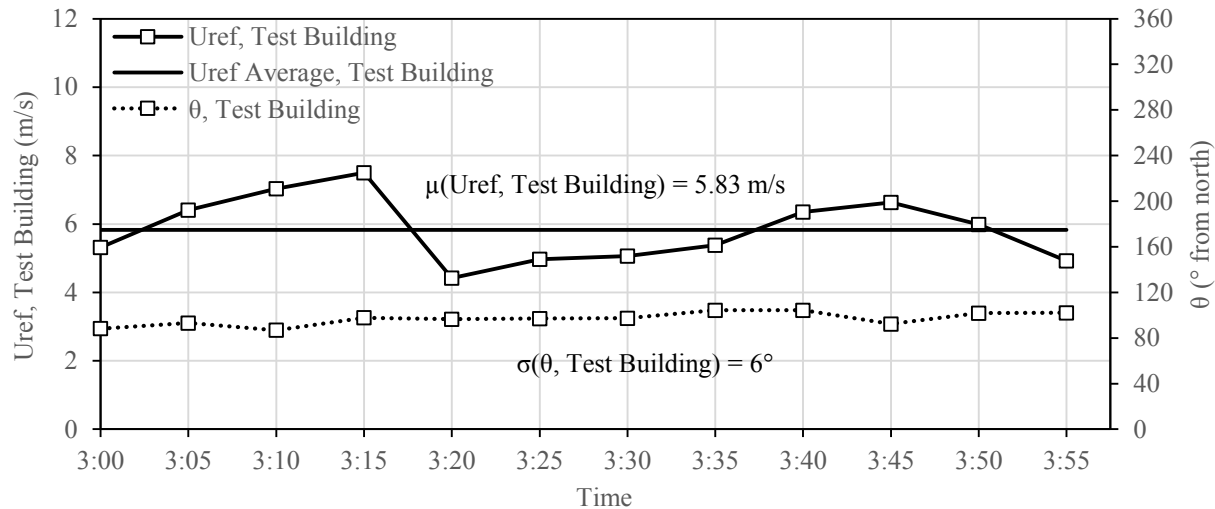


Figure 3.22 – Five-minute data record for 1-hour.

In order to perform a direct comparison between the field data and the wind tunnel data, the wind tunnel model was subjected to wind blowing from the *east* (90°) and from the *south-east* (135°). Figure 3.23 compares the normalized velocities at the wind monitor location between the wind tunnel and the field, when placing a *stand-alone test building* in the wind tunnel. Figure 3.23a is

the result of using the gradient wind speed from Pitt Meadows, while Figure 3.23b is the result of using the gradient wind speed from Vancouver Sea Island. There is a good agreement between the wind tunnel and field measurements for both easterly and south-easterly winds when using Pitt Meadows as a reference station (Figure 3.23a). The same could be said when using Vancouver Sea Island as a reference station (Figure 3.23b), however, the normalized velocity for easterly winds in the field are somewhat lower than that measured in the wind tunnel.

Figure 3.24 compares the normalized velocities at the wind monitor location between the wind tunnel and the field, when placing the *test building with its surroundings* in the wind tunnel. Figure 3.24a is the result of using the gradient wind speed from Pitt Meadows, while Figure 3.24b is the result of using the gradient wind speed from Vancouver Sea Island. There is a good agreement between the wind tunnel and field measurements for both easterly and south-easterly winds when using Pitt Meadows and Vancouver Sea Island as reference stations. As expected, the case with surroundings is a better representation of the field than the stand-alone case.

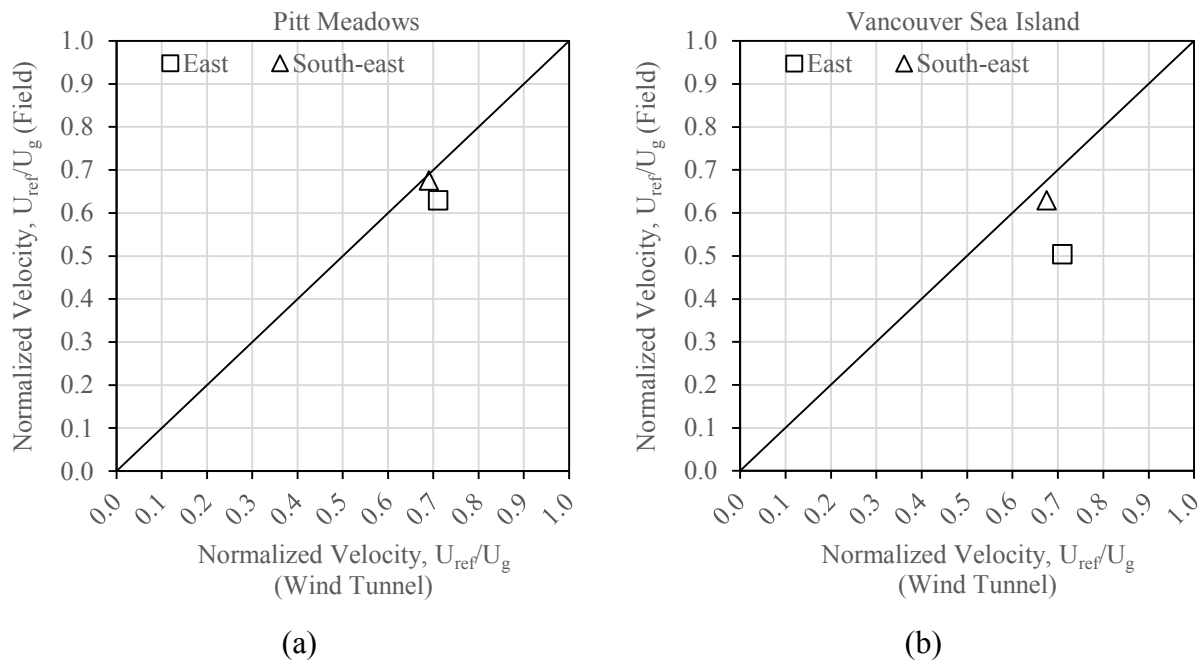


Figure 3.23 – Comparison of the normalized velocity at the wind monitor location in the wind tunnel vs. in the field (Stand-alone test building); for the directions: $\theta=0^\circ$ (East) and $\theta=135^\circ$ (South-east).

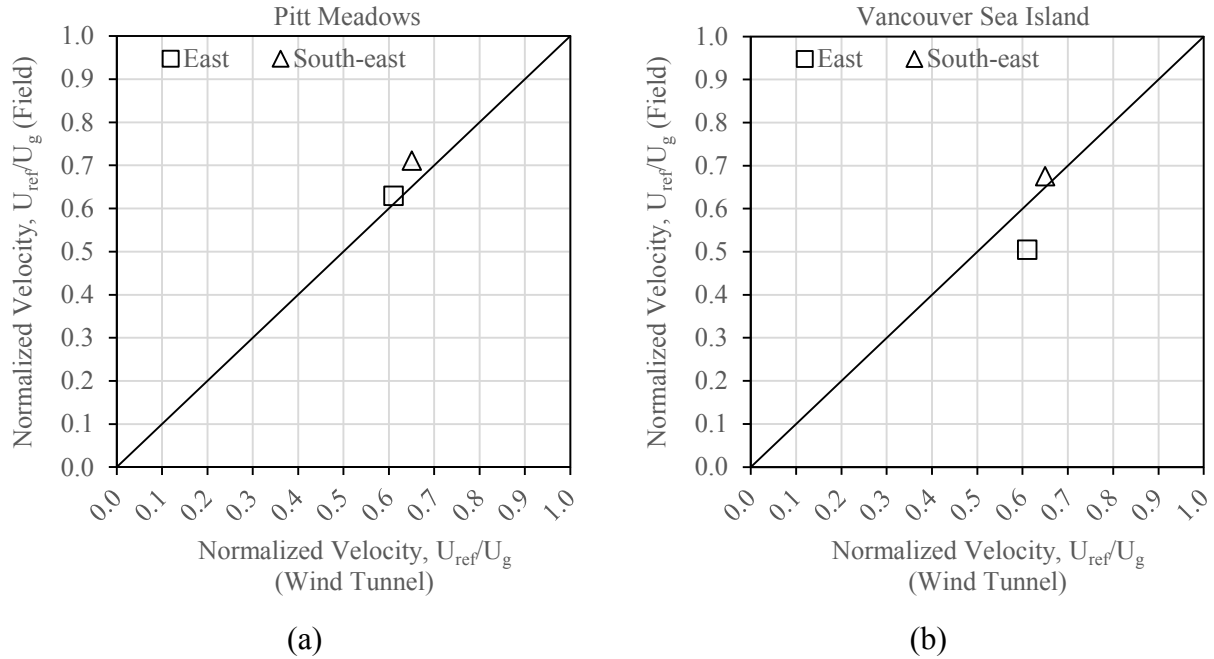


Figure 3.24 – Comparison of the normalized velocity at the wind monitor location in the wind tunnel vs. in the field (Test building with surroundings); for the directions: $\theta=0^\circ$ (East) and $\theta=135^\circ$ (South-east).

3.3.1.2.3. Building Facades

Once the field data and the wind tunnel data were shown to be in good agreement, the velocities near the building facades were conducted. The normalized velocities near the east and north building facades have been measured and are discussed in Section 4.1.2.

3.3.2. On-Site Weather Conditions

Historical weather analysis on the test building has shown that the prevailing wind direction is from the east during rain hours. This, in combination with the fact that the orientation of the building is in line with the cardinal wind directions, provides a good opportunity to study the spatial distribution of WDR and the effectiveness of overhang, especially on the east facade.

To show the consistency of wind speed, wind direction and rainfall experienced at the test site, the on-site weather conditions are separated based on their monitoring period and compared. There are three monitoring periods: (1) No overhang, (2) 0.6 m overhang and (3) 1.2 m overhang. The field measurements started on August 16th, 2013 and ended on December 2nd, 2015.

The results and discussion for the above comparison are presented in Section 4.2.

3.3.3. Airfield Driving Rain Index

The airfield driving rain index (R_{airfield}) expresses the amount of rain incident on an imaginary unobstructed wall surface and is a relative indicator of the severity of a specific wall orientation to the wind-driven rain exposure. The airfield driving rain index may be calculated using ISO 15927-3, 2009, as follows:

$$R_{\text{airfield}} = \frac{2}{9} \sum U \cdot R_h^{\frac{8}{9}} \cdot \cos (\theta - \Theta) \quad (3.2)$$

where U is the hourly wind speed measured by the wind monitor (m/s), R_h is the rainfall intensity (mm/hr), θ is the wind direction relative to the north ($^\circ$), and Θ is the wall orientation relative to the north ($^\circ$).

To convert the wind speed measured at the wind monitor to any given height, the following equation provided by the National Building Code of Canada (NBCC, 2010) is used:

$$U(Z) = U_{10} \times \left(\frac{Z}{10} \right)^\alpha \quad (3.3)$$

where U_{10} is the wind speed 10 m above grade, which is what is typically used by weather stations in Canada, Z is the height above grade, and α is the mean speed exponent.

Using equations 3.2 and 3.3, the airfield driving rain indices are calculated at the height of each rain gauge on the east and north facades. The five-minute data for wind speed, wind direction, and rainfall intensity registered by the data logger have been arithmetically averaged to hourly data and the summation has been taken over all hourly intervals when $\cos (\theta - \Theta)$ is positive (periods when the wind is causing flux through the imaginary wall of interest).

The results and discussion of the airfield driving rain indices are presented in Section 4.3.

3.3.4. Spatial Distribution of Wind-Driven Rain on the Building Facade

The spatial distribution of WDR is reported for the three monitoring periods (no overhang, 0.6 m overhang and 1.2 m overhang) and for each individual rain event in Section 3.3.4.1. The associated errors with WDR experiments using WDR gauges are discussed in Section 3.3.4.2. The spatial distribution of WDR on the building facades is determined as catch ratios and wall factors. The catch ratio is discussed in Section 3.3.4.3, while the wall factor is discussed in Section 3.3.4.4. A wall index, which is the amount of rain that would impact a real wall, obtained by multiplying the airfield driving rain index by several correction factors is introduced in Section 3.3.5.

3.3.4.1. Definition of a Rain Spell

The nature of a “spell” of driving rain as defined by ISO 15927-3 (2009) as a period of driving rain during which the risk of penetration through masonry increases (i.e. a period in which the input of water due to the driving rain exceeds the loss due to evaporation). Generally, spells are periods of one to two hours during a shower and eight to twelve hours during the passage of a depression. However, sometimes there are long spells when successive depressions cause repeated periods of rain with little or no net evaporation in between (such as in Vancouver, British Columbia). Thus, there can be periods of as long as 96 consecutive hours with no driving rain within the spell before evaporative loss exceeds gain from the rain. A gap between two spells is, therefore, defined by a period of at least 96 hours when:

$$U \cdot R_h^{\frac{8}{9}} \cdot \cos(\theta - \Theta) \leq 0 \quad (3.4)$$

where U , θ , and R_h , are the hourly wind speeds, wind directions relative to the north, and rainfall intensities, respectively, and Θ is the wall orientation relative to the north.

The term rain spell will now be referred to as a rain event from here on in. For the application of the present thesis, rain events will be separated if there is a continuous period of no rain lasting more than 96 hours. A total of twenty-three rain events have been selected and are tabulated in Table A.4 in APPENDIX A.

3.3.4.2. Error Analysis

An adequate measurement of WDR should be accompanied by their associated error estimates including: (1) adhesion water evaporation, (2) evaporative losses from the reservoir, (3) splashing of drops from the collection area, (4) condensation on the collection area and (5) wind error. The use of a tipping-bucket mechanism introduces two additional errors: (1) the error caused by the rest water that remains in the bucket at the end of a spell and (2) the error due to loss of incoming water running by and not collected by the bucket due to its brief vertical position during the tip.

1) Adhesion Water Evaporation (E_{AW})

The experimental method of quantifying the errors associated with adhesion water evaporation has been outlined by Blocken & Carmeliet (2006a). To determine the quantity of adhesion water present on a vertical collection area, the plate should be subjected to a predefined amount of “spraying cycles.” In each cycle, spraying occurs until a significant amount of runoff has been collected. After each cycle, the plate is weighed and the mass of adhesion water is registered.

The WDR gauges used in the present study have been tested by Osorio (2013a, 2013b) to determine the average adhesion water on the collection area. The spraying tests were similar to the method mentioned above: (1) the gauge was subjected to 20 spraying cycles, (2) in each cycle, the sample was sprayed at six spots to cover the entire area and the spraying went on until a significant amount of runoff was collected and (3) the plate was then weighed and the mass of adhesion water was calculated. Tap water was used in this experiment.

The average adhesion water measured on the collection area was 4.7 grams, which in relation to its 930.3 cm² area is 0.050 mm. As in the procedure suggested by Blocken & Carmeliet (2006a), total adhesion water evaporation will be assumed to occur when it does not rain for one hour. Therefore, rain events with a large amount of WDR will be selected to reduce the relative error due to adhesion water evaporation.

2) Evaporative Losses from the Reservoir or Tipping Bucket (E_{EVAP})

Evaporative losses from the tipping bucket are losses due to the evaporation of water in the bucket every hour within the rain event. In an analysis conducted by Osorio (2013a), evaporation

from the bucket was small for all rain gauges and rain events. It never accounted for more than 1% of the total relative error, thus, this error is deemed to be negligible.

3 & 4) Rest Water Evaporation (E_{RW}) and Loss of Incoming Water During a Tip (E_{TIP})

The use of a tipping-bucket mechanism introduces two additional errors which must be taken into account: (1) the error caused by the rest water that remains in the bucket at the end of a spell (which eventually evaporates) and (2) the error due to loss of incoming water running by and not collected by the bucket due to its brief vertical position during the tip. The tipping bucket mechanism enclosed within the WDR gauge is shown in Figure 3.25. Water is guided down a drainage hole and fills one of the buckets until it reaches a threshold value. Once this value is reached, the bucket tips and the tip is registered by the data logger. The other bucket then starts to fill with water.

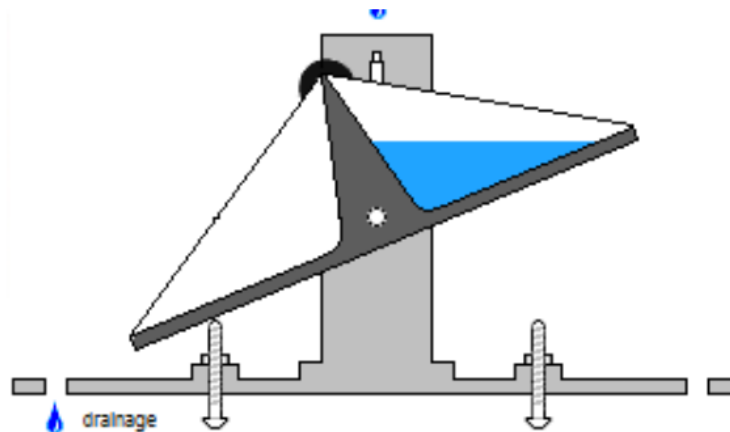


Figure 3.25 – Sketch of the tipping bucket mechanism used to measure the collected rainwater by the WDR gauges (from Osorio, 2013a).

The two errors associated with the tipping bucket mechanism have been tested by Osorio (2013a, 2013b). To determine the maximum amount of rest water that can be present in the bucket, the gauges were subjected to 10 “pouring cycles” using a syringe. In each pouring cycle, a consistent rate of pour and distance of pour was performed until a tip was registered. The syringe was then weighed and the mass of rest water was calculated based on the difference between the mass of the full syringe to that of the emptied syringe. Tap water was used for this experiment.

The average value of rest water (E_{RW}) in the tipping bucket was 5.5 g, which is equivalent to 0.060 mm. The loss of incoming water during a tip (E_{TIP}) was determined from measurement observations and deemed negligible due to the WDR gauge's two bucket design.

5) Splashing of Drops from the Collection Area

Splashing of raindrops mainly occurs during heavy rainfalls with a co-occurrence of high wind speed ($U_{10} = 10$ m/s) and sufficiently large raindrops. Thus, errors caused by splashing may be mitigated by selecting rain events whereby splashing errors will be small or absent. Rain events with wind speeds (U_{10}) of less than 10 m/s and rainfall intensities (R_h) of less than 20 mm/hr should be selected. Given the low wind speeds and low rainfall intensity recorded, this error is considered negligible.

6) Condensation on the Collection Area (E_{UC})

As mentioned in Section 2.5, condensation errors are considered to be small with the typical condensation on a vertical surface on a clear night to be in the order of a few tenths of a millimeter. Osorio (2013a) found that for the aluminum plate type gauges used in the present study, condensation is generally non-existent for all of the gauges analyzed, thus, condensation errors will be deemed negligible.

6) Wind Errors

Wind errors are expected to be lower when the wind is blowing perpendicular to the facade. The potential for wind errors increases for sharp wind angles, as higher wind speeds occur near the surface, which interacts with the rim of the WDR gauge causing errors. Hence, errors due to wind will be lessened by selecting rain events for which the wind direction during rain is approximately perpendicular to the facade. Furthermore, the WDR gauges used have a shallow collection plate, which minimizes wind errors. Given the low profile of the rim of the WDR gauges used, the low wind speed and mostly perpendicular wind direction to the facade, this error is considered negligible.

Total Error

A conservative estimate of the total absolute errors in the WDR measurement at the end of a rain event is made by combining all errors (Osorio, 2013a; Nore et al., 2007), so that:

$$E_{TOT} = E_{AW} + \sum E_{EVAP} + \sum E_{UC} + S_{wdr} \left(\frac{E_{RW} + nE_{TIP}}{nV_{BOWL}} \right) \quad (3.5)$$

where, E_{AW} is the adhesion water evaporation error during and at the end of the rain event (mm) assuming the worst case scenario (complete evaporation of adhesion water after every break or dry period in the rain event), E_{EVAP} is the hourly evaporation error from the tipping bucket at every hour in the rain event (mm), E_{UC} is the hourly condensation error at every hour in the rain event (mm), E_{RW} is the rest water error (g), E_{TIP} is the collection loss during every tip (g), n is the amount of tips during the rain event, V_{BOWL} is the content of the bowls (g) and S_{wdr} is the total accumulated WDR for the rain event (mm).

Adhesion water evaporation (E_{AW}) is determined by multiplying the adhesion water for a single occurrence by the number of interruptions of the rainfall by dry periods, so that:

$$E_{AW} = AW \times \text{Number of interruptions} \quad (3.6)$$

Based on the conclusions made by Osorio (2013a), E_{EVAP} , E_{UC} , and E_{TIP} are considered negligible and are omitted, simplifying equation 3.5 to:

$$E_{TOT} = E_{AW} + E_{RW} \quad (3.7)$$

Finally, the relative error associated with the WDR measurement with a wall mounted WDR gauge can be expressed as:

$$e_{TOT} = \frac{E_{TOT}}{S_{wdr}} \quad (3.8)$$

An example of error analysis will be provided in Section 4.6 together with the measurement results for rain event 7. The relative errors for each rain event are tabulated in Table A.5 and Table A.6 in APPENDIX A for the east and north facades, respectively.

3.3.4.3. Catch Ratio

The catch ratio (η) is the total amount of WDR collected on a wall surface divided by the total amount of horizontal rainfall over the same time period, so that:

$$\text{Catch Ratio } (\eta) = \frac{S_{\text{wdr}}}{S_h} \quad (3.9)$$

where S_{wdr} is the total accumulated WDR amount (mm) and S_h is the total accumulated horizontal rainfall amount (mm).

The analysis includes:

- 1) Catch ratios plotted on the east and north facades for the monitoring periods with: (1) no overhang, (2) a 0.6 m overhang and (3) a 1.2 m overhang to show the spatial distribution of WDR across the building facades.
- 2) The relationship between catch ratio with wind speed and direction given that the spatial distribution of WDR is significantly influenced by the wind speed and direction.

The results for catch ratio analysis are presented in Section 4.4.1.

3.3.4.4. Wall Factor

The actual WDR rain received on a building surface at a specific location is influenced by the airflow along the building surface(s), which is a product of the wind and building interaction. As outlined in ISO 15927-3 (2009), the airfield driving rain indices (R_{airfield}) can be converted to wall indices (I_{WS}) – which is the amount of rain that would impact a real wall – by multiplying the airfield driving rain indices by several factors, as follows:

$$I_{\text{WS}} = R_{\text{airfield}} \cdot C_R \cdot C_T \cdot O \cdot W \quad (3.10)$$

where C_R is the roughness coefficient which accounts for the variability of mean wind speed due to the height above ground and the upstream roughness of the terrain, C_T is the topography coefficient which accounts for the increase in mean wind speed over hills and escarpments, O is the obstruction factor which accounts for nearby obstacles that are of equal or greater height to the building and W is the wall factor which considers the effect the building geometry and building details have on the WDR load. The amount of WDR varies significantly over the surface of a wall due to the flow of air around edges, corners, over the roof, etc. (International Standard Organization (ISO), 2009).

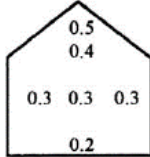
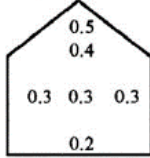
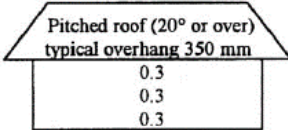
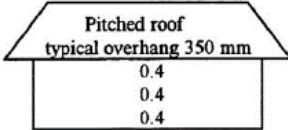
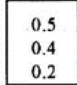
Since the on-site meteorological data (i.e. wind speed, wind direction, horizontal rainfall, WDR) are available at the test building, the roughness factor (C_R), topography factor (C_T), and obstruction factor (O) can be set equal to 1. Thus, the wall factor becomes the quantity of measured WDR divided by the airfield driving rain index. Equation 3.10 then becomes:

$$W = \frac{S_{\text{wdr}}}{R_{\text{airfield}}} = \frac{S_{\text{wdr}}}{\frac{2}{9} \cdot U \cdot R_h^{8/9} \cdot \cos(\theta - 90^\circ)} \quad (3.11)$$

where S_{wdr} is the total accumulated WDR amount (mm) and R_{airfield} is the amount of rain incident on an imaginary unobstructed wall surface calculated from equation 3.2.

ISO 15927-3 (2009) suggests several wall factors for different building configurations (i.e. height, type of roof, roof overhang) as shown in Table 3.2. These wall factors are based on long-term field measurements and do not take in account the specific wind and rain conditions. For a six-storey building with a flat roof (as the one considered in this thesis), a “Multi-storey flat roof” would be selected. For this type of building, a wall factor of 0.5 is assigned to the top 2.5 m of the facade, while the remainder of the facade is assigned with a wall factor of 0.2. It is noted that these are general and conservative values of wall factors for this particular type of building since there is no variation across the building facade nor does it take into consideration the orientation of the building, assuming all the facades of the building have the same wall factor values assigned.

Table 3.2 – Wall Factor, W provided by the International Organization for Standardization to take into account different building configurations (height, type of roof, roof overhangs) (from ISO 15927-3 2009).

Description of wall	Average value	Distribution
Two storey gable	0.4	
Three storey gable	0.3	
Multi storey flat roof	0.2 for e.g. ten storey, but higher intensity at top	0.5 for top 2.5 m 0.2 for remainder
two storey eaves wall	0.3	
three storey eaves wall	0.4	
two storey flat roof (pitch <20°)	0.4	

The analysis includes:

- 1) Wall factors plotted on the east and north facades for each monitoring period to show the spatial distribution of WDR and the influence of building geometry on the WDR load.
- 2) Comparison of measured wall factors to the wall factors suggested by the ISO standard.

The results for wall factor analysis are presented in Section 4.4.2.

3.3.5. Wall Index

As discussed in Section 3.3.4.4, the wall index (I_{WS}) is the amount of rain that would impact a real wall by multiplying the airfield driving rain indices ($R_{airfield}$) by a number of correction factors – see equation 3.10.

Meteorological data is typically not available at the building site, therefore, data from the closest weather station is normally used. The terrain roughness coefficient (C_R) and the topography coefficient (C_T) are used to convert the mean wind speed measured at the weather station to the building site at the building height of interest. The obstruction factor (O) takes into account the sheltering effect provided by the obstacles nearby, while wall factors (W) describes the spatial distribution of WDR on the building facade(s) as a result of the complex interaction between the wind flow and the building. The airfield driving rain indices ($R_{airfield}$) have been calculated using meteorological data from Vancouver Sea Island station (i.e. wind speed and wind direction), next to Vancouver International Airport, using equation 3.2. Since, hourly rainfall is not recorded at typical weather stations, the hourly rainfall measured at the test building is used. The determination of terrain roughness coefficient (C_R), topography coefficient (C_T), obstruction factor (O) and wall factor (W), are discussed below.

Roughness Coefficient (C_R)

The roughness coefficient accounts for the variability of mean wind velocity due to the height above ground and the upstream roughness of the terrain. Using the procedure outlined in ISO 15927 (2009), the roughness coefficient at height z is given by equations 3.12 and 3.13.

$$C_R(Z) = K_R \ln \left(\frac{Z}{Z_0} \right) \quad \text{for} \quad Z \geq Z_{min} \quad (3.12)$$

$$C_R(Z) = C_R(Z_{min}) \quad \text{for} \quad Z < Z_{min} \quad (3.13)$$

The parameters above depend on the terrain category given in Table 1 of ISO 15927 (2009). Since the terrain category for the test building is suburban and the height (Z) of each gauge is greater than 8 m (Z_{min}), equation 3.12 is used to calculate the roughness coefficient at the height of each gauge.

Topography Coefficient (C_T)

The topography coefficient (C_T) accounts for the increase of mean wind speed over isolated hills and escarpments. The procedure outlined in the ISO 15927-3, 2009 suggests including C_T for locations (1) more than half-way up the slope of the hill and (2) within 1.5 times the height of the cliff from the base of a cliff. It is defined as follows:

$$C_T = 1 \quad \text{for} \quad \phi < 0.05 \quad (3.14)$$

$$C_T = 1 + 2s\phi \quad \text{for} \quad 0.05 \leq \phi < 0.3 \quad (3.15)$$

$$C_T = 1 + 0.6s \quad \text{for} \quad \phi < 0.3 \quad (3.16)$$

where s is a factor obtained from Figure 2 and 3 in the ISO 15927-3, 2009 and ϕ is the upwind slope (H/L_u).

Obstruction Factor (O)

The obstruction factor (O) accounts for nearby obstacles that are of equal or greater height to the building. Table 3 in ISO 15927 (2009) suggests an obstruction factor of 1.0 if the distance of the obstruction to the wall is over 120 m, which is the case for the test building since it is the tallest building in its approximate area. There are a number of trees about 10 m away from the east facade, however, they are shorter than the building and are bare of leaves during the winter, which is the season that receives the majority of rainfall in the area.

The Wall Factor (W)

The wall factor (W) accounts for the building geometry and the building details on the WDR load. As mentioned earlier, the ISO suggests wall factors depending on the building configuration shown in Table 3.2.

The wall index analysis includes:

- 1) Wall indices calculated on the east and north facade for each monitoring period.

- 2) The actual measured WDR at each gauge location compared to: (1) the wall indices using the measured wall factors and (2) the wall indices using the ISO suggested wall factors.

The wall indices are presented and discussed in Section 4.5

3.4. Effectiveness of Overhang

To assess the effectiveness of overhang with two different widths (0.6 m and 1.2 m), the percent reduction of WDR, in terms of catch ratios, is used. The overhang effectiveness is assessed by:

- 1) Comparing similar rain events.
- 2) Using a symmetrical WDR deposition pattern on the building facade.

3.4.1. Similarity

The overhang effectiveness can be assessed by choosing rain events with similar meteorological characteristics (wind speed, wind direction and horizontal rainfall intensity) and comparing the catch ratios on the gauges that are directly under the overhang (gauges EN1 to EN9), in one rain event, with the same gauges (with the overhang completely retracted), in a different but similar rain event.

In order to determine if a rain event is similar to another rain event, both rain events should have similar meteorological characteristics, ultimately leading to similar catch ratios on the gauges that are not influenced by the overhang. For instance, when considering the east facade, the catch ratios on the gauges ES1 to ES7 and EC1 & EC2 (in the case without overhang), should be similar to the catch ratios on the same gauges (in the case with overhang) if the meteorological characteristics are similar between the two rain events. Once this similarity has been established, the catch ratios on gauges EN1 to EN9 in the case without overhang may be compared to the same gauges in the case with overhang.

3.4.2. Symmetry

In order for a symmetrical WDR deposition pattern on the building facade to exist, the prevailing wind direction must be blowing approximately perpendicular to the facade. Since the prevailing wind direction is predominantly from the east during rain hours, it is quite easy to find rain events to meet this criteria.

The effectiveness of overhang can then be assessed by comparing gauges EN1 to EN7 (under the overhang) to gauges ES1 to ES7 (no overhang above it). This comparison is possible because the predominant wind direction is from the east during rain hours, which creates a symmetrical WDR distribution across the east facade.

The effectiveness of overhang has been assessed for the two cases: (1) 0.6 m overhang and (2) 1.2 m overhang by:

- 1) Comparing similar rain events on the east and north facades.
- 2) Assuming a symmetrical WDR deposition pattern on the east facade.

In addition, the overhang effectiveness, with respect to wind speed and wind direction, has been investigated to determine the influence of these meteorological parameters.

The effectiveness of overhang is presented and discussed in Section 4.6.

CHAPTER 4: RESULTS AND DISCUSSION

4.1. On-Site Weather Comparisons

4.1.1. Surrounding Weather Stations

The comparison between on-site weather data with data recorded at nearby weather stations confirms the reliability of on-site weather data measurements. The following observations are made:

- 1) The on-site measured meteorological data of wind speed and wind direction are reliable as they compare well with two nearby airport weather stations, especially Vancouver Sea Island station for wind speed and wind direction.
- 2) The suburban exposure assigned to the test building is reasonable, at least from the east, which is the predominant wind direction during rain hours at the test site.
- 3) The horizontal rainfall amount measured at the test building is in good agreement with two surrounding airport stations; the test building and Pitt Meadows receives almost the same amount of rain on a day to day basis. Vancouver Sea Island receives relatively less rain than the other two stations.
- 4) The temperature and relative humidity measured at the test building is also in good agreement with the airport weather stations.

4.1.2. Wind Tunnel Measurements

The normalized velocities at the wind monitor location and near the building facades, in the form of point measurements, are plotted in Figure B.1 to Figure B.5 in APPENDIX B. The normalized velocities near the east and north building facades, in the form of contour lines, for different approaching angles are shown in Figure 4.1 and Figure 4.2 for the *stand-alone test building* and Figure 4.3 to Figure 4.5 for the *test building with its surroundings*.

Stand-Alone Building, $\theta = 0^\circ$

The normalized velocity contours for the *stand-alone test building* with the wind approaching normal to the east facade (0°) are shown in Figure 4.1. Looking at the east facade (Figure 4.1a), several observations are made: (1) there is a symmetrical distribution of velocities across the facade, (2) the lowest velocities are encountered in the center of the facade and (3) the velocities

increase from the center of the facade to the top and side edges of the facade. Looking at the north facade (Figure 4.1b), the velocities are highest at the windward edge and decreases towards the leeward edge.

Stand-Alone Building, $\theta = 45^\circ$ (from North-East)

The normalized velocity contours for the *stand-alone test building* with the wind approaching the east facade from the north-east (45°) are shown in Figure 4.2. The velocities are smallest at the windward edge and increases towards the leeward edge of the east facade. The same phenomenon is observed on the north facade.

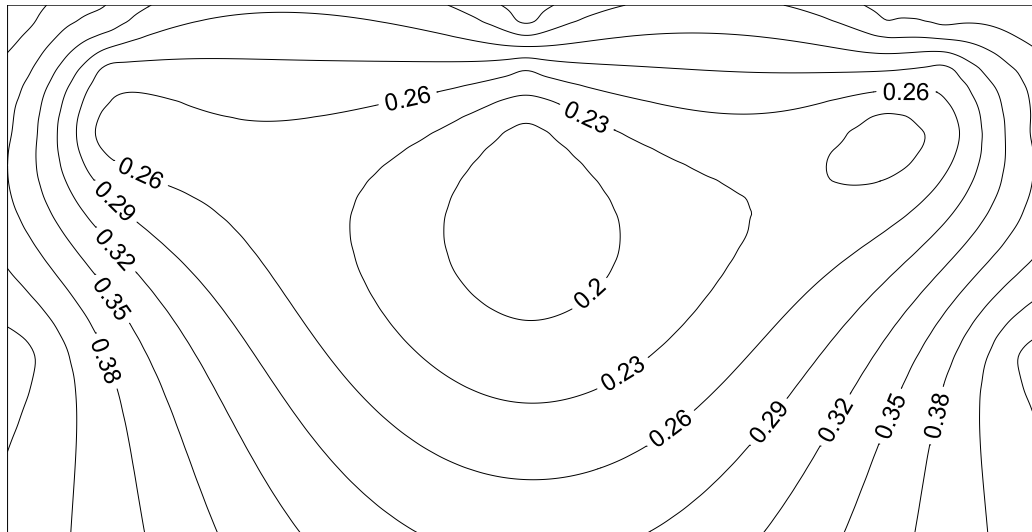
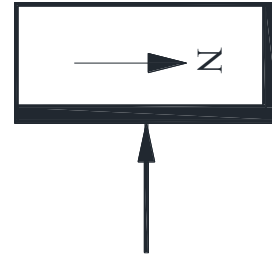
Building with Surroundings, $\theta = 0^\circ$

The normalized velocity contours for the *test building with its surroundings* with the wind approaching normal to the east facade (0°) are shown in Figure 4.3. The influence of the surroundings on the test building is evident. The added “roughness” reduces the relative speed on the east facade (Figure 4.3a), when compared the the east facade in the stand-alone model (Figure 4.1a). The velocities on the north facade (Figure 4.3b) are similar in pattern to the stand-alone model (Figure 4.1b). However, there is a marked increase in velocities encountered across the north facade for the case with surroundings.

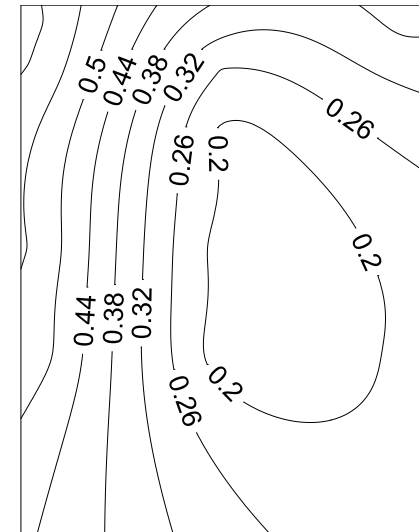
Building with Surroundings, $\theta = 45^\circ$ (from North-East and South-East)

The normalized velocity contours for the *test building with its surroundings* with the wind approaching the east facade from the north-east (45°) and south-east (45°) are shown in Figure 4.4 and Figure 4.5, respectively. For winds approaching from the north-east, the influence of the surrounding buildings on the east facade is apparent when comparing the stand-alone model (Figure 4.2a) with the model with surroundings (Figure 4.4a); the velocities are relatively lower when the surroundings are present. On the north facade, the velocities are similar for both the stand-alone building (Figure 4.2b) and the building with surroundings (Figure 4.4b), except near the top edge, where there is a drop in velocities for the case with surroundings. For winds approaching from the south-east, the influence of the surrounding buildings result in a unique wind distribution pattern across the east facade (Figure 4.5a).

Stand-Alone Building, $\theta = 0^\circ$

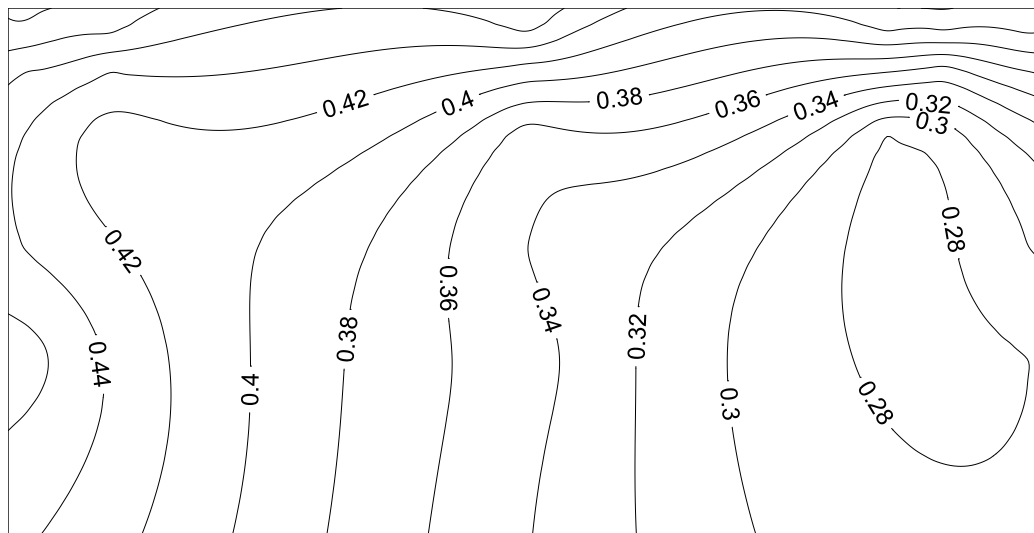


(a)



(b)

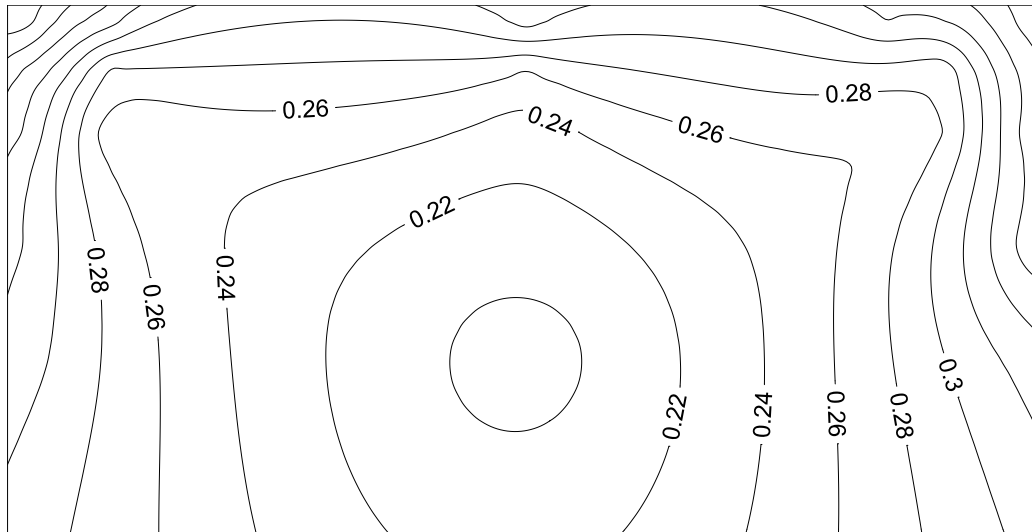
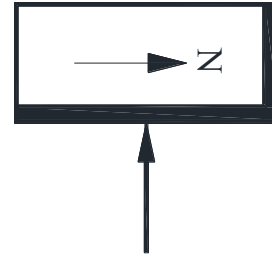
Figure 4.1 – Normalized velocities on the (a) East facade, (b) North facade
Stand-alone test building, $\theta = 0^\circ$.



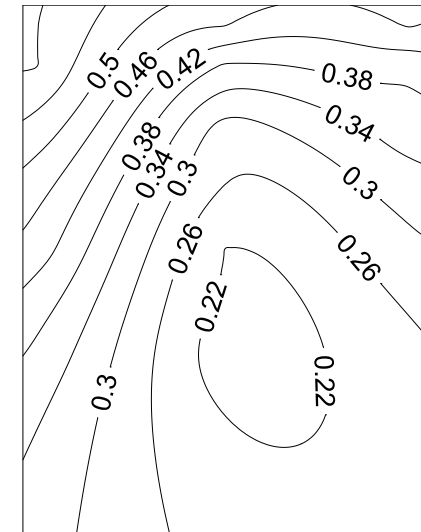
(b)

64

Building with Surroundings, $\theta = 0^\circ$



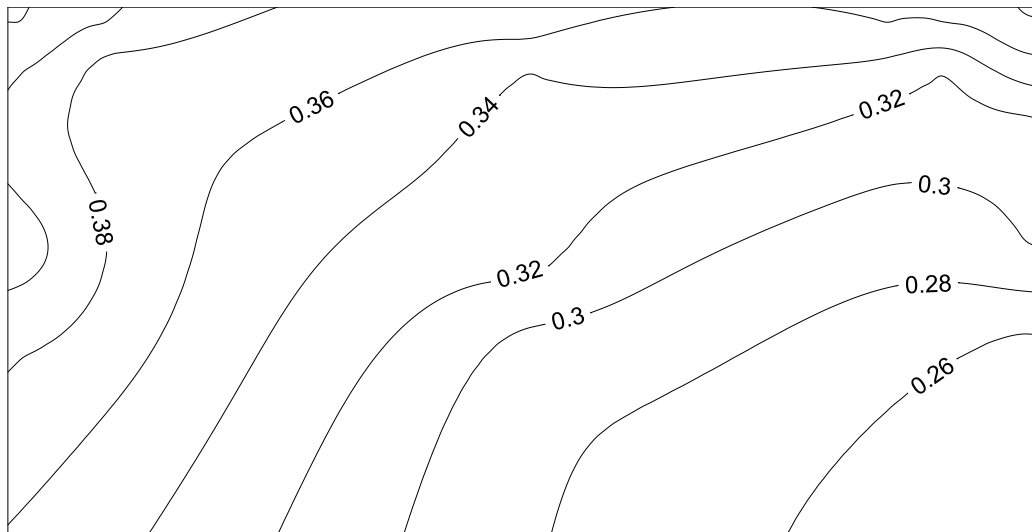
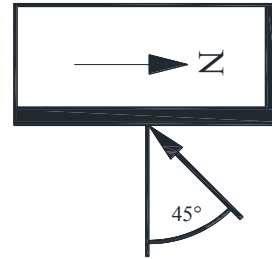
(a)



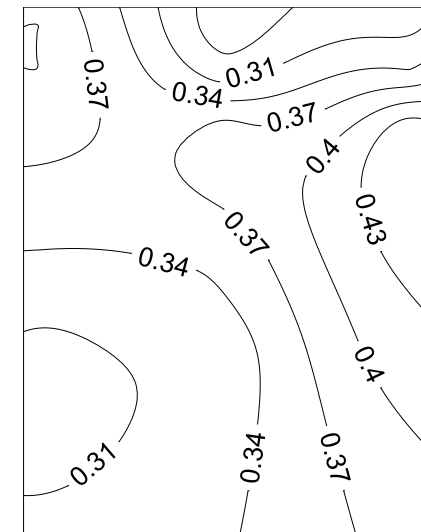
(b)

Figure 4.3 – Normalized velocities on the (a) East facade, (b) North facade
Test building with surrounding buildings, $\theta = 0^\circ$.

Building with Surroundings, $\theta = 45^\circ$ (from North-East)



(a)



(b)

Figure 4.4 – Normalized velocities on the (a) East facade, (b) North facade
Test building with surrounding buildings, $\theta = 45^\circ$ (from north-east).

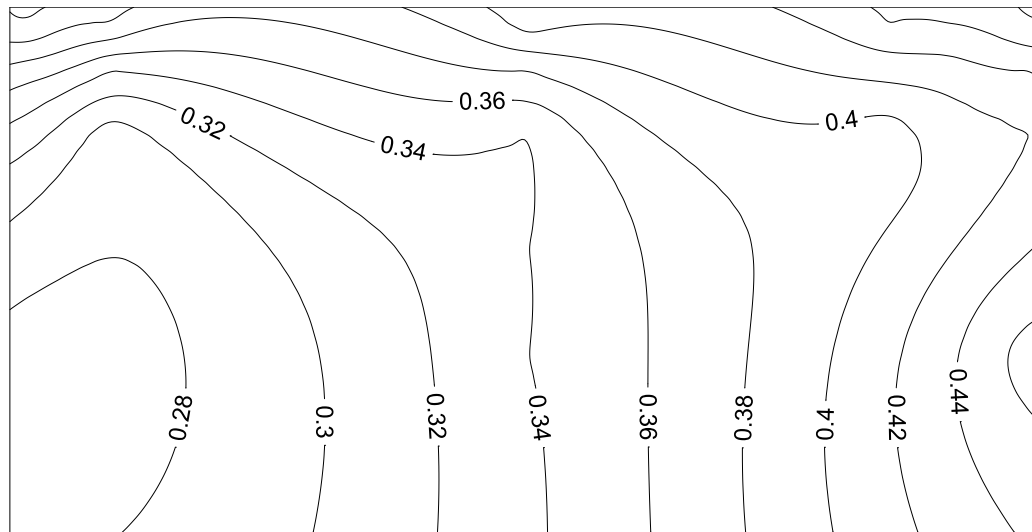


Figure 4.5 – Normalized velocities on the (a) East facade, (b) North facade
Test building with surrounding buildings, $\theta = 45^\circ$ (from north-east)

4.2. On-site Weather Conditions

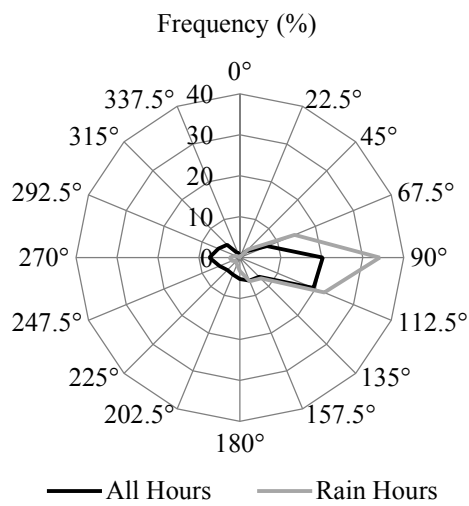
The on-site measurements began on August 16, 2013 and ended December 2, 2015. A sufficiently long period of measurements has been collected in order to obtain reliable and useful measurements. The measurements have been separated into three monitoring periods: (1) No overhang, (2) with a 0.6 m overhang and (3) with a 1.2 m overhang. A summary of the on-site weather conditions for the different monitoring periods is shown in Table B.1 in APPENDIX B.

4.2.1. Entire Monitoring Period

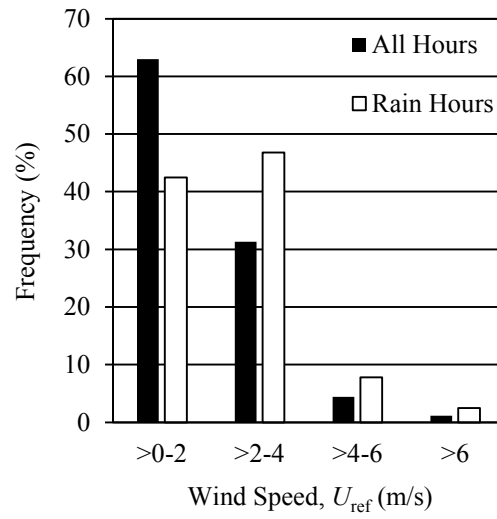
The wind and precipitation conditions at the test site for the entire monitoring period are shown in Figure 4.6a-c. The wind characteristics have been plotted for “all hours” and “rain hours”.

The prevailing wind direction for “all hours” and “rain hours” is from the east, however, the frequency of easterly winds increases significantly during rain hours, as seen in Figure 4.6a. There is also a noticeable increase in the frequency of higher wind speeds during “rain hours”. For “all hours”, the majority of wind speeds are in the range of 0 to 2 m/s; during rain hours the majority of wind speeds are in the range of 2 to 4 m/s. Wind speeds between 4 to 6 m/s are occasionally seen, most of them occurring during “rain hours” (~10%). The frequency of wind speeds greater than 6 m/s is low.

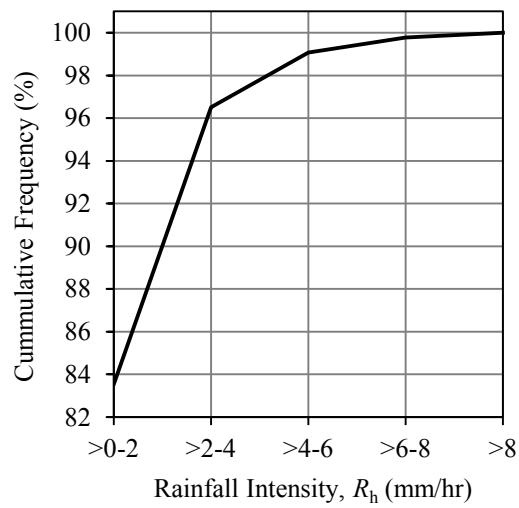
The rainfall intensity is mostly light to moderate, with a rainfall intensity of less than 2 mm/hr the majority of the time (84%), 2 to 4 mm/hr sometimes (~15%) and rarely over 4 mm/hr, as shown in Figure 4.6c. The total horizontal rainfall amount for the entire period is 3461 mm.



(a)



(b)



(c)

Figure 4.6 – (a) Wind direction frequency; (b) Wind speed frequency; and (c) Rainfall intensity cumulative frequency at the test building for the entire monitoring period (from August 16, 2013 to July 13, 2015).

4.2.2. Weather Conditions for Different Monitoring Periods

As mentioned earlier, one method to assess the effectiveness of overhang is to carefully select and compare similar rain events (i.e. compare the catch ratios for an event with overhang to a similar event without overhang). In addition to that, the entire monitoring periods with overhang (0.6 m and 1.2 m), may both be compared to the entire period without overhang to obtain the general effectiveness of overhang under real-life conditions. For this comparison to be feasible, the meteorological parameters of wind direction, wind speed, and rainfall intensity should be similar for all three monitoring periods. This similarity should also result in a similar wetting pattern, i.e. similar catch ratios (to be discussed) on the east and north facades.

A comparison of wind direction, wind speed and horizontal rainfall intensity, for the three monitoring periods, is shown in Figure 4.7, Figure 4.8 and Figure 4.9, respectively. The values are also tabulated in Table B.1 in APPENDIX B.

Wind Direction

The prevailing wind direction for all three monitoring periods is from the east during rain hours, as seen in Figure 4.7a-c. Winds are also quite frequent from the east-south-east and east-north-east directions. This narrow band of wind directions coming from the east-north-east to east-south-east, creates an ideal opportunity to study WDR on the east facade, since the prevailing wind is blowing approximately normal to the wall.

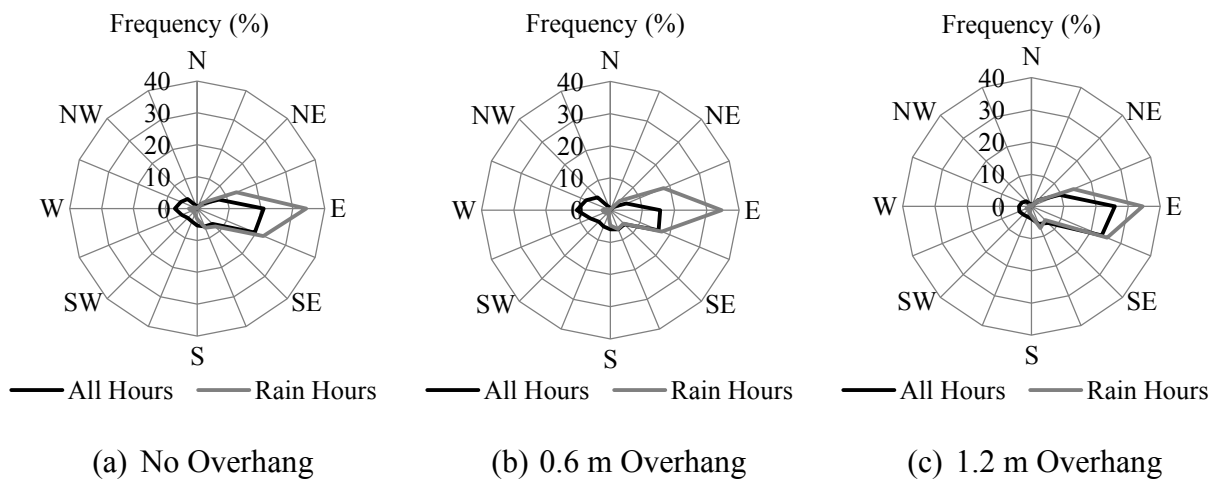


Figure 4.7 – Wind direction frequency at the test building.

Wind Speed

The amount of airfield WDR has been shown to increase linearly in proportion to wind speed, therefore, a comparison between monitoring periods requires relatively similar wind speeds. The wind speed characteristics are very similar during “rain hours” for all three monitoring periods, as shown in Figure 4.8a-c. The frequency of wind speeds in the range of 0 to 2 m/s is around 40 to 45% and in the range of 2 to 4 m/s around 45 to 50% of the time. Wind speeds in the range of 4 to 6 m/s are seen less than 10% of the time.

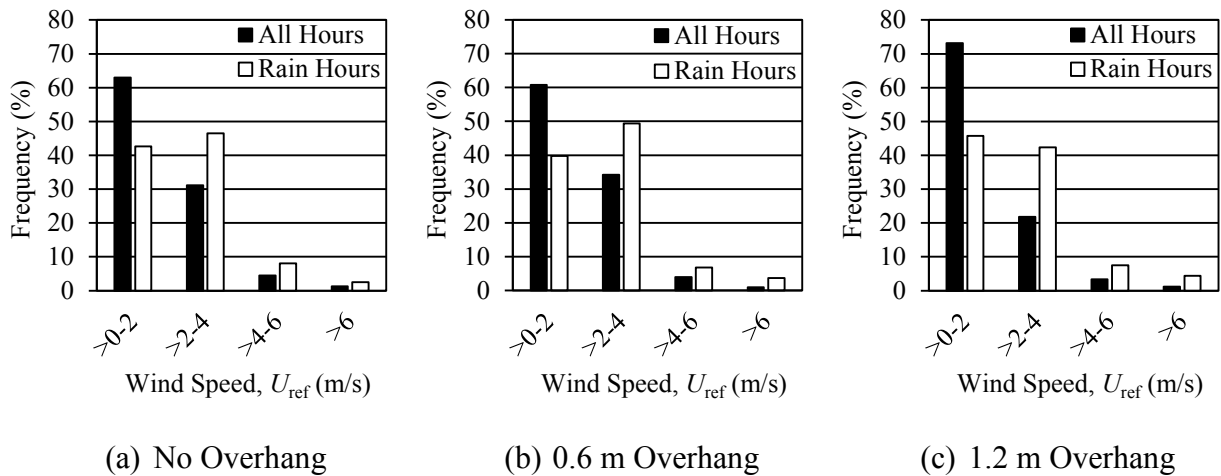


Figure 4.8 – Wind speed frequency at the test building.

Rainfall Intensity

It has been observed that the fraction of large raindrops in rain increases as the rainfall intensity increases (Best, 1950). The influence of drop size on the spatial distribution of WDR across the facade has been documented in several CFD simulations (Sepehr, 2013; Blocken, 2004). Smaller raindrops are influenced mainly by the wind drag force, so tends to follow the flow of the wind, resulting in highly curved trajectories. Larger raindrops are mainly gravity driven and less influenced by the wind flow, resulting in straighter trajectories.

The Greater Vancouver area is known for its rainy season with periods of light rain lasting for days. These systems are normally a result of stratiform clouds, which are wide with little vertical depth resulting in rainfall that is steady and of low intensity. As a result, rainfall intensities of

less than 2 mm/hr are seen about 80 to 85% of the time, as seen in Figure 4.9a-c.

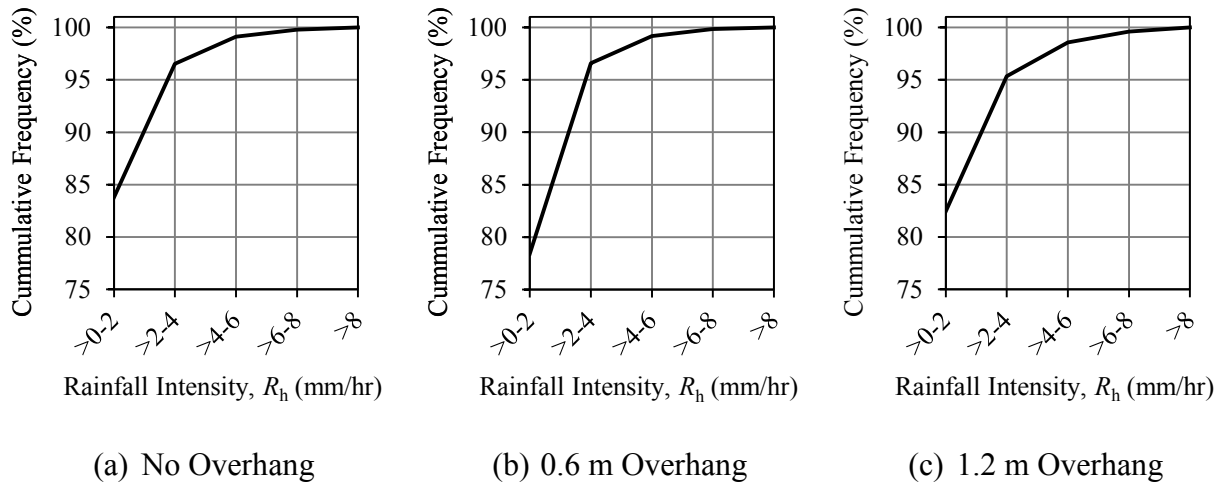


Figure 4.9 – Rainfall intensity cumulative frequency at the test building.

Similarity has been established between each monitoring period for wind direction, wind speed and rainfall intensity. This allows the direct comparison of catch ratios (to be discussed) between monitoring periods to assess the effectiveness of overhangs. It also forms the basis as to how the rain events will be compared to each other.

4.3. Airfield Driving Rain Index

As mentioned earlier, the airfield driving rain index (R_{airfield}) expresses the amount of rain incident on an imaginary unobstructed wall surface and is a relative indicator of the severity of a specific wall orientation to the wind-driven rain exposure.

To calculate the airfield driving rain indices, the wind speed measured on top of the roof is converted to each row of WDR gauges using equation 3.3. The WDR gauges are located 0.6 m, 2.4 m, 4.9 m and 9.1 m below the roofline on the east facade and 0.6 m, 2.4 m, 3.7 m, 4.9 m and 9.1 m below the roofline on the north facade, therefore, the wind speed is converted to seven different heights. The mean speed exponent (α) of 0.25 is used, which represents the suburban terrain category of the test building.

The airfield driving rain index and the measured wind-driven rain have been compared for the three monitoring periods (no overhang, 0.6 m overhang and 1.2 m overhang). Figure 4.10 to

Figure 4.12 show the results on the east facade. Figure 4.13 to Figure 4.15 show the results on the north facade.

The airfield driving rain indices increase with height because of the increase in wind speed with height. The values in the legend are distances with respect to the rooftop. There is a significant difference between the calculated airfield driving rain index and the actual measured driving rain impinging on the building facade implying that the building geometry and its design details (i.e. overhangs) have a significant influence on the amount of rain deposited on the building facade. The influence of building geometry and building details are accounted for by using the wall factor, which will be presented in Section 4.4.2.

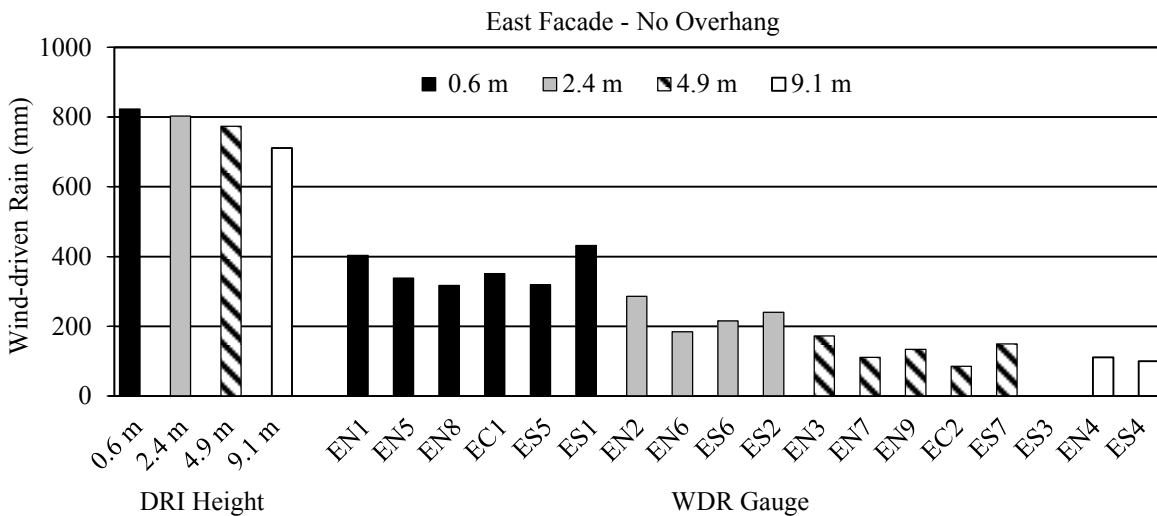


Figure 4.10 – Airfield driving rain index and measured WDR on the east facade.

No overhang.

DRI height refers to the distance from the roofline.

(Data collected from August 16, 2013 to December 2, 2014)

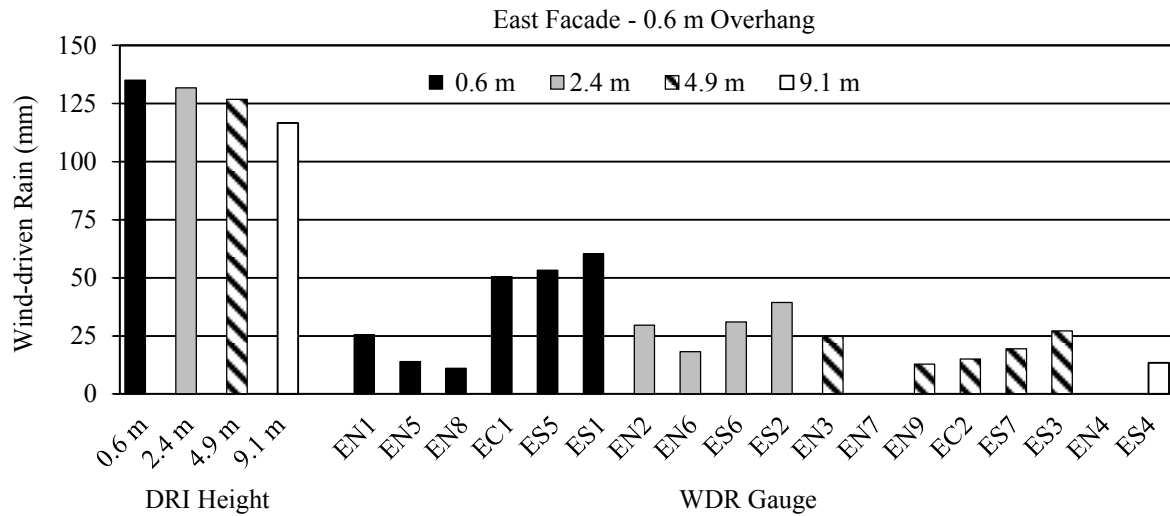


Figure 4.11 – Airfield driving rain index and measured WDR on the east facade.
With a 0.6 m overhang.

DRI height refers to the distance from the roofline.
(Data collected from March 2, 2015 to July 13, 2015)

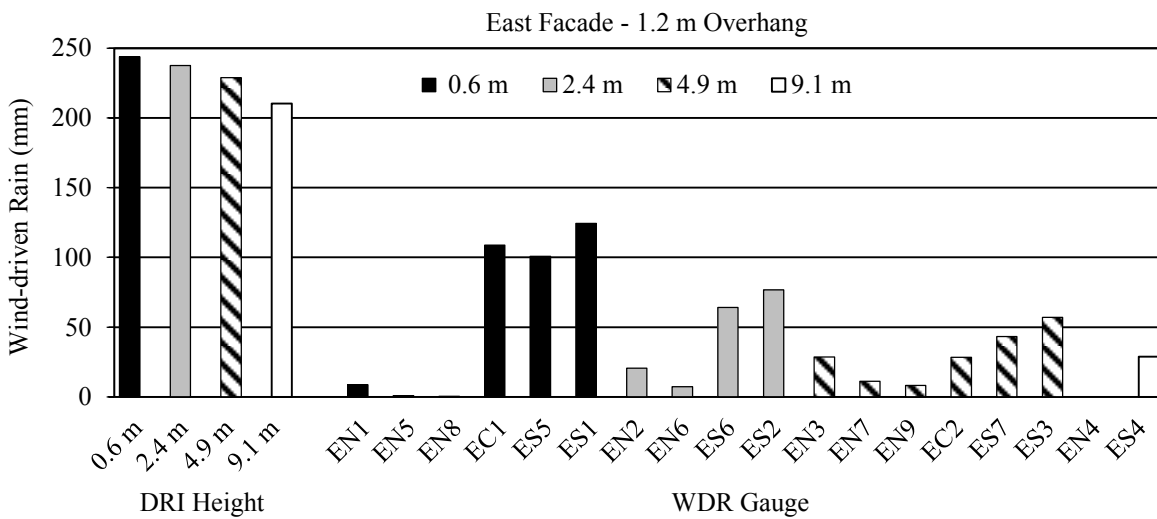


Figure 4.12 – Airfield driving rain index and measured WDR on the east facade.
With a 1.2 m overhang.

DRI height refers to the distance from the roofline.
(Data collected from December 2, 2014 to March 2, 2015)

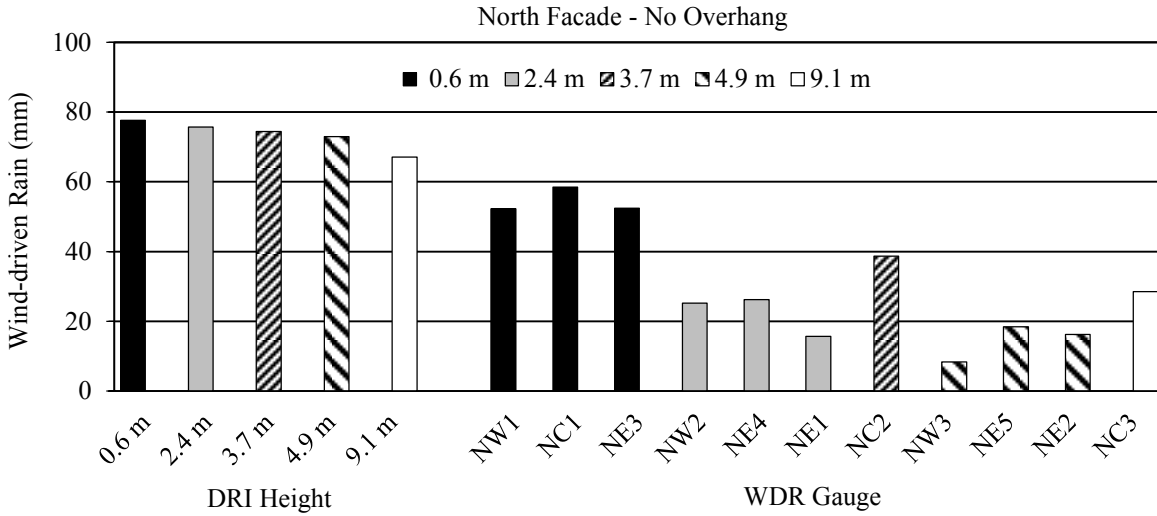


Figure 4.13 – Airfield driving rain index and measured WDR on the north facade.
No overhang.
DRI height refers to the distance from the roofline.
(Data collected from August 16, 2013 to December 2, 2014)

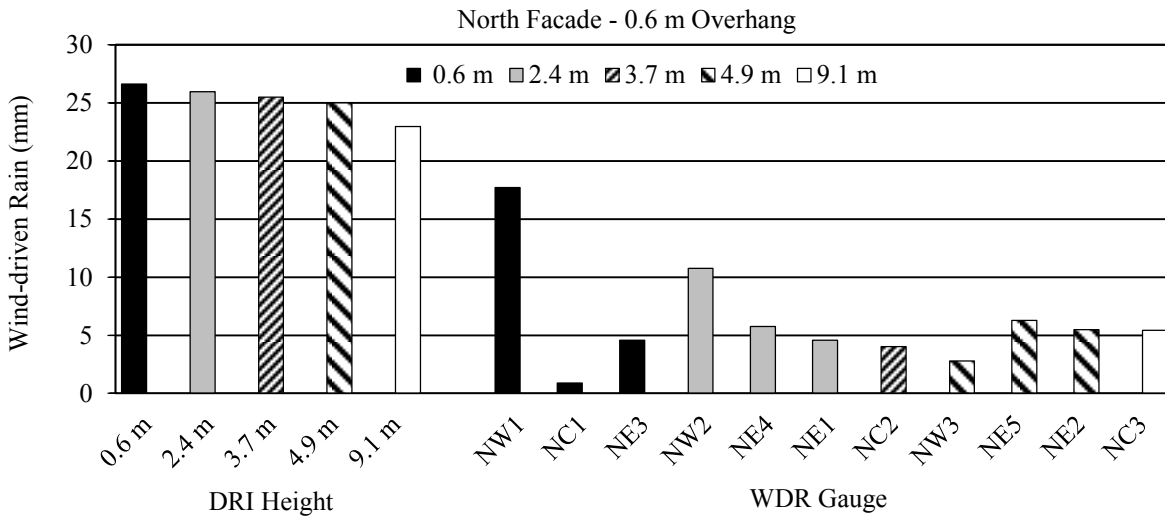


Figure 4.14 – Airfield driving rain index and measured WDR on the north facade.
With a 0.6 m overhang.
DRI height refers to the distance from the roofline.
(Data collected from March 2, 2015 to July 13, 2015)

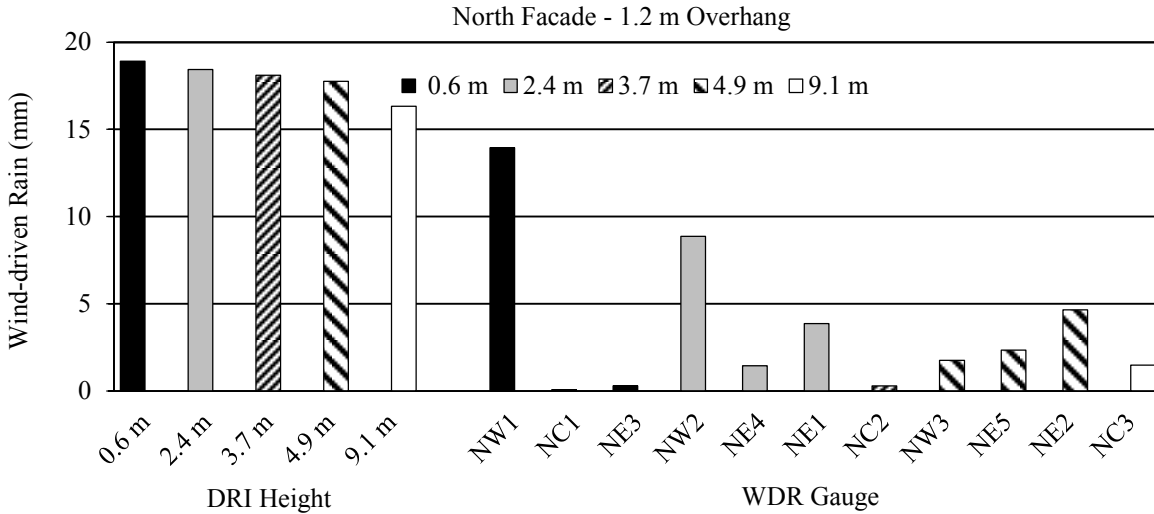


Figure 4.15 – Airfield driving rain index and measured WDR on the north facade.
With a 1.2 m overhang.
DRI height refers to the distance from the roofline.
(Data collected from December 2, 2014 to March 2, 2015)

4.4. Spatial Distribution of Wind-Driven Rain on the Building Facade

4.4.1. Catch Ratio

Catch ratio analysis has been performed for the test building over three monitoring periods: (1) no overhang, (2) 0.6 m overhang and (3) 1.2 m overhang. The catch ratios on the east and north facades for the monitoring period with (1) no overhang, (2) a 0.6 m overhang and (3) a 1.2 m overhang are shown in Figure 4.16, Figure 4.17 and Figure 4.18, respectively. Table B.2 in APPENDIX B summarizes the catch ratios for the rain events within each monitoring period.

Phase I: No Overhang

The amount of rain deposited on the building facade varies with locations, however, a symmetrical distribution of WDR across the east facade can be seen because the prevailing wind direction is from the east, resulting in the wind blowing normal to the facade (Figure 4.16). The classic wetting pattern can be seen from Figure 4.16a: (1) the top corners are the most wetted followed by the top and side edges and (2) wetting increases from the bottom of the facade to the top and from the middle of the facade to the sides.

Since the prevailing wind direction is from the east, the catch ratios on the north facade are not symmetrical, as shown in Figure 4.16b. The gauges on the left edge of the facade (NE1 and NE2) receive less rain than the gauges located to their right. This may be explained by considering the wind flow around the building. Since the prevailing wind direction during rain hours is from the east, flow separation occurs at the edges of the east facade, resulting in a wetting pattern on the north facade that is reflective of the wind flow around the north-east edge.

Phase II: 0.6 m Overhang

The catch ratios for the monitoring period with a 0.6 m overhang are shown in Figure 4.17. The majority of the catch ratios on the east facade are similar to that of the monitoring period without overhang since both prevailing wind directions are from the east with similar wind speeds and horizontal rainfall intensities. However, it is evident that the gauges below the 0.6 m overhang on the east facade have lower catch ratios when compared to (1) other gauges of similar height and distance from edge and (2) the same gauges in the monitoring period without overhang (Figure 4.16a). The gauges right below the overhang are the most protected (EN1, EN5, EN8). The protection provided by the 0.6 m overhang seems to extend until the second row of gauges when compared to the period without overhang.

The catch ratios on the north facade are slightly higher for the monitoring period with a 0.6 m overhang when compared to the monitoring period without overhang. This is due to an increase in frequency of north-easterly winds for the monitoring period with a 0.6 m overhang, as seen in Figure 4.7b. The gauges right below the 0.6 m overhang (NE3 and NC1), are the most protected; the gauges have significantly lower catch ratios when compared to NW1, which is at the same height. This is also apparent when compared to the north facade without overhang (Figure 4.16b). The remaining gauges below the 0.6 m overhang are protected to various degrees.

Phase III: 1.2 m Overhang

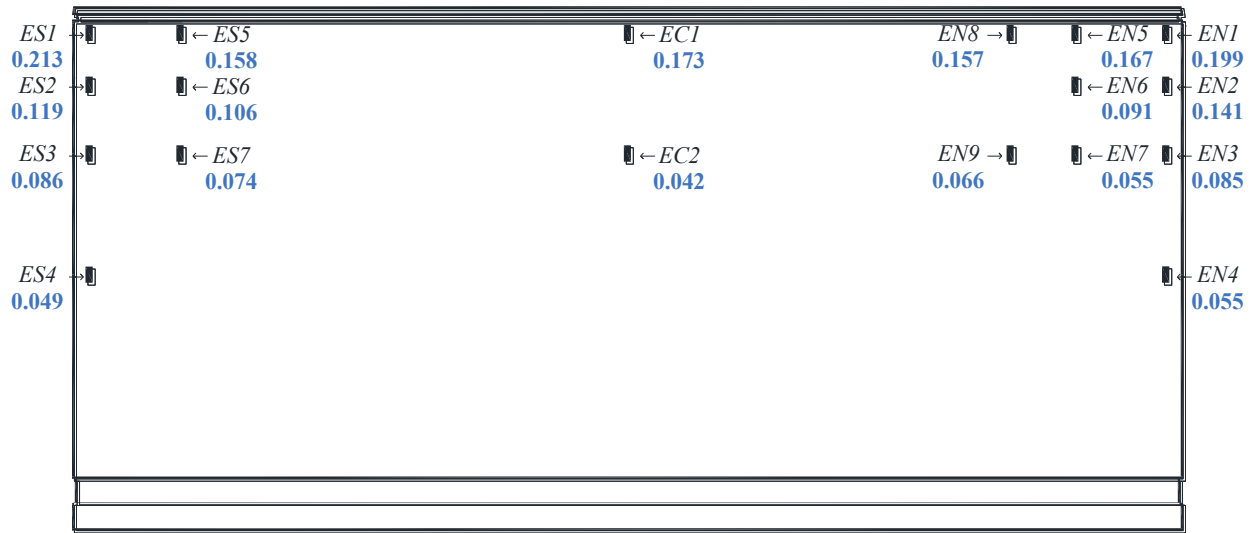
The catch ratios for the monitoring period with a 1.2 m overhang are shown in Figure 4.18. The majority of the catch ratios on the east facade are similar to those found in the other two monitoring periods. However, all of the WDR gauges below the 1.2 m overhang have lower catch ratios when compared to (1) other WDR gauges of similar height and distance from edge and (2) the same WDR gauges in the monitoring period without overhang (Figure 4.16a). The

gauges right below the overhang are almost entirely protected (EN1, EN5, EN8). The protection provided by the 1.2 m overhang seems to extend until the third row of gauges when compared to the period without overhang.

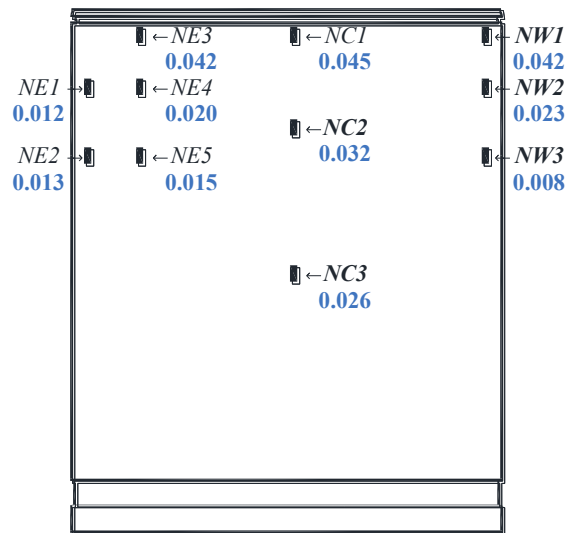
The catch ratios on the north facade are similar to the catch ratios for the period without overhang because of the similar on-site weather conditions. The gauges right below the overhang (NE3 to NC1) are entirely protected. The remaining gauges below the overhang are protected to various degrees and seem to extend until the fourth row of gauges.

In summary, the analyses of catch ratio over the three monitoring periods shows that:

- 1) The classic wetting pattern is observed on the east facade of the building: (1) the top corners are the most wetted followed by the top and side edges and (2) wetting increases from the bottom of the facade to the top and from the middle of the facade to the sides.
- 2) The wetting pattern observed on the north facade is not symmetrical because the prevailing wind direction during rain hours is from the east. Flow separation occurs at the edges of the east facade, resulting in a wetting pattern on the north facade that is reflective of the wind flow blowing around the north-east edge.
- 3) The 0.6 m overhang reduces the WDR deposition on the facade, especially areas right below the overhang. The protection provided by the overhang extends 2.4 m to 4.9 m (second to third row of WDR gauges).
- 4) The 1.2 m overhang significantly reduces the WDR deposition on the facade, almost eliminating the WDR in the areas right below the overhang. The protection provided by the 1.2 m overhang extends 4.9 m to 9.1 m (third to fourth row of WDR gauges).
- 5) The overhang is less effective in reducing WDR deposition near the edge of the wall. The protection increases from the side edge to the center of the facade and from the bottom to the top of the facade.

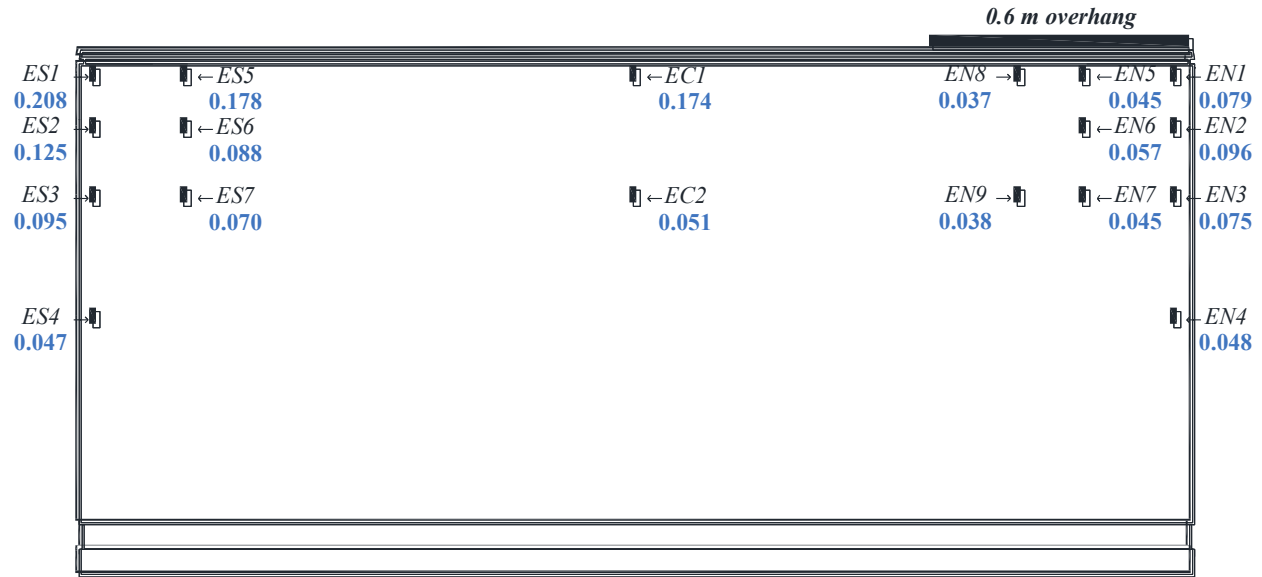


(a)

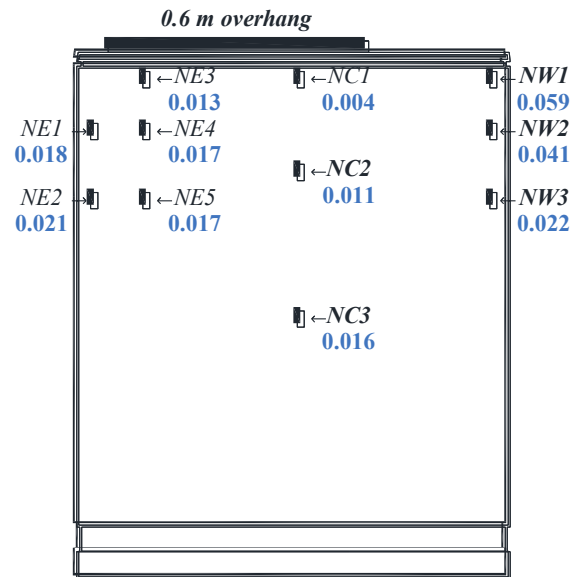


(b)

Figure 4.16 – Catch ratios on the (a) East facade and (b) North facade.
No overhang.
(Data collected from August 16, 2013 to December 2, 2014)

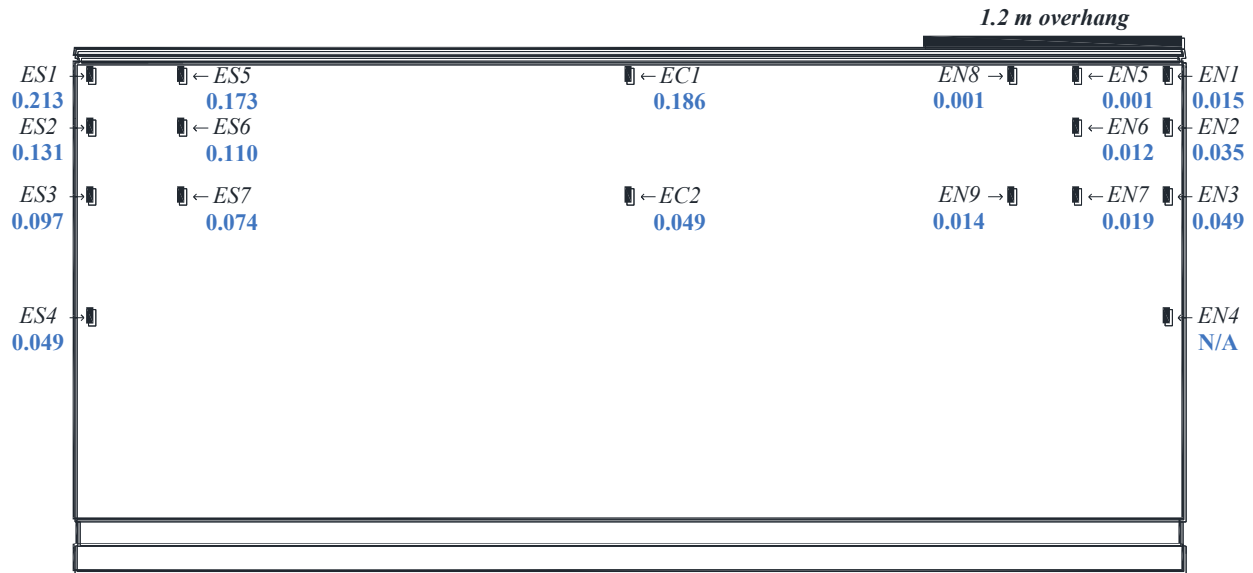


(a)

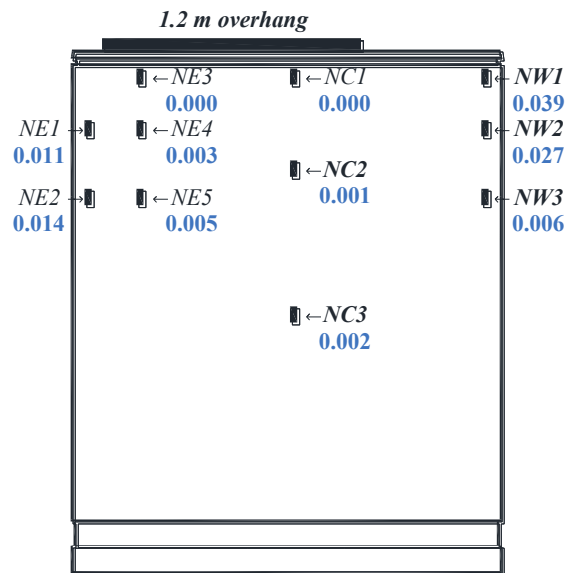


(b)

Figure 4.17 – Catch ratios on the (a) East facade and (b) North facade.
With a 0.6 m overhang.
(Data collected from March 2, 2015 to December 2, 2015)



(a)



(b)

Figure 4.18 – Catch ratios on the (a) East facade and (b) North facade.
With a 1.2 m overhang.
(Data collected from December 2, 2014 to March 2, 2015)

As mentioned earlier, there is a linear correlation between wind speed and the amount of wind-driven rain that impinges onto a vertical building surface. Wind angle also plays a vital role in the amount of wind-driven rain received, with decreasing amounts of impinged rain, as the angle between the approaching wind and the normal to the facade becomes more oblique. The wind angle is shown in Figure 4.19 with the direction normal to the wall being $\theta = 0$.

Figure 4.20 shows the relationship between catch ratio and wind speed on corner gauge ES1 for four approaching wind angles: $\theta = 0 \pm 15^\circ$, $\theta = 30 \pm 15^\circ$, $\theta = 60 \pm 15^\circ$ and $\theta = 90 \pm 15^\circ$. The catch ratios increase proportionally with wind speed, especially for winds blowing normal to the facade. As the wind becomes more oblique, the influence of wind speed diminishes and the catch ratios decrease.

Figure 4.21 shows the relationship between catch ratio and wind speed on the far left column of gauges on the east facade (ES1 to ES4) for winds blowing normal to the facade ($\theta = 0 \pm 15^\circ$). The influence of the building on the wind flow and rain deposition is apparent; the catch ratios decrease with decreasing height. The catch ratios measured by gauge ES1 are significantly higher than those measured by gauge ES4, for wind speeds of 4 m/s measured on top of the roof.

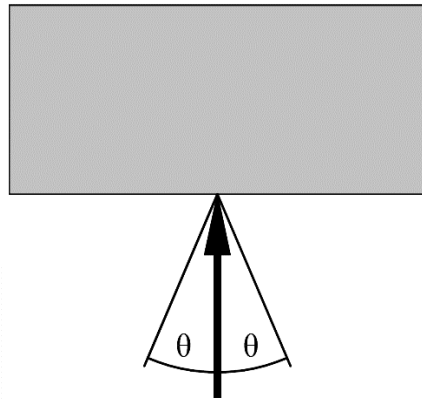
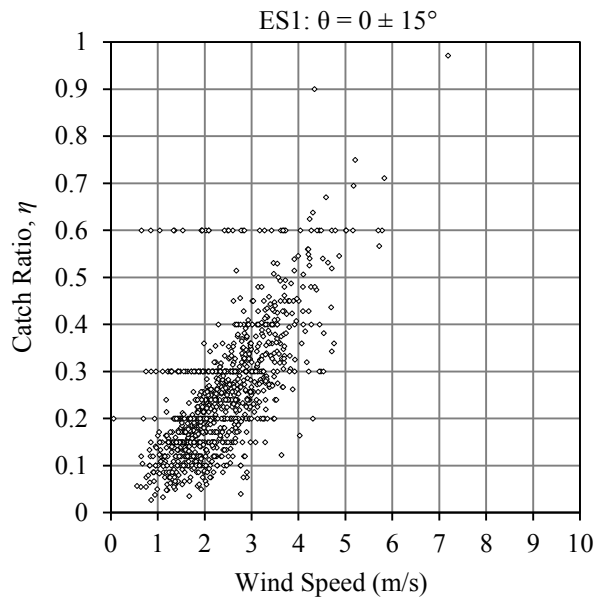
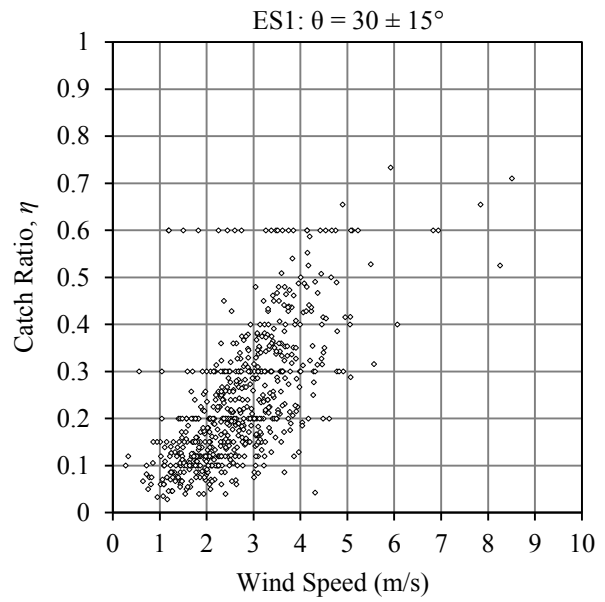


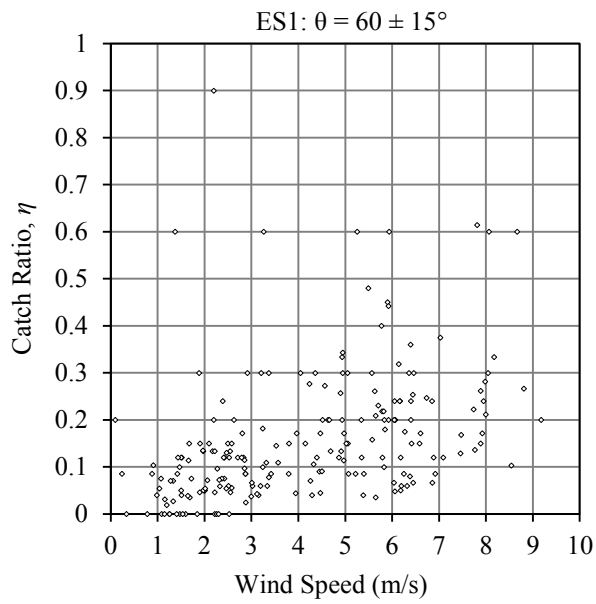
Figure 4.19 – Wind angle, θ (Plan View).



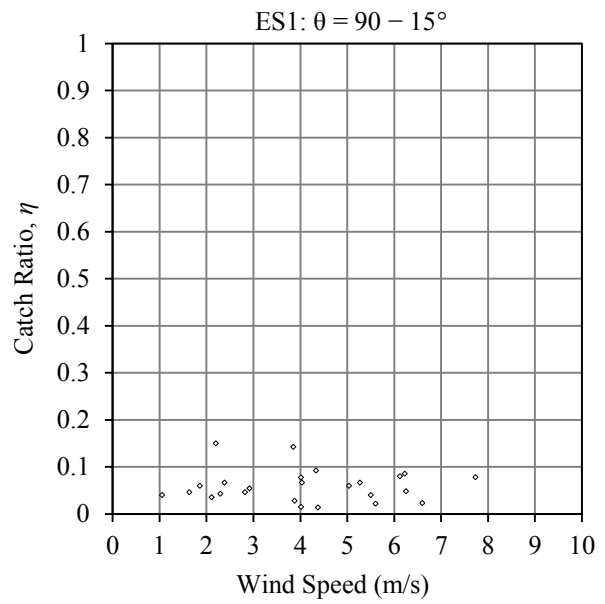
(a)



(b)

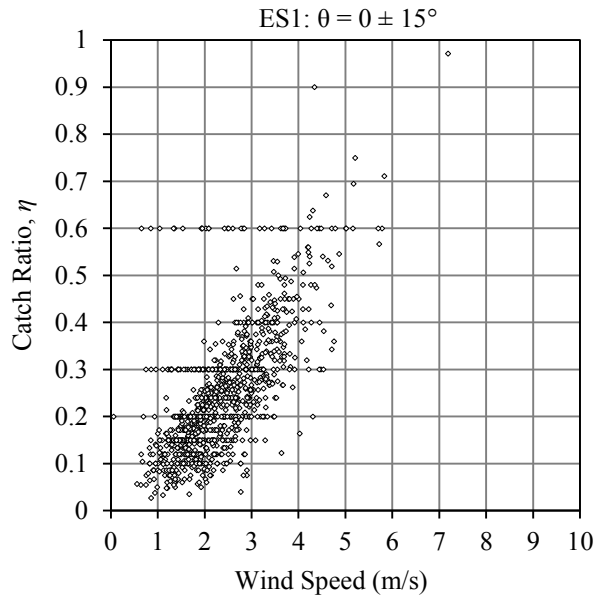


(c)

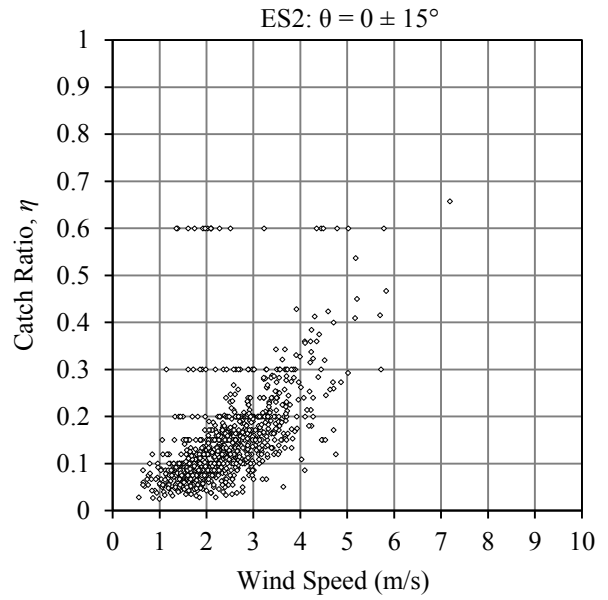


(d)

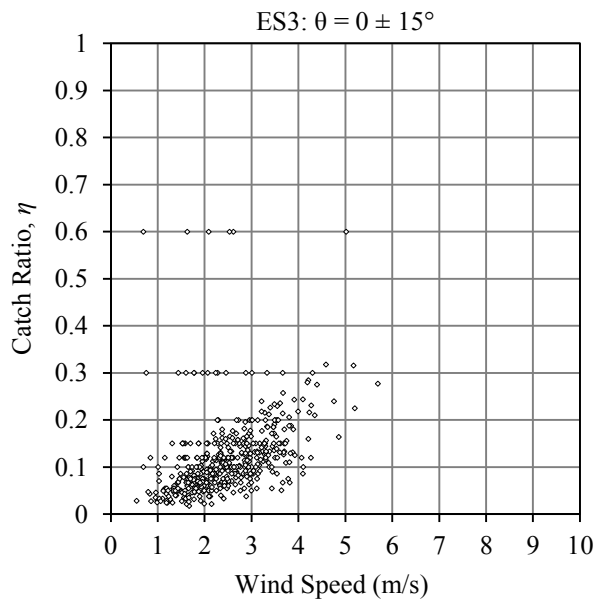
Figure 4.20 – Catch ratio vs. wind speed for four approaching wind angles on gauge ES1.
(a) $\theta = 0 \pm 15^\circ$; (b) $\theta = 30 \pm 15^\circ$; (c) $\theta = 60 \pm 15^\circ$; (d) $\theta = 90 \pm 15^\circ$.



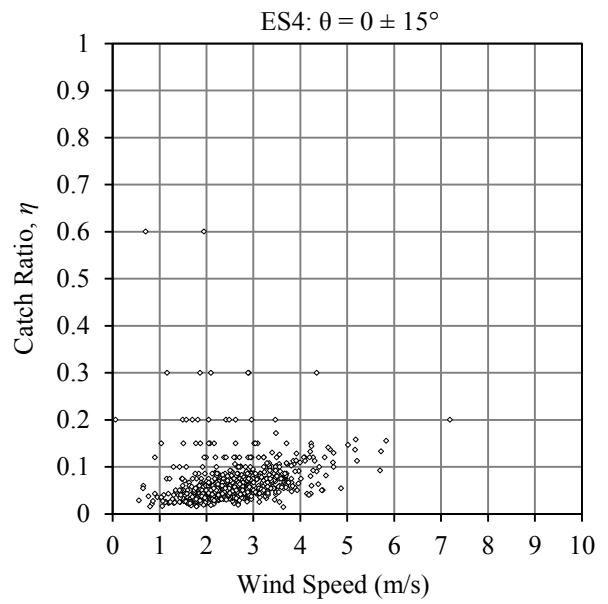
(a)



(b)



(c)



(d)

Figure 4.21 – Catch ratio vs. wind speed when $\theta = 0 \pm 15^\circ$ for gauges ES1 to ES4.
(a) ES1, (b) ES2; (c) ES3 and (d) ES4.

4.4.2. Wall Factor

Wall factors have been calculated using on-site measured wind speed, wind direction and rainfall intensity for the test building over the three monitoring periods: (1) no overhang, (2) 0.6 m overhang and (3) 1.2 m overhang. A comparison is made between the on-site measured and the ISO suggested wall factors.

The wall factors on the east and north facades for entire monitoring period with (1) no overhang, (2) a 0.6 m overhang and (3) a 1.2 m overhang are shown in Figure 4.22, Figure 4.23 and Figure 4.24, respectively. The ISO suggested wall factors are shown in gray, while the measured wall factors are shown in black. A summary of wall factors can be found in Table B.3 in APPENDIX B.

Phase I: No Overhang

As shown in Figure 4.22, there is a symmetrical distribution of wall factors across the east facade since the prevailing wind direction during rain hours is from the east. The measured wall factors on the east facade decreases from the top of the facade to the bottom and from the side of the facade to the center. The highest wall factors encountered on the east facade are at the corner gauges ES1 and EN1, with values of 0.52 and 0.49, respectively; ISO suggests a wall factor of 0.50 at these locations. In general, the ISO suggested wall factors are an overestimation of the wall factors across the east facade; although they provide a good estimation at the top corners and at the third row of gauges, except for the center gauge EC2. There are significant overestimations at the second row of gauges when compared to the measured values.

The measured wall factors on the north facade show similar and contrasting wall factors when compared to the east facade. The similarities lie in the fact that the ISO suggested values are a significant overestimation at the second row of gauges. The differences lie in the fact that the WDR deposition on the north facade is significantly different than that of the east facade, resulting in large wall factors at the top edge (NE3, NC1, NW1) and with a gradient that is low at the left edge of the facade (NE1, NE2), increases towards the center of the facade (NC1, NC2, NC3) and then levels off towards the right edge (NW1, NW2, NW3).

Phase II: 0.6 m Overhang

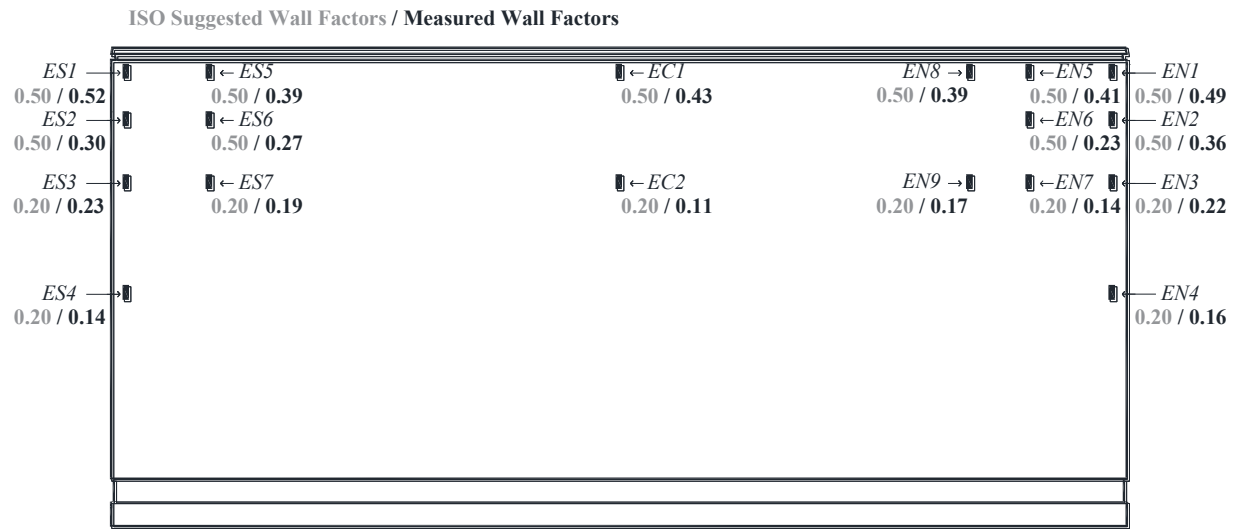
Figure 4.23 shows the wall factors on the east and north facades for the monitoring period with a 0.6 m overhang. On the east facade, the presence of a 0.6 m overhang reduces the wall factor values on the top row of gauges (EN1, EN5, EN8), with increasing wall factors towards the edge of the facade. The protection provided by the 0.6 m overhang extends until the second row of gauges (2.4 m) on the east facade. On the north facade, the presence of a 0.6 m overhang reduces the wall factors on all the gauges beneath the overhang, with smaller influences to the gauges NE4 and NE5, when compared to the monitoring period without overhang (Figure 4.22b). The protection provided by the 0.6 m overhang extends to gauge NC3, which is 9.1 m below the roofline. This suggests that the protection provided by the overhang is significantly influenced by the approaching wind angle, since the majority of WDR deposited on the north facade is from the north-east.

Phase III: 1.2 m Overhang

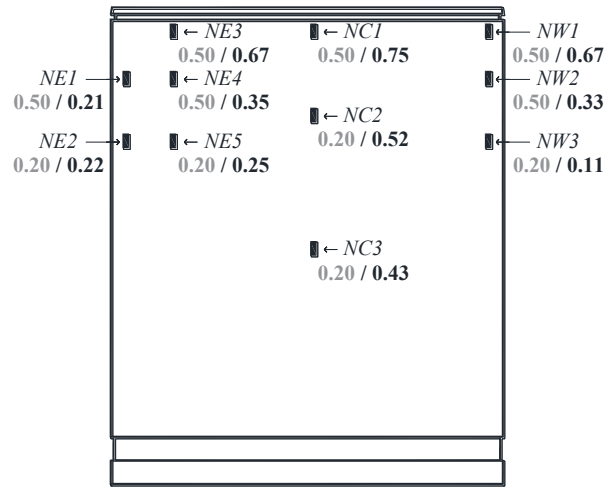
Figure 4.24 shows the wall factors on the east and north facades for the monitoring period with a 1.2 m overhang. On the east facade, the presence of a 1.2 m overhang further reduces the wall factor values on the top row of gauges (EN1, EN5, EN8), rendering a wall factor of 0 for gauges EN5 and EN8 and drastically reducing the wall factor of EN4 to 0.04. The protection provided by the 1.2 m overhang extends until the third row of gauges (4.9 m) on the east facade. On the north facade, the presence of a 1.2 m overhang drastically reduces the wall factors on all the gauges beneath the overhang when compared to the other two monitoring periods.

The wall factor analysis indicates that:

- 1) The ISO standard only suggests 2 wall factors for a multi-storey building with a flat roof and assumes the same wall factor across all four facades, however, site measurements show that wall factors vary widely with respect to the location on the facade and the facade orientation.
- 2) By neglecting building specific features a significant overestimation or underestimation may be encountered when using the ISO standard. More wind-driven rain data is needed to improve the current ISO Standard.

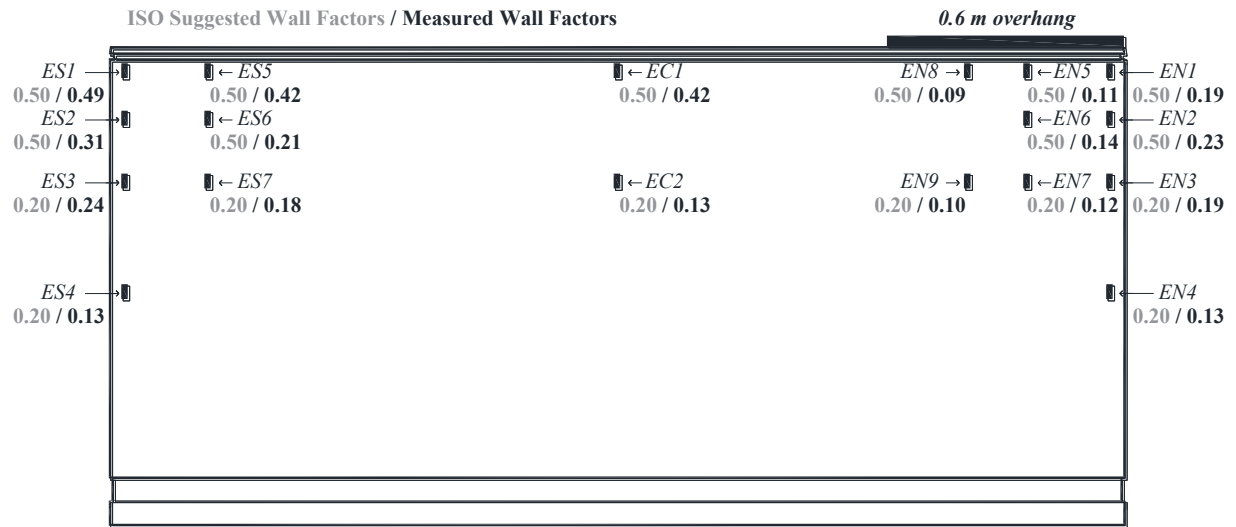


(a)

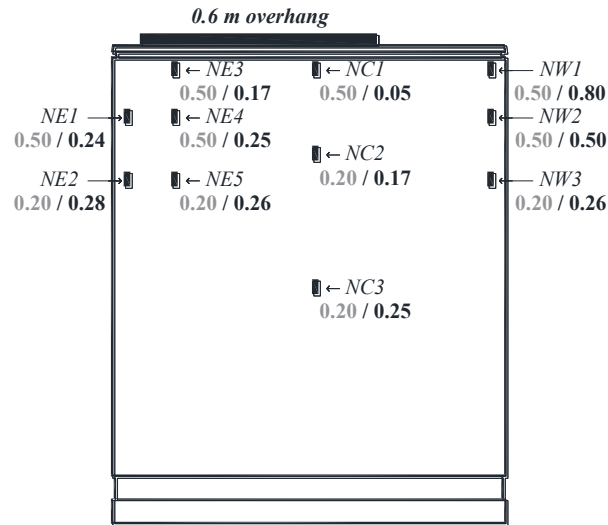


(b)

Figure 4.22 – Wall Factors on the (a) East facade and (b) North facade.
No overhang.
(Data collected from August 16, 2013 to December 2, 2014)

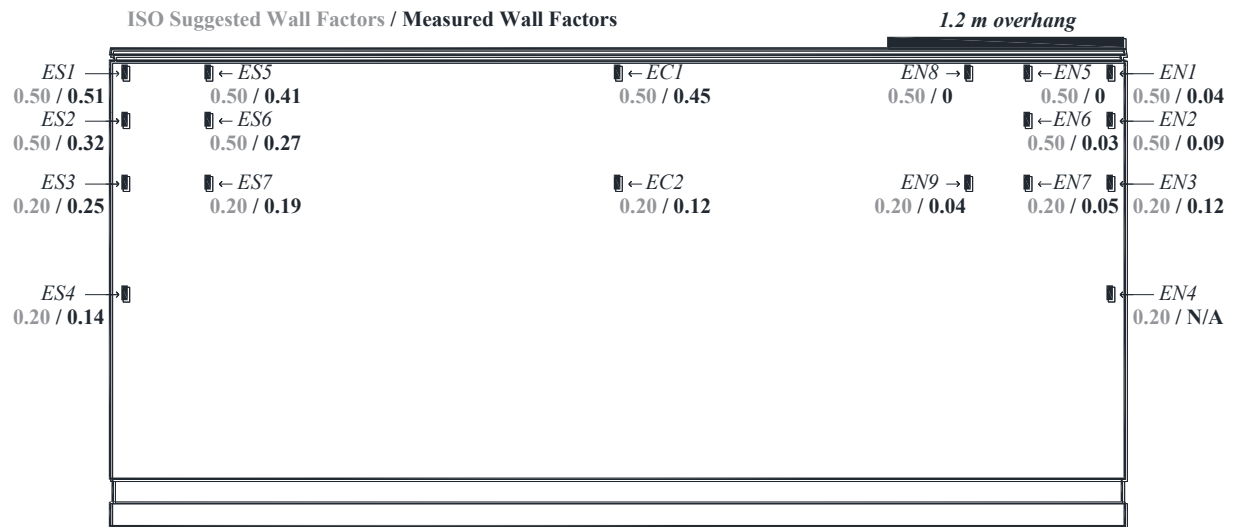


(a)

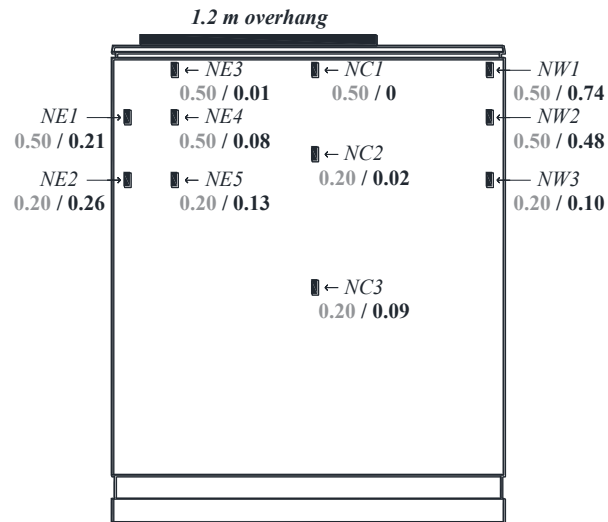


(b)

Figure 4.23 – Wall Factors on the (a) East facade and (b) North facade.
With a 0.6 m overhang.
(Data collected from March 2, 2015 to December 2, 2015)



(a)



(b)

Figure 4.24 – Wall Factors on the (a) East facade and (b) North facade.
With a 1.2 m overhang.
(Data collected from December 2, 2014 to March 2, 2015)

4.5. Wall Index

The wall indices, which are the amounts of rain that impinges on a real wall, have been calculated for the test building over the three monitoring periods: (1) no overhang, (2) 0.6 m overhang and (3) 1.2 m overhang. Comparisons between the measured WDR and the calculated WDR are presented.

The wall indices on the east and north facades for entire monitoring period with (1) no overhang, (2) a 0.6 m overhang and (3) a 1.2 m overhang are shown in Figure 4.25, Figure 4.26 and Figure 4.27, respectively. The values shown in black are the actual WDR amounts measured by the WDR gauges with their associated errors. The values shown in gray are the wall indices calculated using the measured wall factors presented in Section 4.4.2. The values shown in white are the wall indices calculated using the two wall factor values suggested by ISO, also presented in Section 4.4.2.

From Figure 4.25a, the calculated WDR using the ISO suggested wall factors results in an overestimation of WDR amounts at all measured locations on the east facade. The calculated WDR using the measured wall factors also leads to an overestimation, although the difference is not as prominent. The same can be said of the north facade (Figure 4.25b); the calculated WDR amount using the ISO suggested wall factors also lead to overestimations at most measured locations, except at NC2 and NC3.

The reasons for these differences lies in the values assigned to the various factors in equation 3.10 (roughness factor, topography factor, obstruction factor, and wall factor). To obtain a perfect correlation between the measured values and the calculated wall indices, the values assigned to each factor must be exactly representative of the field conditions. The test building and its surroundings have an inherent roughness and topology with local obstructions, such as nearby buildings, trees, etc. and building details (balconies and overhangs). Although the values suggested in ISO 15927-3 (2009) can depict a general picture of the WDR exposure, it is difficult to obtain a perfect representation of the test building due to the complex nature of the building within its suburban environment.

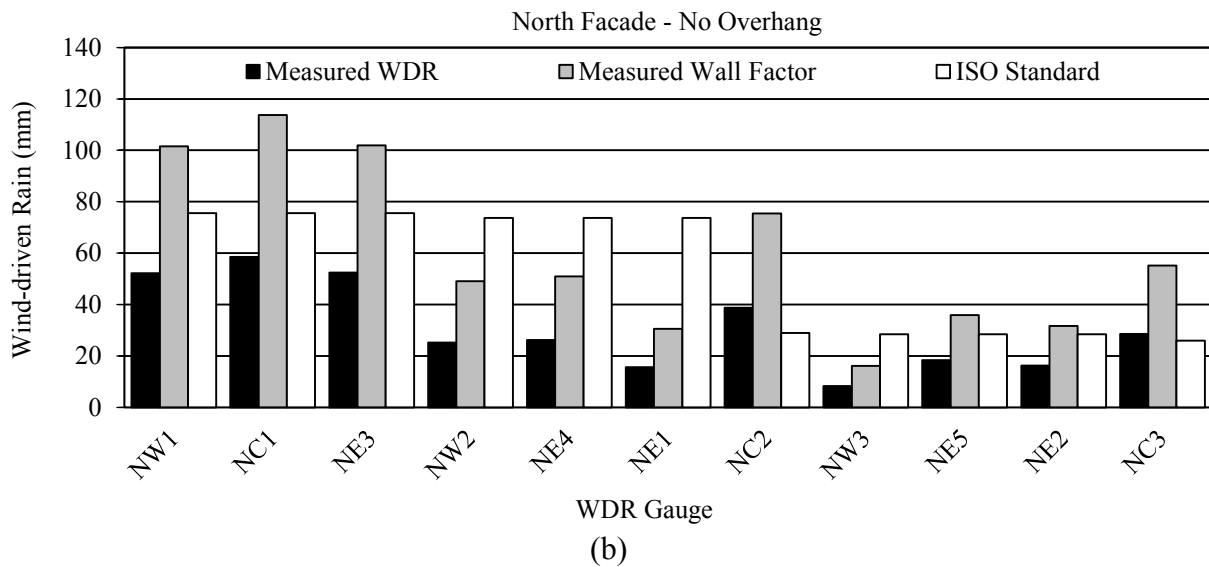
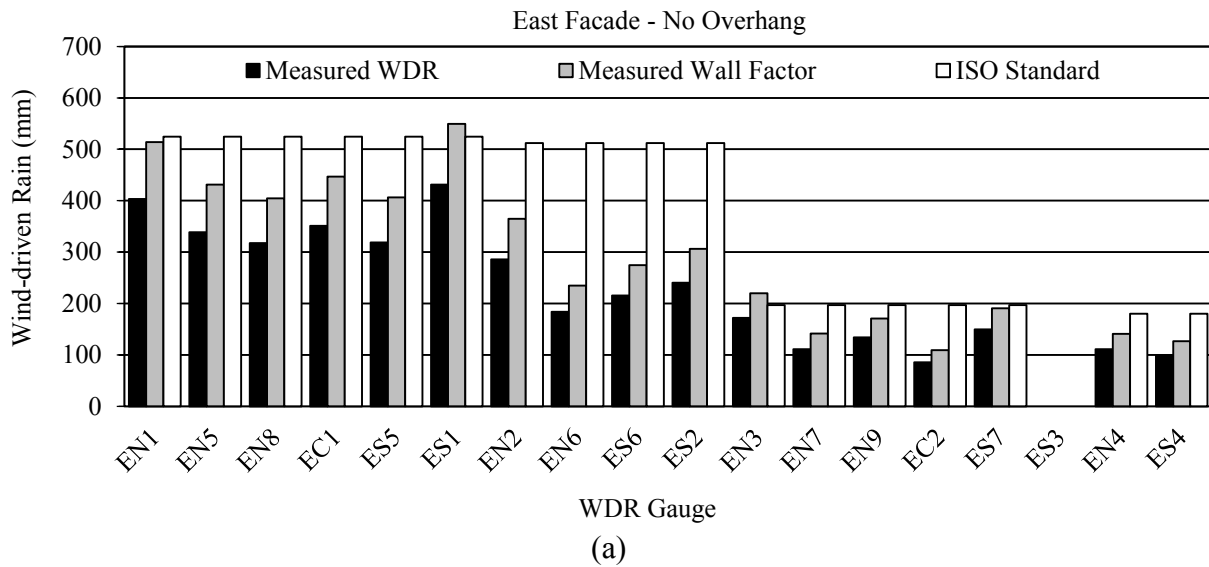


Figure 4.25 – Comparison between measured WDR and calculated WDR using (1) measured wall factors and (2) ISO suggested wall factors
 (a) east facade and (b) north facade
 No overhang

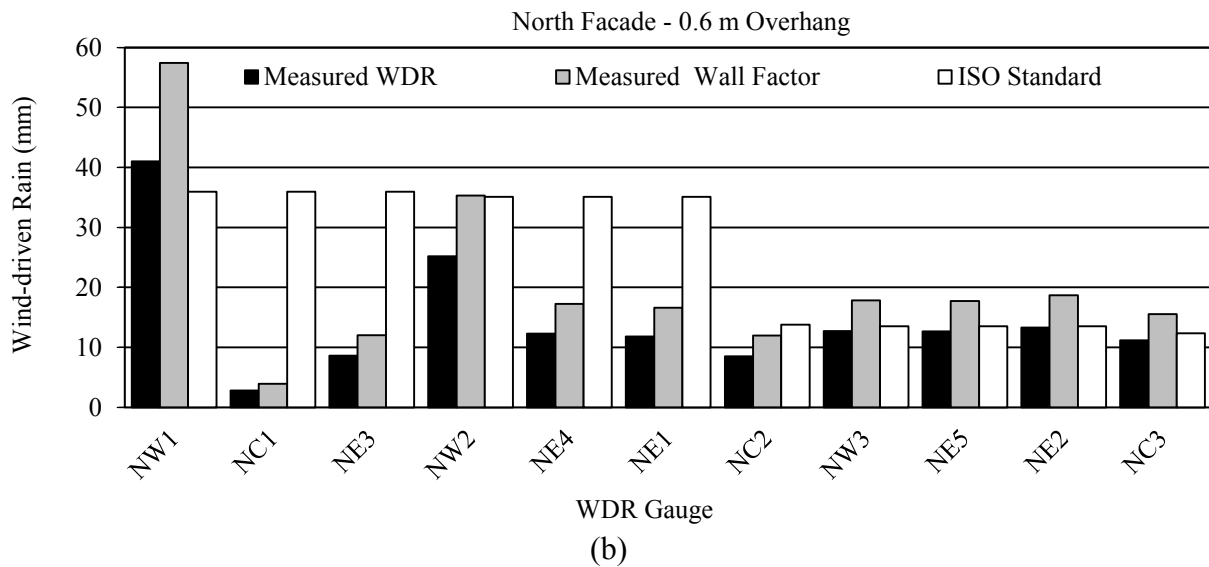
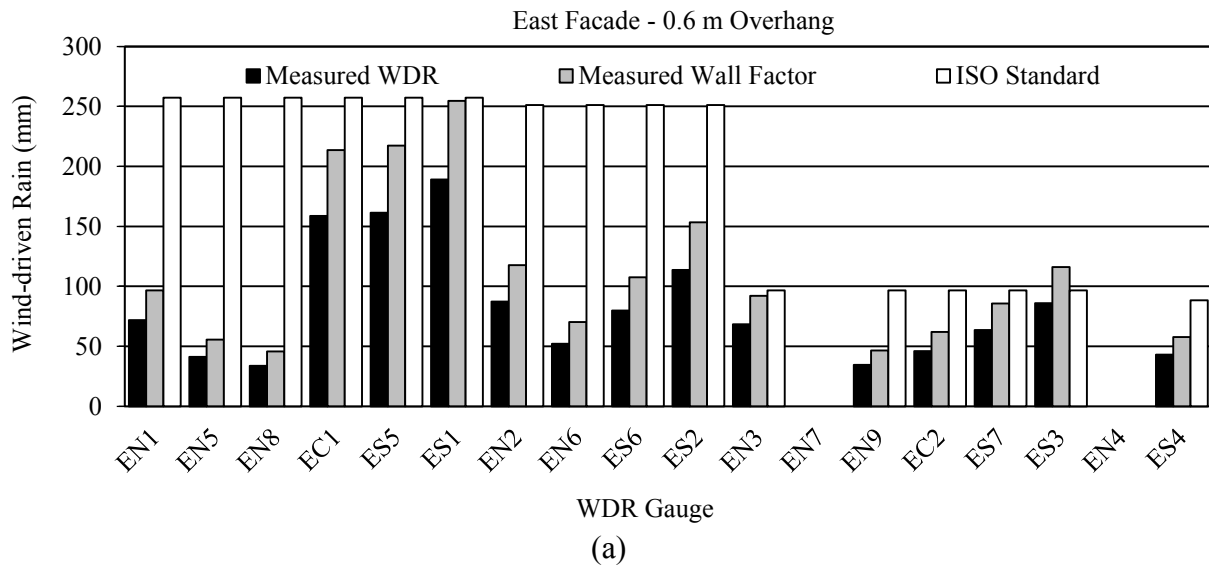


Figure 4.26 – Comparison between measured WDR and calculated WDR using (1) measured wall factors and (2) ISO suggested wall factors
 (a) east facade and (b) north facade
 With a 0.6 m overhang

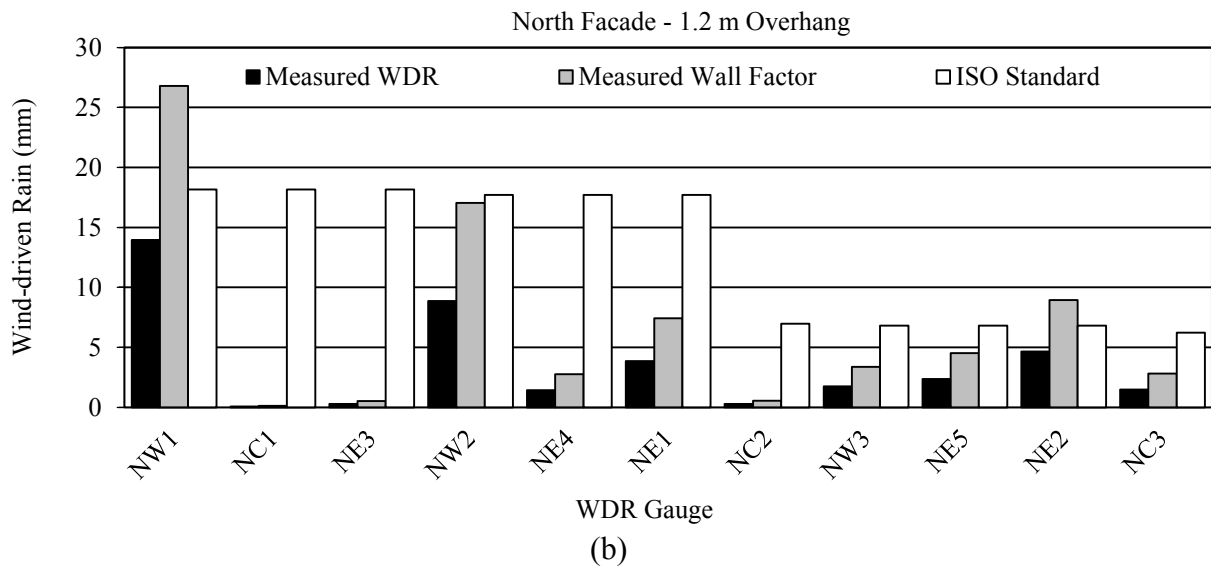
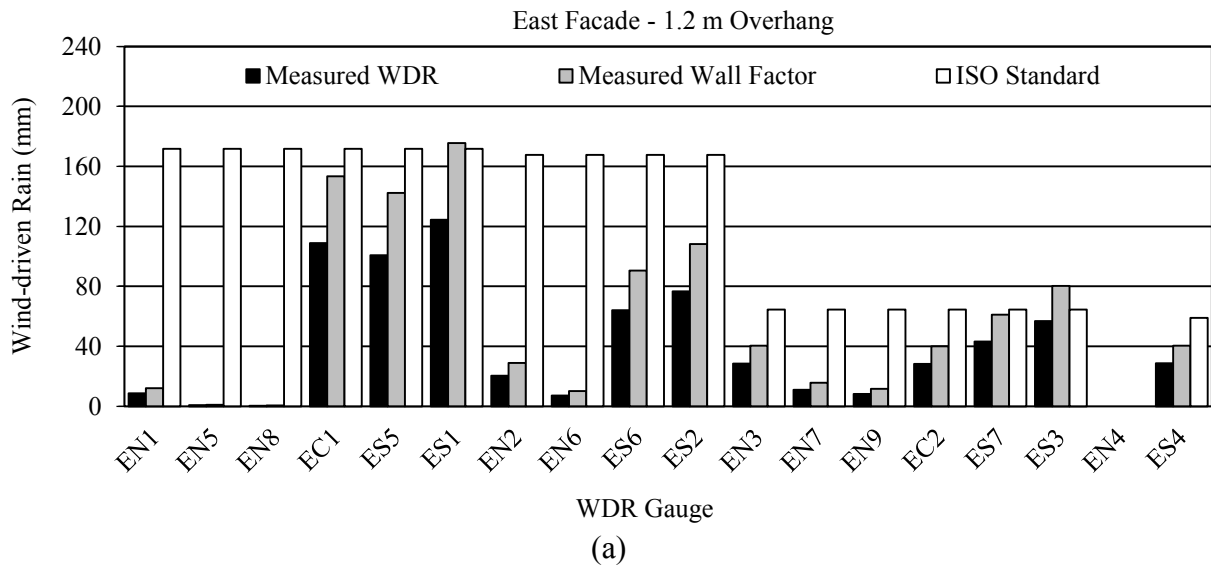


Figure 4.27 – Comparison between measured WDR and calculated WDR using (1) measured wall factors and (2) ISO suggested wall factors
 (a) east facade and (b) north facade
 With a 1.2 m overhang

4.6. The Effectiveness of Overhang

The effectiveness of overhang has been assessed by (1) similarity (comparing similar rain events) and (2) using a symmetrical distribution of wind-driven rain across the building facade during a rain event. The rain events considered in this section and their catch ratios can be found in Table B.4 in APPENDIX B.

In this section, a description of two similar rain events is provided, one rain event from the monitoring period without overhang and the other from the monitoring period with a 1.2 m overhang. The effectiveness of overhang assessed by using similarity and symmetry, and the two methods are compared. Lastly, the effectiveness of overhang with respect to wind speed and wind incident angle is presented and discussed.

4.6.1. Similarity

To assess the effectiveness of overhang using similarity, two similar rain events are compared; one without overhang and one with overhang. The meteorological parameters of rainfall intensity, wind speed and wind direction for two similar rain events (rain event 7 and rain event 16) are shown in Figure 4.28 and Figure 4.29, respectively. Rain event 7 occurred during the monitoring period without overhang while rain event 16 occurred during the monitoring period with a 1.2 m overhang.

Rain event 7 started on February 10 and ended on February 25, 2014. It is characterized by a light to moderate rainfall intensity with less than 2 mm/hr the majority of the time (80%), 2-4 mm/hr occasionally (18%) and rarely reaching above 4 mm/hr (2%). The total horizontal rainfall amount of this rain event is 162.8 mm. The wind speed during rain hours is mostly in the range of 0-4 m/s (86%) and occasionally above 4 m/s (14%). The wind direction during rain hours is predominantly from the east followed by the east-south-east.

Rain event 16 began on December 4, 2014 and ended on December 11, 2014. In comparison to rain event 7, the rainfall intensity is similar with a rainfall intensity under 2 mm/hr the majority of the time (74%), 2-4 mm/hr occasionally (21%) and rarely reaching above 4 mm/hr (4%). The total horizontal rainfall amount of this rain event is 132 mm. The wind speed during rain hours is

mostly in the range of 0-4 m/s (74%) and occasionally above 4 m/s (26%). The wind direction during rain hours is predominantly from the east-south-east followed by the east.

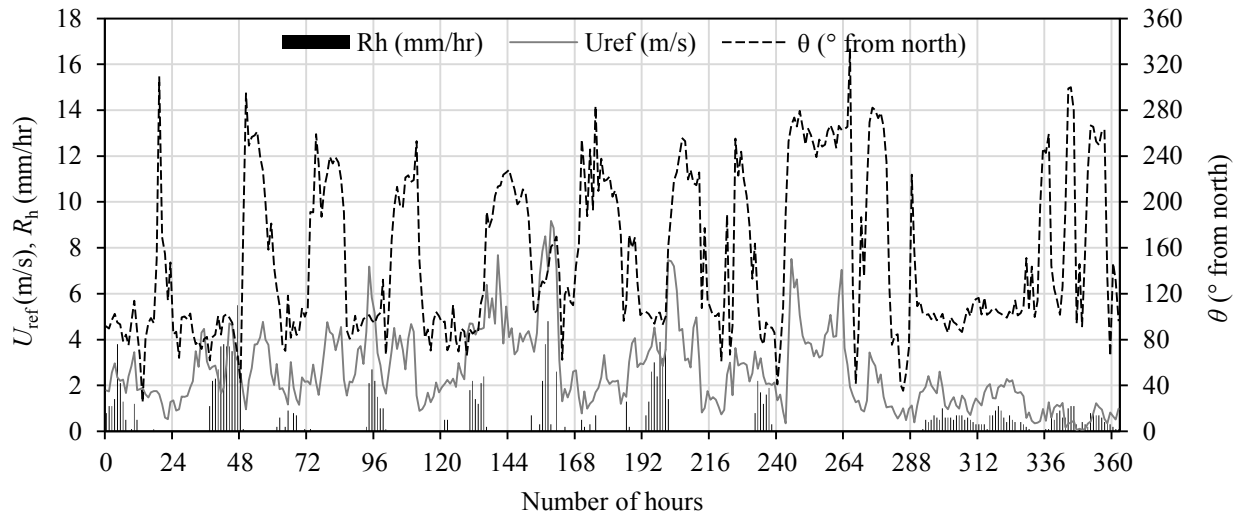


Figure 4.28 – Rainfall intensity (R_h), wind speed (U_{ref}), and wind direction (θ) for rain event 7. (February 10 to February 25, 2014)

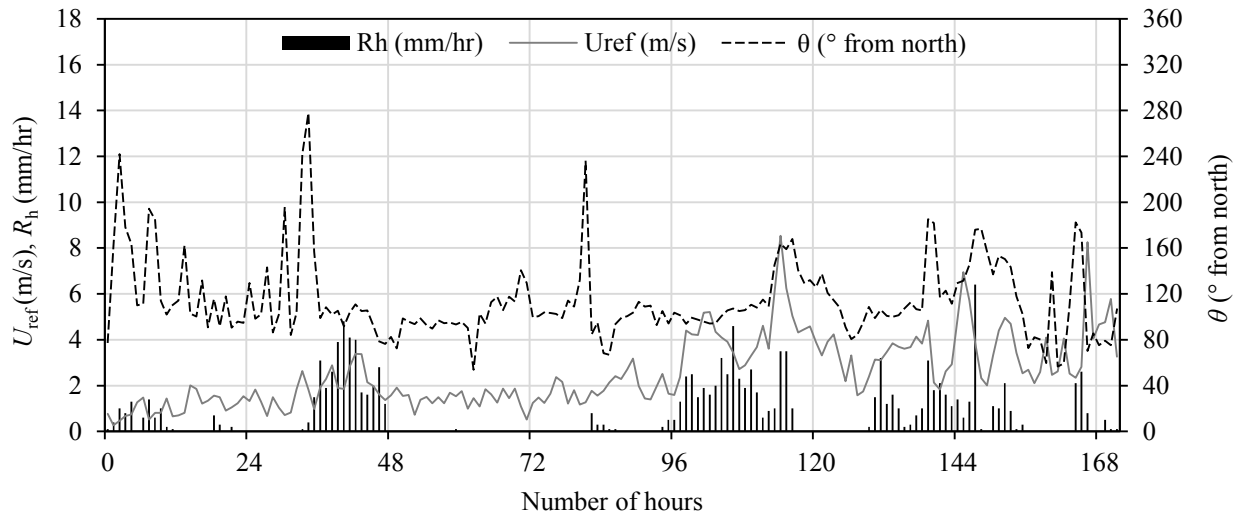


Figure 4.29 – Rainfall intensity (R_h), wind speed (U_{ref}), and wind direction (θ) for rain event 16. (December 4, 2014 to December 11, 2014)

The errors associated with the WDR measurements on the east facade of rain event 7 are shown in Table 4.1. The absolute error is the sum of the adhesion water plus the rest water at the end of the rain event. The relative error is smaller for gauges that register more tips, as shown in Figure

4.30. Therefore, large errors may be avoided by selecting rain events with greater amounts of WDR measured at the gauges.

Table 4.1 – Error estimates for the accumulated WDR measured on the east facade for rain event 7.

WDR Gauge	No. of Tips	No. of Interruptions	Swdr (mm)	E_{AW} (mm)	E_{RW} (mm)	E_{TOT} (mm)	e_{TOT} (%)
EN1	549	10	32.94	0.5	0.06	0.560	1.7
EN2	348	10	20.88	0.5	0.06	0.560	2.7
EN3	260	11	15.60	0.55	0.06	0.610	3.9
EN4	165	13	9.90	0.65	0.06	0.710	7.2
EN5	411	11	24.66	0.55	0.06	0.610	2.5
EN6	251	13	15.06	0.65	0.06	0.710	4.7
EN7	154	13	9.24	0.65	0.06	0.710	7.7
EN8	436	13	26.16	0.65	0.06	0.710	2.7
EN9	172	12	10.32	0.6	0.06	0.660	6.4
EC1	446	7	26.76	0.35	0.06	0.410	1.5
EC2	87	12	5.22	0.6	0.06	0.660	12.6
ES1	486	10	29.16	0.5	0.06	0.560	1.9
ES2	239	13	14.34	0.65	0.06	0.710	5.0
ES3	n/a	n/a	n/a	n/a	n/a	n/a	n/a
ES4	109	16	6.54	0.8	0.06	0.860	13.1
ES5	356	10	21.36	0.5	0.06	0.560	2.6
ES6	230	10	13.80	0.5	0.06	0.560	4.1
ES7	169	13	10.14	0.65	0.06	0.710	7.0

The catch ratios for rain events 7 and 16 are shown in Table 4.2. The similar meteorological parameters between these two rain events yield similar catch ratios on the gauges not sheltered by the overhang, which are the unshaded values (EC1, EC2, ES1 to ES7). The gauges located under the retractable overhang in rain event 16, which are shaded (EN1 to EN9), may then be compared to the same gauges in rain event 7 to determine the percent reduction in catch ratios.

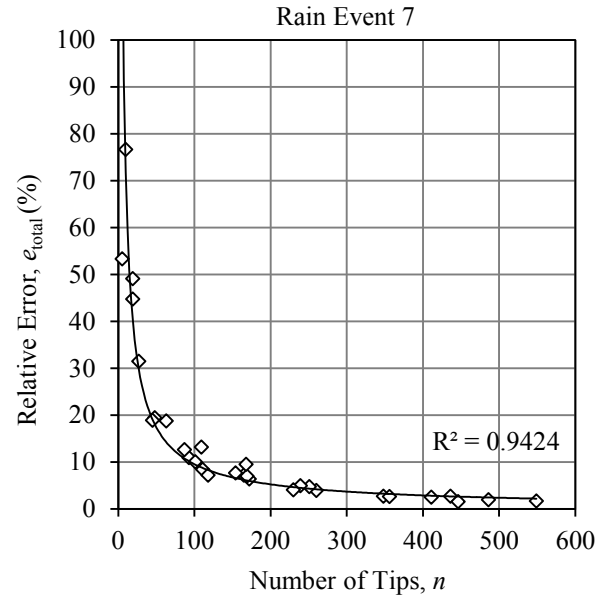


Figure 4.30 – Relative error of WDR measurements as a function of the number of tips.

Table 4.2 – Catch ratios on the east facade for rain events 7 and 16.

WDR Gauge	Catch Ratios	
	RE 7 (No OH)	RE 16 (1.2 m OH)
EN1	0.281	0.019
EN2	0.169	0.051
EN3	0.118	0.056
EN4	0.074	n/a
EN5	0.228	0.005
EN6	0.121	0.024
EN7	0.070	0.026
EN8	0.210	0.003
EN9	0.073	0.017
EC1	0.217	0.202
EC2	0.050	0.057
ES1	0.284	0.266
ES2	0.162	0.168
ES3	n/a	0.117
ES4	0.066	0.059
ES5	0.210	0.186
ES6	0.143	0.132
ES7	0.104	0.091

* Shaded rows contain gauges which are located under the retractable overhang.

By comparing similar rain events (similarity), the percent reductions in catch ratios for a 0.6 m overhang and 1.2 m overhang are obtained, and are shown in Table 4.3 and 4.4, respectively.

The effectiveness of overhang is highly dependent on the meteorological parameters. Although the meteorological parameters between two similar rain events may be alike, they are different when compared to other rain events, therefore, each comparison yields a different percent reduction in catch ratio for the same gauge, as shown in Table 4.3 and Table 4.4.

Table 4.3 – Percent reduction in catch ratios when comparing similar rain events.
East facade with a 0.6 m overhang.

East Facade – 0.6 m Overhang					
WDR Gauge	11 vs. 20	9 vs. 21	3 vs. 22	3 vs. 23	Average
EN1	73	64	81	83	75
EN2	50	44	59	61	54
EN3	32	12	46	52	36
EN4	n/a	18	35	47	33
EN5	84	82	91	93	88
N6	51	41	60	66	55
EN7	n/a	29	48	49	42
EN8	83	80	92	90	86
EN9	46	43	65	73	57

Table 4.4 – Percent reduction in catch ratios when comparing similar rain events.
East facade with a 1.2 m overhang.

East Facade – 1.2 m Overhang					
WDR Gauge	7 vs. 16	13 vs. 17	11 vs. 18	9 vs. 19	Average
EN1	93	85	94	99	93
EN2	70	66	79	94	77
EN3	52	10	50	79	48
EN4	n/a	n/a	n/a	n/a	n/a
EN5	98	99	100	100	99
EN6	80	85	90	96	88
EN7	63	55	71	87	69
EN8	98	99	100	100	99
EN9	76	77	78	93	81

4.6.2. Symmetry

To assess the effectiveness of overhang using symmetry, the gauges beneath the overhang (EN1 to EN7) are directly compared to the gauges on the other side of the facade (ES1 to ES7), which are not sheltered by an overhang. As mentioned earlier, this is possible because the prevailing wind direction during rain hours is from the east, which is normal to the east facade. By applying symmetry, the percent reduction in catch ratios for a 0.6 m overhang and 1.2 m overhang are obtained and are shown in Table 4.5 and Table 4.6, respectively.

Table 4.5 – Percent reduction in catch ratios when using symmetry.
East facade with a 0.6 m overhang.

East Facade – 0.6 m Overhang					
WDR Gauge	RE 20	RE 21	RE 22	RE 23	Average
EN1 vs. ES1	59	54	82	79	69
EN2 vs. ES2	31	24	49	45	37
EN3 vs. ES3	12	5	37	39	23
EN4 vs. ES4	n/a	50	18	39	36
EN5 vs. ES5	78	76	92	94	85
EN6 vs. ES6	45	38	57	49	47
EN7 vs. ES7	n/a	19	48	52	40

Table 4.6 – Percent reduction in catch ratios when using symmetry.
East facade with a 1.2 m overhang.

East Facade – 1.2 m Overhang					
WDR Gauge	RE 16	RE 17	RE 18	RE 19	Average
EN1 vs. ES1	93	89	91	98	93
EN2 vs. ES2	70	65	69	91	74
EN3 vs. ES3	52	29	38	77	49
EN4 vs. ES4	n/a	n/a	n/a	n/a	n/a
EN5 vs. ES5	97	99	100	100	99
EN6 vs. ES6	82	89	89	96	89
EN7 vs. ES7	71	68	70	87	74

The approximate winds that are normal to the east facade during rain, along with their corresponding wind speeds and horizontal rainfall intensities, yield slightly different wetting patterns on the east facade that are not so “symmetric”. Therefore, a comparison with the method

of similarity is required. In addition, the meteorological parameters between rain events differ from one another resulting in different percent reductions in catch ratio for the same gauge, as shown in Table 4.5 and Table 4.6.

4.6.3. Similarity vs. Symmetry

The average percent reductions in catch ratio on the east facade for both methods (similarity and symmetry) are shown in Figure 4.31 and Figure 4.32, for the 0.6 m overhang and 1.2 m overhang, respectively.

For the 0.6 m overhang, the average percent reductions in catch ratios are higher when comparing similar rain events, however, in general, there is a good agreement between both methods with 8 to 36% difference. The highest discrepancy is for gauge EN3 (36%) followed by EN2 (31%) and EN6 (14%). For other gauges, the discrepancy is below 10%. For the 1.2 m overhang, the average percent reductions in catch ratios are almost identical for both methods (0-7% difference). This consistently better agreement for the 1.2 m overhang indicates that the wider overhang is more capable of protecting the facade below it than the 0.6 m overhang when exposed to different meteorological parameters.

The average percent reductions in catch ratios, on the north facade, obtained from similarity, for the 0.6 m and 1.2 m overhang, are shown in Figure 4.33 and Figure 4.34, respectively. The predominantly easterly winds do not allow for symmetry analysis on the north facade. Therefore, the similarity approach is used to compare the average percentage reduction in catch ratios over the entire monitoring periods to the average of similar rain events.

For the 0.6 m overhang, there is a good agreement between the two, however, there are large discrepancies at NE4 and NE5. These gauges are believed to be in a transition zone, where the influence of the 0.6 m overhang begins to take hold, therefore, the area is extremely sensitive to fluctuations in wind speed, wind direction and rainfall intensity. For the 1.2 m overhang, there is a very good agreement between the two methods.

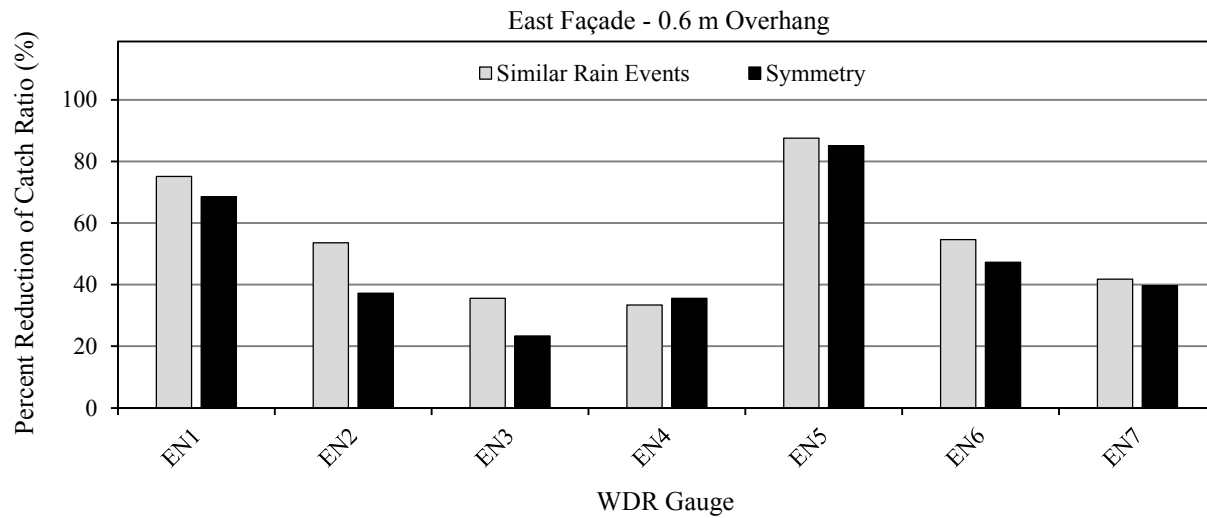


Figure 4.31 – Percent reduction in catch ratios.
(Average of similar rain events vs. average using symmetry)
East facade with a 0.6 m overhang.

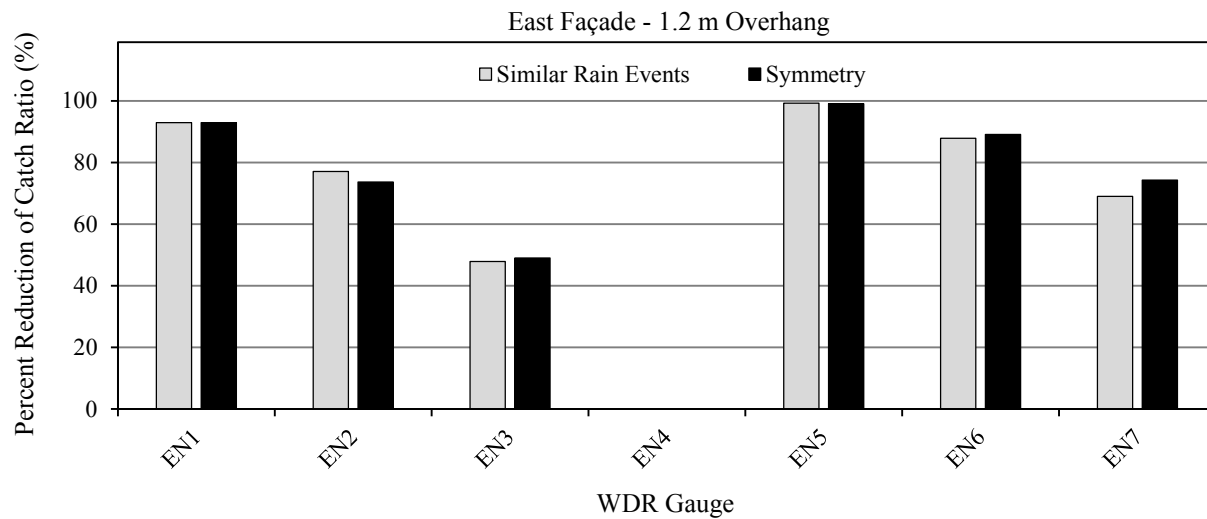


Figure 4.32 – Percent reduction in catch ratios.
(Average of similar rain events vs. average using symmetry)
East facade with a 1.2 m overhang.

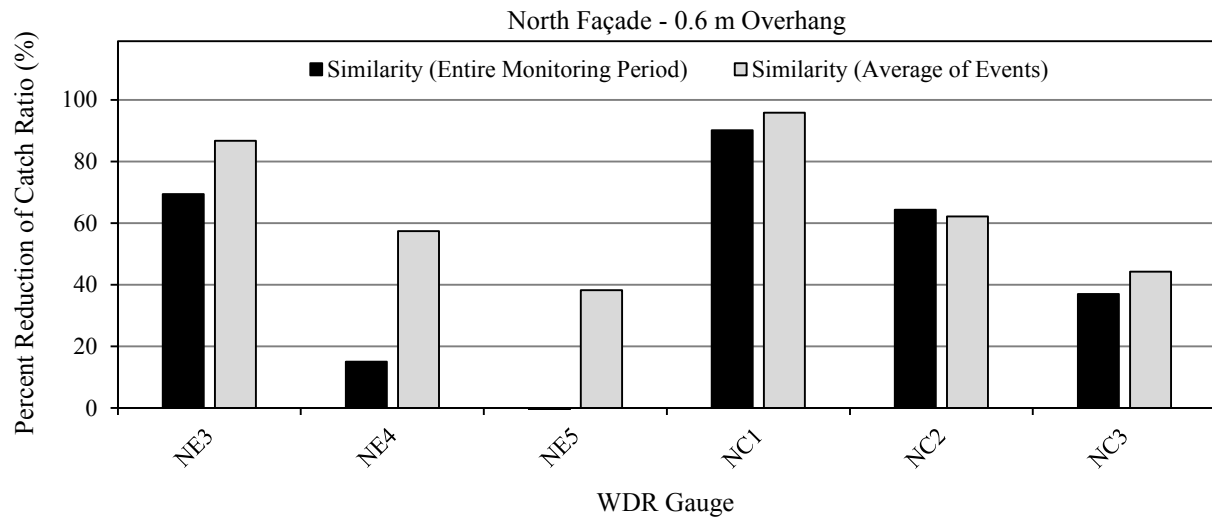


Figure 4.33 – Percent reduction in catch ratios using the similarity approach.
(Average of similar rain events vs. average of the entire monitoring period)
North facade with a 0.6 m overhang.

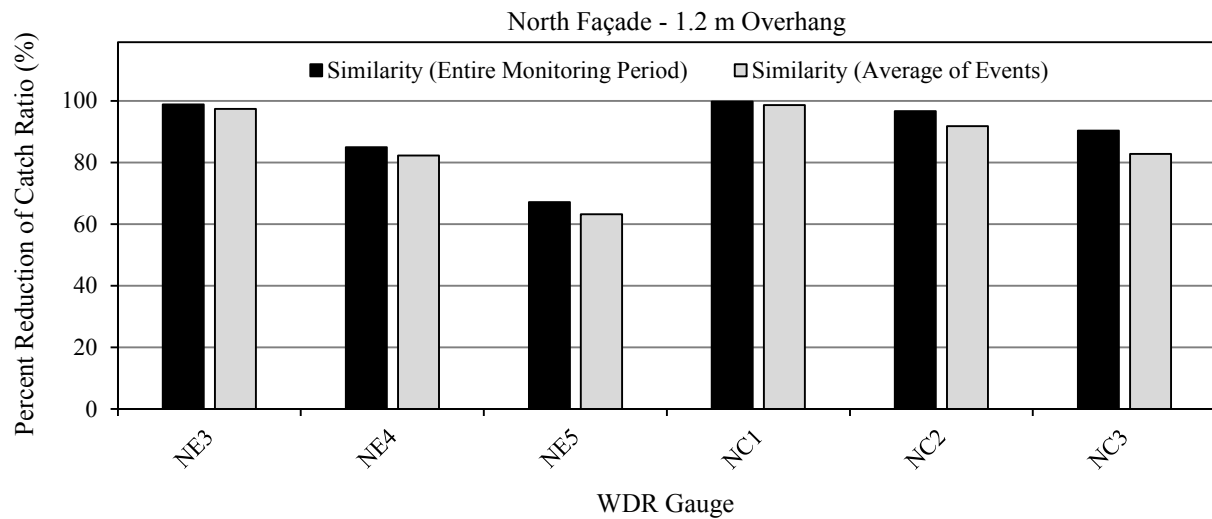


Figure 4.34 – Percent reduction in catch ratios using the similarity approach.
(Average of similar rain events vs. average of the entire monitoring period)
North facade with a 1.2 m overhang.

4.6.4. Overhang Effectiveness

For the sake of brevity, the effectiveness of overhang in the following sections is based off similarity. Given the similar results obtained by similarity and symmetry approaches, the effectiveness of overhang calculated using the similarity approach is used in the following sections for discussion. The effectiveness of the 0.6 m overhang and 1.2 m overhang are also plotted in Figure 4.35 for the east facade and in Figure 4.36 for the north facade, respectively. The following observations are made:

For a 0.6 m overhang:

- 1) The effectiveness of the overhang decreases when moving from the upper edge towards the ground and from the center of the facade towards the side edge.
- 2) The 0.6 m overhang reduces the WDR deposited on the facade, especially the area right beneath the overhang by about 70 to 90%.
- 3) At a distance of 2.4 m below the roofline (EN2 and EN6), the WDR is reduced by 50%.
- 4) At a distance of 4.9 m below the roofline (EN3, EN7, EN9), the WDR is reduced by about 30 to 60%.
- 5) The protection provided by the 0.6 m overhang extends up to 2.4 m below the overhang (EN2, EN6). The protection below this point is dependent on the wind and rain conditions and will be explored in the next sections.

For a 1.2 m overhang:

- 1) The effectiveness of the overhang decreases when moving from the upper edge towards the ground and from the center of the facade towards the side edge.
- 2) The 1.2 m overhang significantly reduces the WDR deposited on the facade, especially the area right beneath the overhang by over 90%.
- 3) At a distance of 2.4 m below the roofline (EN2 and EN6), the WDR is reduced by about 80 to 90%.
- 4) At a distance of 4.9 m below the roofline (EN3, EN7, EN9), the WDR is reduced by about 50 to 80%.

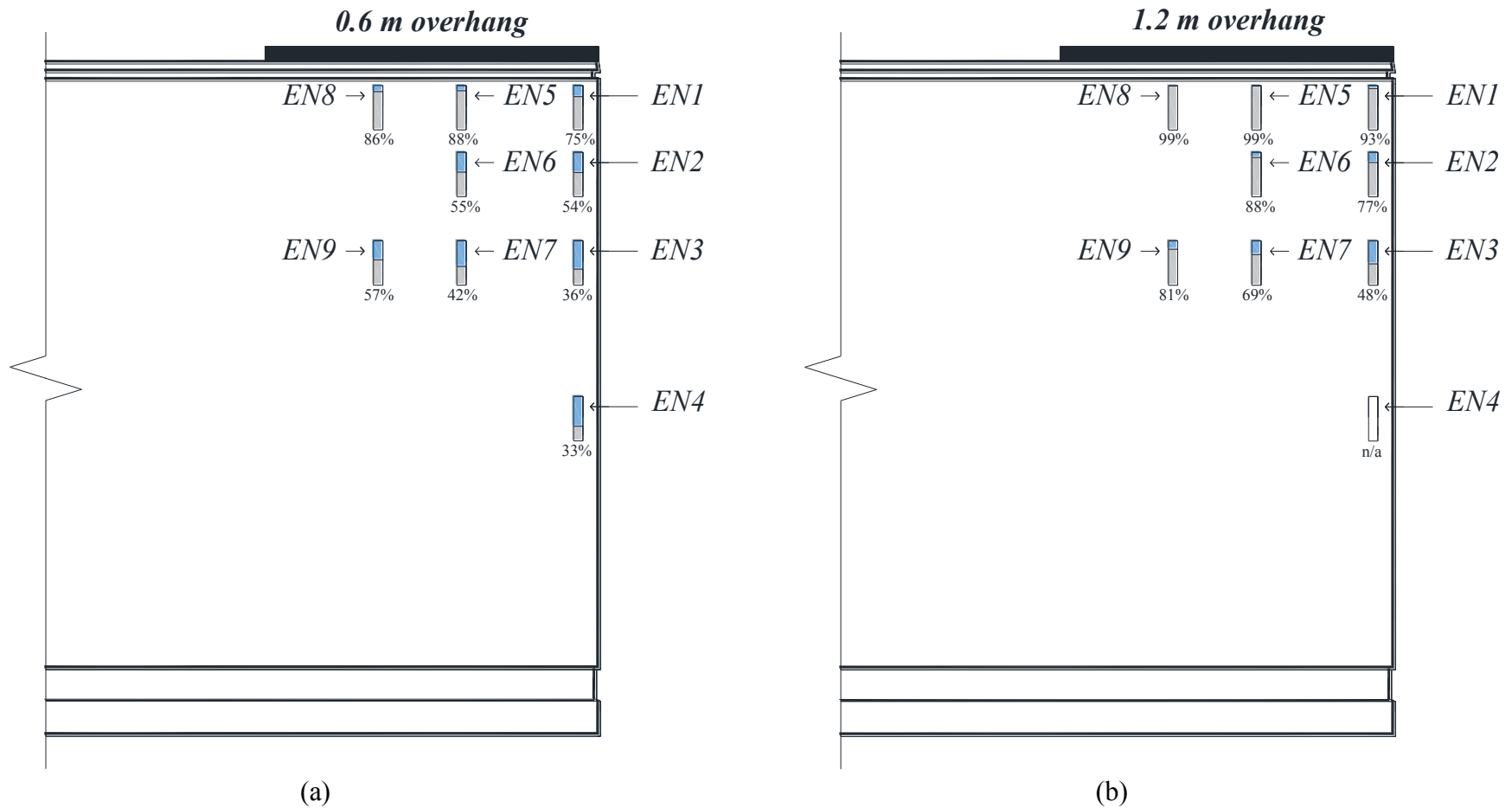
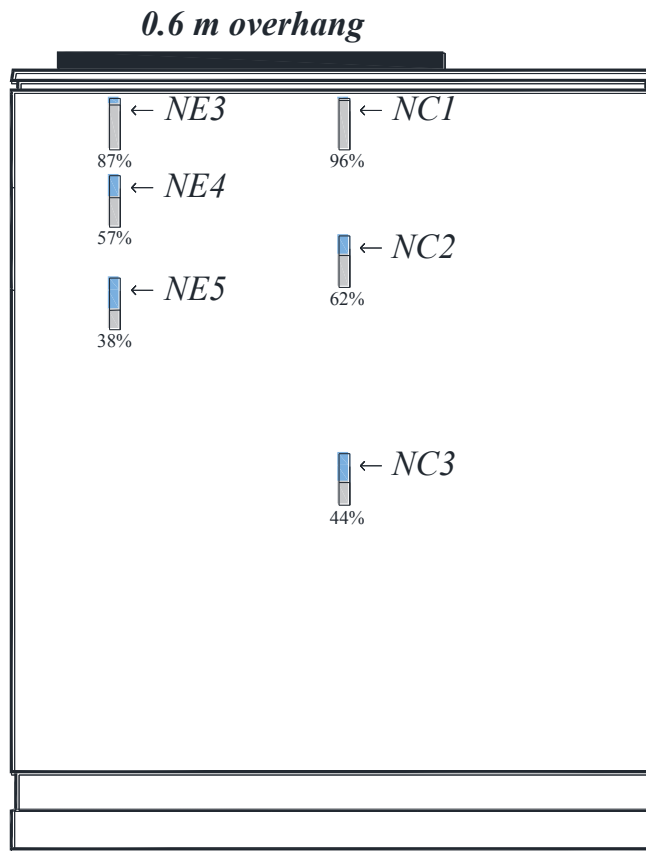


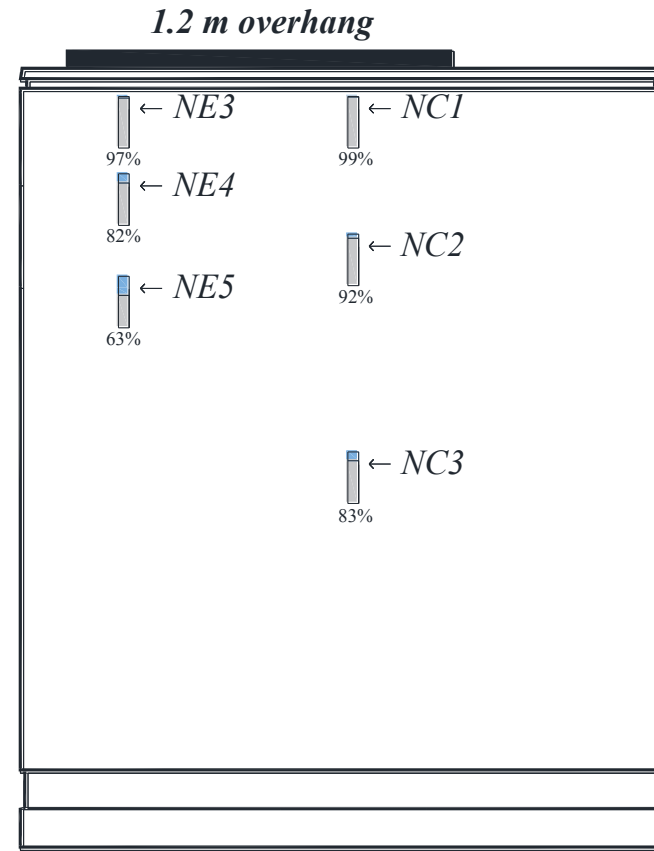
Figure 4.35 – Percent reduction in catch ratios.

East facade with (a) 0.6 m overhang and (b) 1.2 m overhang.

The percentage reduction in catch ratio is displayed (average of similar rain events). The wind speeds are predominantly in the range of 0 to 4 m/s. The wind direction is approximately normal to the east facade.



(a)



(b)

Figure 4.36 – Percent reduction in catch ratios.

North facade with (a) 0.6 m overhang and (b) 1.2 m overhang.

The percentage reduction in catch ratio is displayed (average of similar rain events). The wind speeds are predominantly in the range of 0 to 4 m/s. The wind direction is approximately normal to the east facade.

- 5) The protection provided by the 1.2 m overhang extends up to 4.9 m below the roofline (EN3, EN7, EN9).

The percent reductions of WDR on the north facade are in-line with the observations made on the east facade.

4.6.4.1. Overhang Effectiveness with Respect to Wind Speed

The overhang effectiveness with respect to wind speed is shown in Figure 4.37 and Figure 4.38 for a 0.6 m overhang and 1.2 m overhang, respectively. Only winds perpendicular to the east facade have been considered to eliminate the more complex wetting patterns caused by oblique winds. There is a direct correlation between the wind speed and the percent reduction in catch ratio for both overhang widths. The following observations are made:

For a 0.6 m overhang:

- 1) The protection provided by the overhang, with respect to wind speed, decreases as the distance from the top edge increases. For example looking at the column of gauges on the right edge of the east facade (EN1 to EN4), the protection that is provided by the overhang for the top gauge (EN1) is considerably greater compared to the protection provided by the overhang for the bottom gauge (EN4) for each wind speed range.
- 2) As the wind speed increases, the effectiveness of the overhang decreases, irrespective of the location.
- 3) The 0.6 m overhang is able to significantly reduce the amount of WDR deposited on the top edge of the facade (EN1, EN5, EN8) for low wind speeds (90 to 100%). This protection drops significantly for higher wind speeds of 2 to 4 m/s (50 to 70%) and again, albeit less drastically, for wind speeds greater than 4m/s (40 to 60%).
- 4) The gauges further down the facade (EN3, EN4, EN7, EN9) receive little to no protection from the 0.6 m overhang during higher wind speeds.

For a 1.2 m overhang:

- 1) Much like the 0.6 m overhang, the protection provided by the 1.2 m overhang, with respect to wind speed, decreases as the distance from the top edge increases. For example

looking at the column of gauges on the right edge of the east facade (EN1 to EN4), the protection at provided at the top gauge (EN1) is considerable compared to the protection provided by the bottom gauge (EN4) for every wind speed. However, the top gauge (EN1) is almost unaffected by higher wind speeds.

- 2) As the wind speed increases, the effectiveness of the overhang decreases, irrespective of the location.
- 3) The 1.2 m overhang totally eliminates the WDR deposited on the top edge of the facade (EN1, EN5, EN8) for low wind speeds (100%). This protection remains significant for higher wind speeds of 2 to 4 m/s (90 to 100%) and for wind speeds greater than 4 m/s (80 to 100%).
- 4) Contrary to the 0.6 m overhang, the 1.2 m overhang remains quite effective, further down the facade (EN3, EN7, EN9), for higher wind speeds of 2 to 4 m/s (40 to 70%) and for wind speeds greater than 4 m/s (20 to 60%).

Wind speed plays a significant role in the effectiveness of the overhangs. The wider overhang not only provides more direct shelter but is more effective during periods of higher wind speeds.

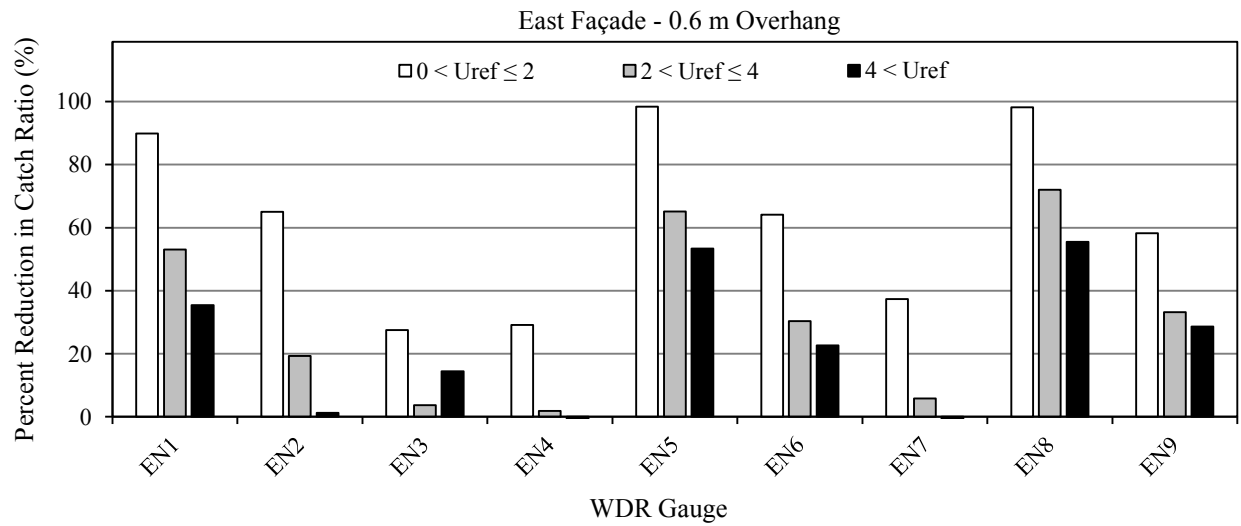


Figure 4.37 – Percent reduction in catch ratio with respect to wind speed, $\theta = 0 \pm 15^\circ$.
East facade with a 0.6 m overhang.

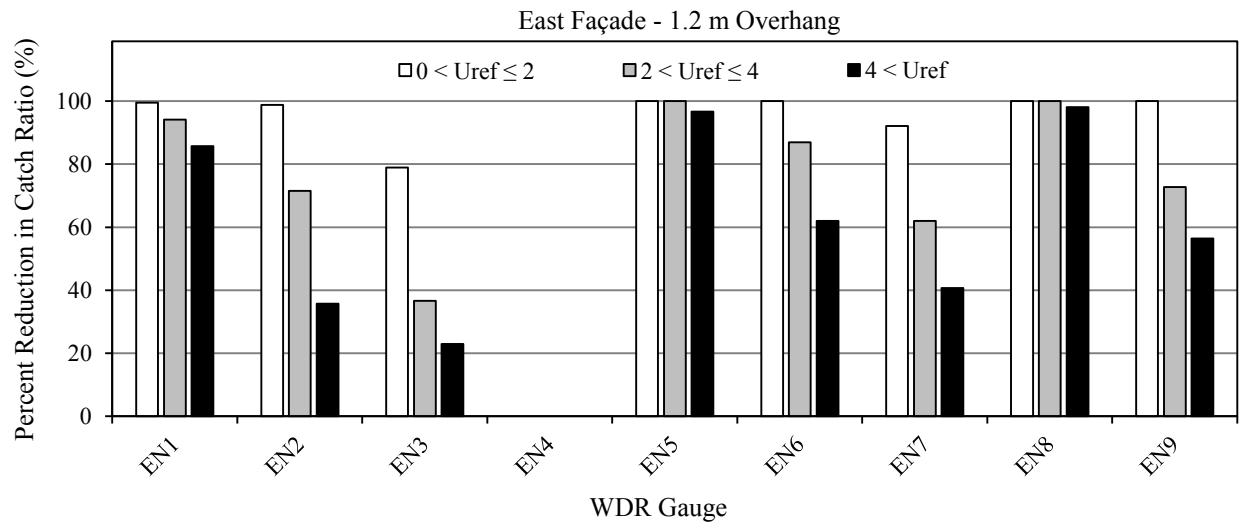


Figure 4.38 – Percent reduction in catch ratio with respect to wind speed, $\theta = 0 \pm 15^\circ$.
East facade with a 1.2 m overhang.

4.6.4.2. Overhang Effectiveness with Respect to Wind Direction

The following approaching wind angles towards the east facade are considered: 60° (left of the normal), 30° (left of the normal), 0° (normal to facade), and 30° (right of the normal), as shown in Figure 4.39. All wind speeds are considered due to limited data for oblique wind angles. The overhang effectiveness with respect to wind direction on the east facade, is shown in Figure 4.40 and Figure 4.41, for a 0.6 m overhang and 1.2 m overhang, respectively.

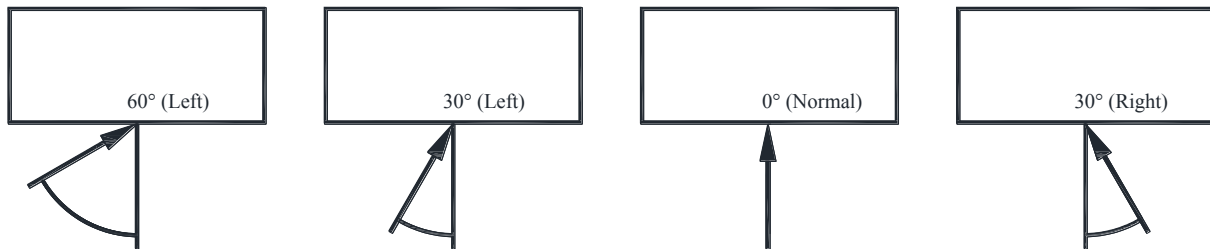


Figure 4.39 – Plan view of approaching wind angles towards the east facade.

The influence of wind direction is not as consistent as the influence of wind speed, in terms of percent reduction in catch ratios. However, a few general trends are observed.

In general, the overhang is more effective in reducing WDR for oblique winds. For example, from Figure 4.40, looking at gauge ES1 (located at the top right corner of the east facade), the effectiveness drops from 80% to 60% for wind incidence angles of 60° and 0° (normal to the facade), respectively, with the presence of a 0.6 m overhang.

However, the effectiveness of overhang depends on the location on the facade with respect to wind incidence angle. Again, looking at EN1 in Figure 4.40 (located at the right edge of the east facade), the effectiveness drops from 60% to about 50% for wind incidence angles of 0° (normal to the facade) and 30° (right of the normal), respectively. This is because EN1 is located on the right edge of the facade and is therefore prone to WDR coming from the right of the normal.

The trend observed above is more consistent for a 1.2 m overhang shown in Figure 4.41. Locations EN5 and EN8 are fully protected by the 1.2 m overhang, therefore, the effectiveness is not influenced by the wind incidence angle. Locations EN6, EN7 and EN9 are better protected when compared to the 0.6 m overhang, therefore, the effectiveness increases with the increase of

wind incidence angle - with the least protection when the wind is blowing normal to the facade. For locations on the right edge of the east facade (EN1 to EN3), the effectiveness increases for oblique winds coming from the left of the normal (30° and 60°) and decreases for oblique winds coming from the right of the normal (30°).

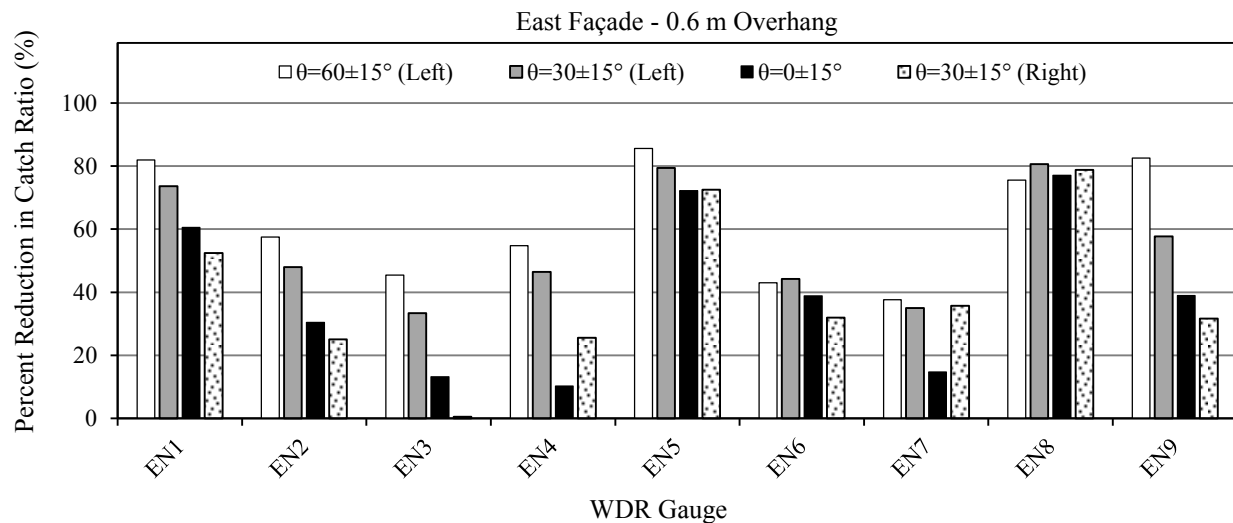


Figure 4.40 – Percent reduction in catch ratios with respect to wind direction; all wind speeds. East facade with a 0.6 m overhang.

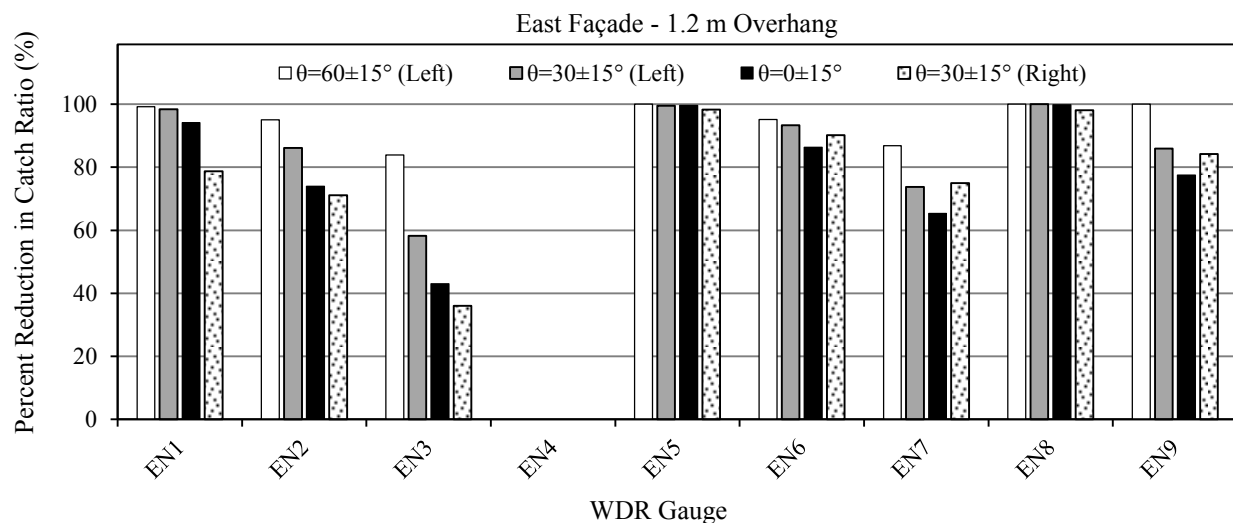


Figure 4.41 – Percent reduction in catch ratios with respect to wind direction; all wind speeds. East facade with a 1.2 m overhang.

Concluding Remarks:

- 1) The two methods of assessing the effectiveness of overhang (similarity and symmetry) compare well, however, each has its disadvantages. When comparing similar rain events, although the meteorological parameters between two similar rain events may be alike, they are different when compared to other rain events, therefore, each comparison yields a different percent reduction in catch ratio for the same gauge. When applying symmetry, the approximate easterly wind directions along with their corresponding wind speeds and horizontal rainfall intensities yield slightly different wetting patterns on the east facade that are not so “symmetric”. In addition, the meteorological parameters between rain events differ from one another resulting in different percent reductions in catch ratio for the same gauge.
- 2) The effectiveness of overhang is directly correlated to its width. Simply said, wider overhangs provide more shelter to the building facade than narrower ones. The extent of the protection is highly dependent on the meteorological parameters of wind speed and wind direction, especially for the narrower overhang. The overhangs are most effective in reducing WDR wetting on the top part of the facade, which is typically the part of the facade that receives the most rain. The overhang effectiveness decreases near the side edges and further down the facade. The protection provided by the 0.6 m generally extends to 2.4 m below the roofline, while the protection provided by the 1.2 m overhang generally extends 4.9 m below the roofline.
- 3) The effectiveness of the overhangs decrease as the wind speed increases. The wider overhang is more capable of reducing WDR deposition during higher winds speeds than the narrower overhang.
- 4) The influence of wind angle on the overhang effectiveness is not as significant as wind speed. The overhangs are more effective in reducing WDR wetting for oblique winds than winds blowing normal to the facade.

CHAPTER 5: CONCLUSION AND FUTURE WORK

Although overhangs are a classical approach in protecting building facades from rain, the effectiveness of overhang in reducing WDR wetting of building facades has never been quantified and requires further investigation. This is the first field experiment known to the author that studies the effectiveness of overhang in reducing wind-driven rain wetting on a building equipped with a retractable overhang. For the first time, the effectiveness of various widths of overhang is assessed under real-life conditions on the same part of the building. The effectiveness of overhang has been assessed using two methods: similarity and symmetry for two overhang widths. The effectiveness of overhang with respect to wind speed and wind incidence angle is analyzed. This chapter summarizes the main findings of this study and recommendations for future work.

5.1. Conclusions

A six-storey test building with a flat roof in Vancouver, British Columbia, has been equipped with a retractable overhang extendable to 1.2 m, partially covering both east and north facades. The building has been equipped to measure the meteorological parameters of wind speed, wind direction, horizontal rainfall intensity, rainfall intensity, temperature and relative humidity. To ensure the reliability of measurements, meteorological data collected on site are compared to those reported by Environment Canada at two nearby airport weather stations. The suburban exposure of the test building has been verified by comparing the wind speed and wind direction converted to the airport terrain using the measured on-site data.

Prior to assessing the effectiveness of overhangs, the characterization of the WDR load on the building facade is required. The catch ratios and wall factors are used to represent the spatial distribution of WDR across the building facade(s). The classic wetting pattern is observed on the east facade - the top corners are most wetted followed by the top and side edges; the middle of the facade remained relatively dry. The measured wall factors are compared to the ISO suggested wall factors for a multi-storey building with a flat roof. The ISO standard suggests two wall factors across all four facades, however, site measurements show that wall factors vary with respect to the location on the facade and the orientation of the facade with respect to the

prevailing wind direction during rain. The ISO suggested wall factors lead to significant overestimation of wall indices, expressing the amount of rain that would impact a real wall.

Previous experimental work on the effect of overhangs has been carried out but quantitative results are only based on single overhang widths or overhang widths on different parts of the building. Since the WDR load on any given location on the facade is highly governed by the wind flow near the building facade due to the wind and building interaction, studying various widths of overhang on the same location of the facade is crucial in understanding the effectiveness of overhangs. To measure the effectiveness of overhang, the percentage reduction of WDR in terms of catch ratios are used. The overhang effectiveness was assessed by comparing similar rain events and by applying a symmetrical distribution of WDR on the east facade, due to the predominantly easterly winds during rain. These two methods were compared and a good agreement was achieved.

The provision of overhang reduces the amount of WDR deposited on the facades, especially the areas right beneath the overhang. The 1.2 m overhang provides significantly more protection than the 0.6 m overhang. The effectiveness of the overhang(s) decreases when moving from the upper edge towards the ground and from the side edge towards the center of the facade. The wider 1.2 m overhang significantly reduces the WDR deposition on the upper portion of the facade, especially the area right below the overhang by over 90%. At a distance of 2.4 m below the roofline, the WDR is reduced by about 80 to 90%. At a distance of 4.9 m below the roofline, the WDR is reduced by about 50 to 80%. At a distance of 9.1 m below the roofline, the WDR is reduced by about 50%. The 0.6 m overhang reduces the WDR deposited on the facade, especially the area right beneath the overhang by about 70 to 90%. At a distance of 2.4 m below the roofline the WDR is reduced by 50%. At a distance of 4.9 m below the roofline, the WDR is reduced by about 20 to 50% - the same is seen at a distance 9.1 m below the roofline.

The protection provided by the overhang(s) is highly dependent on the wind speed and wind direction. As the wind speed increases, the effectiveness of the overhang decreases, irrespective of the location. The 0.6 m overhang is quite effective in protecting the upper portion of the facade: (90% to 100%) for low wind speeds between 0 to 2 m/s, however, this protection drops significantly for winds speeds higher than 4 m/s (40 to 60%). On the contrary, the 1.2 m

overhang remains quite effective at the same location, even for wind speeds higher than 4 m/s (80 to 100%).

The influence of wind direction is not as consistent as the influence of wind speed. In general, the overhangs are more effective in reducing WDR for oblique winds. For locations better protected by the overhang, with the increase of wind incidence angle, no matter which direction the wind comes from, the effectiveness of overhang increases. For locations less protected by the overhang such as locations at the right edge (EN1 to EN3), the effectiveness of overhang decreases when the wind incidence angle is from the right of the normal.

5.2. Recommendations for Future Work

As mentioned earlier, experimental data is invaluable in providing validation for semi-empirical models and CFD modelling. The wind-driven rain measurements at the test building are conducted at a sufficiently high resolution in space and time with two overhang widths. This data, in combination with future data from the test building, will be useful in quantifying the WDR loads much needed for CFD validation studies.

The long term goal of this part of the research is to develop a methodology to assess the WDR loads on any given mid-rise building and to develop a correlation between overhang width and the protection it provides for the facade below it; ultimately leading to design recommendations for roof overhang widths to effectively protect mid-rise buildings. Further research into different overhang widths is required and the results should be entered into a database where a correlation between the various widths can be made. Furthermore, since the effectiveness of overhang is highly dependent on the wind speed, a correlation between overhang protection with respect to wind speed, should be developed for various overhang widths.

REFERENCES

- Abuku, M., Blocken, B., Nore, K., Thue, J. V., Carmeliet, J., & Roels, S. (2009). On the validity of numerical wind-driven rain simulation on a rectangular low-rise building under various oblique winds. *Building and Environment*, 44(3), 621–632.
- Avendano, P. (1966). Present state of EXCO's research on rain penetration of buildings. In *CIB Working Commission on Rain Penetration*. Madrid.
- Aynsley, R. M., Melbourne, W., & Vickery, B. J. (1977). *Architectural aerodynamics*. London: Applied Science Publishers Ltd.
- Beranek, W. J., & Van Koten, H. (1979). *Limiting wind discomfort around buildings*.
- Best, A. C. (1950). The size distribution of raindrops. *Quarterly Journal of the Royal Meteorological Society*, 76, 16–36.
- Blociszewski, S. (1966). Driving rain in Poland. In *CIB Working Commission on Rain Penetration*. Madrid.
- Blocken, B. (2004). *Wind-driven rain on buildings - measurements, numerical modelling, and applications*. Ph.D. Thesis, Katholieke Universiteit Leuven, Leuven, Belgium.
- Blocken, B., & Carmeliet, J. (2000). Driving rain on building envelopes - I. Numerical estimation and full -scale experimental verification. *Journal of Building Physics*, 24(1), 61–85.
- Blocken, B., & Carmeliet, J. (2004). A review of wind-driven rain research in building science. *Journal of Wind Engineering and Industrial Aerodynamics*, 92(13), 1079–1130.
- Blocken, B., & Carmeliet, J. (2005). High-resolution wind-driven rain measurements on a low-rise building—experimental data for model development and model validation. *Journal of Wind Engineering and Industrial Aerodynamics*, 93(12), 905–928.
- Blocken, B., & Carmeliet, J. (2006a). On the accuracy of wind-driven rain measurements on buildings. *Building and Environment*, 41(12), 1798–1810.
- Blocken, B., & Carmeliet, J. (2006b). On the validity of the cosine projection in wind-driven rain calculations on buildings. *Building and Environment*, 41, 1182–1189.
- Blocken, B., & Carmeliet, J. (2006c). The influence of the wind-blocking effect by a building on its wind-driven rain exposure. *Journal of Wind Engineering and Industrial Aerodynamics*, 94(2), 101–127.
- Blocken, B., & Carmeliet, J. (2007). Validation of CFD simulations of wind-driven rain on a low-rise building facade. *Building and Environment*, 42(7), 2530–2548.
- Blocken, B., Dezsö, G., van Beeck, J., & Carmeliet, J. (2009). The mutual influence of two buildings on their wind-driven rain exposure and comments on the obstruction factor. *Journal of Wind Engineering and Industrial Aerodynamics*, 97(5-6), 180–196.





- Blocken, B., Roels, S., & Carmeliet, J. (2007). A combined CFD–HAM approach for wind-driven rain on building facades. *Journal of Wind Engineering and Industrial Aerodynamics*, 95(7), 585–607.
- Blocken, B., Van Mook, F. J. R., & Höberg, A. (1999). *Full-scale driving rain simulation in the Jules Verne Climatic Wind Tunnel. Training and mobility of researchers, access to large-scale facilities-access for researchers. Research Proposal.*
- British Standards Institution. (1984). *Draft for Development 93, Methods for assessing exposure to wind-driven rain.*
- British Standards Institution. (1992). *BS8104, Code of practice for assessing exposure of walls to wind-driven rain.*
- Campbell Scientific. (2013a). HC2-S3-L Rotronic HygroClip Relative Humidity & Temperature Probe Instruction Manual, (June).
- Campbell Scientific. (2013b). TE525 Tipping Bucket Rain Gauge Instruction Manual, (October).
- Camuffo, A. (1998). *Microclimate for Cultural Heritage.* Elsevier. Amsterdam.
- CEN. (1997). *Hygrothermal performance of buildings — Climatic data — Part 3: calculation of a driving rain index for vertical surfaces from hourly wind and rain data, Draft prEN 13013-3.*
- Choi, E. C. C. (1993). Simulation of wind-driven-rain around a building. *Journal of Wind Engineering and Industrial Aerodynamics*, 46, 721–729.
- Choi, E. C. C. (1994a). Determination of wind-driven-rain intensity on building faces. *Journal of Wind Engineering and Industrial Aerodynamics*, 51(1), 55–69.
- Choi, E. C. C. (1994b). Parameters affecting the intensity of wind-driven rain on the front face of a building. *Journal of Wind Engineering and Industrial Aerodynamics*, 53(1-2), 1–17.
- Choi, E. C. C. (2001). Wind-driven rain and driving rain coefficient during thunderstorms and non-thunderstorms. *Journal of Wind Engineering and Industrial Aerodynamics*, 89(3-4), 293–308.
- City of Vancouver. (2014). VanMap. Retrieved August 1, 2014, from <http://vancouver.ca/your-government/vanmap.aspx>
- El-Shimi, M., White, R., & Fazio, P. (1980). Influence of facade geometry on weathering. *Canadian Journal of Civil Engineering*, 7, 597–613.
- Gandemer, J. (2001). *Final report: large scale facilities, Jules Verne Climatic Wind Tunnel, Contract ERB 4062PL970118.*
- Ge, H., & Krpan, R. (2009). *Wind-driven rain study in the coastal climate of British Columbia.* Final Report, Prepared for Homeowner Protection Office, BC. Burnaby.

- Government of Canada (Environment Canada). (2013). Historical Climate Data - Access hourly, daily or monthly data for stations across Canada. Retrieved September 15, 2013, from <http://climate.weather.gc.ca/>
- Gunn, R., & Kinzer, G. D. (1949). The terminal velocity of fall for water droplets in stagnant air. *Journal of Meteorology*.
- Högberg, A. (2002). *Microclimate load: transformed weather observations for use in design of durable buildings*. Ph.D. Thesis, Chalmers University of Technology, Gothenburg, Sweden.
- Högberg, A., Kragh, M., & Van Mook, F. J. R. (1999). A comparison of driving rain measurements with different gauges. *Proceedings of the 5th Symposium on Building Physics in the Nordic Countries*, (August), 24–26.
- Hutcheon, N. B., & Handegord, G. (1995). *Building science for a cold climate* (3rd ed.). National Research Council of Canada.
- Inculet, D., & Surry, D. (1995). *Simulation of wind-driven rain and wetting patterns on buildings*. Research report for Canadian Mortgage and Housing Corporation. Ottawa.
- International Standard Organization (ISO). (2009). *Hygrothermal performance of buildings — Calculation and presentation of climatic data — Part 3: Calculation of a driving rain index for vertical surfaces from hourly wind and rain data*. ISO 15927-3:2009.
- Jessing, J. (1966). An index of driving rain in Denmark. In *CIB Working Commission on Rain Penetration*. Madrid.
- Jonesen, C., & Marcu, J. (1966). Some aspects on the rain penetration problem through the building walls in Rumania. In *CIB Working Commission on Rain Penetration*. Madrid.
- Kerr, D. (2004). *Keeping walls dry*. Canadian Mortgage and Housing Corporation (CMHC). Ottawa.
- Kragh, M. K. (1998). *Microclimatic conditions at the external surface of building envelopes*. Ph.D. Thesis, Technical University of Denmark, Kongens Lyngby, Denmark.
- Lacy, R. E. (1965). Driving-rain maps and the onslaught of rain on buildings. In *RILEM/CIB symposium on moisture problems in buildings* (p. vol.3). Helsinki.
- Lacy, R. E. (1971). An index of exposure to driving rain. *Building Research Station Digest* 127, 1–8.
- Lacy, R. E., & Shellard, H. C. (1962). An index of driving rain. *Meteorol. Mag.* 91, 177–184.
- NBCC. (2010). *National Building Code of Canada*.
- Nore, K., Blocken, B., Petter Jelle, B., Thue, J. V., & Carmeliet, J. (2007). A dataset of wind-driven rain measurements on a low-rise test building in Norway. *Building and Environment*, 42(5), 2150–2165.

- Osorio, M. (2013a). *Error analysis of the wind-driven rain measurements taken on a six-storey building in Lower Mainland, British Columbia*. Concordia University, Montreal, Canada.
- Osorio, M. (2013b). *Report on the errors associated with a wind-driven rain gauge*. Concordia University, Montreal, Canada.
- Ricketts, D., & Lovatt, J. (1996). *Survey of building envelope failures in the coastal climate of british columbia*. CMHC.
- Sepehr, S. (2013). *A numerical study of the effects of overhangs on the wind-driven rain wetting of building facades*. Master's Thesis, Ryerson University, Toronto, Canada.
- Sepehr, S., Ge, H., & Naylor, D. (2014). Effects of roof overhangs on wind-driven rain wetting of a low-rise cubic building : a numerical study. *Journal of Wind Engineering and Industrial Aerodynamics*, 125, 38–51.
- Stathopoulos, T. (1984). Design and fabrication of a wind tunnel for building aerodynamics. *Journal of Wind Engineering and Industrial Aerodynamics*, 16(2-3), 361–376.
- Straube, J., & Schumacher, C. (2006). *Driving rain loads for Canadian building design*. Research report for Canadian Mortgage and Housing Corporation, Ottawa.
- Surry, D., & Hangan, H. (2000). *Wind-driven Rain Study for the Governor's Road Project*. Research report for Canadian Mortgage and Housing Corporation, Ottawa.
- TurbulentFlow Instrumentation. (2011). *Getting Started - Series 100 Cobra Probe*. Victoria, Australia: Turbulent Flow.
- Turner, D. B. (1994). *Workbook of atmospheric dispersion estimates: an introduction to dispersion modeling* (2nd ed.). CRC Press.
- Van der Hoven, I. (1957). Power Spectrum of Horizontal Wind Speed in the Frequency Range From 0.0007 To 900 Cycles Per Hour. *Journal of Meteorology*.
- Wind Power Program. (2015). Estimating mean wind speed. Retrieved September 3, 2015, from <http://www.wind-power-program.com/windestimates.htm>

APPENDIX A

Table A.1 – Instrumentation technical specifications.

Instrument	Model	Function	Photograph	Range/Accuracy
Wind Monitor	05103	Measures wind speed and wind direction.		Range: 0–50 m s ⁻¹ Accuracy: ±0.2 m s ⁻¹ 1% of reading
Temperature & Relative Humidity Probe	HC2-S3-L	Measures temperature and relative humidity.		Temperature Sensor: Range: -50°C to +50°C Accuracy: ±0.1° C RH Sensor: Range: 0 to 100% non-condensing Accuracy: 0.8%
Horizontal Rain Gauge	TE525M	Measures the horizontal rainfall intensity.		Collection Diameter: 24.5 cm Rainfall per tip: 0.1 mm/tip Accuracy: 1% up to 50 mm/hr
Wind-Driven Rain Gauges	BSC custom made	Measures the quantity of WDR on the facade.		Collection Area: 30.5 cm by 30.5 cm Wind-driven rainfall per tip: 0.06 mm/tip

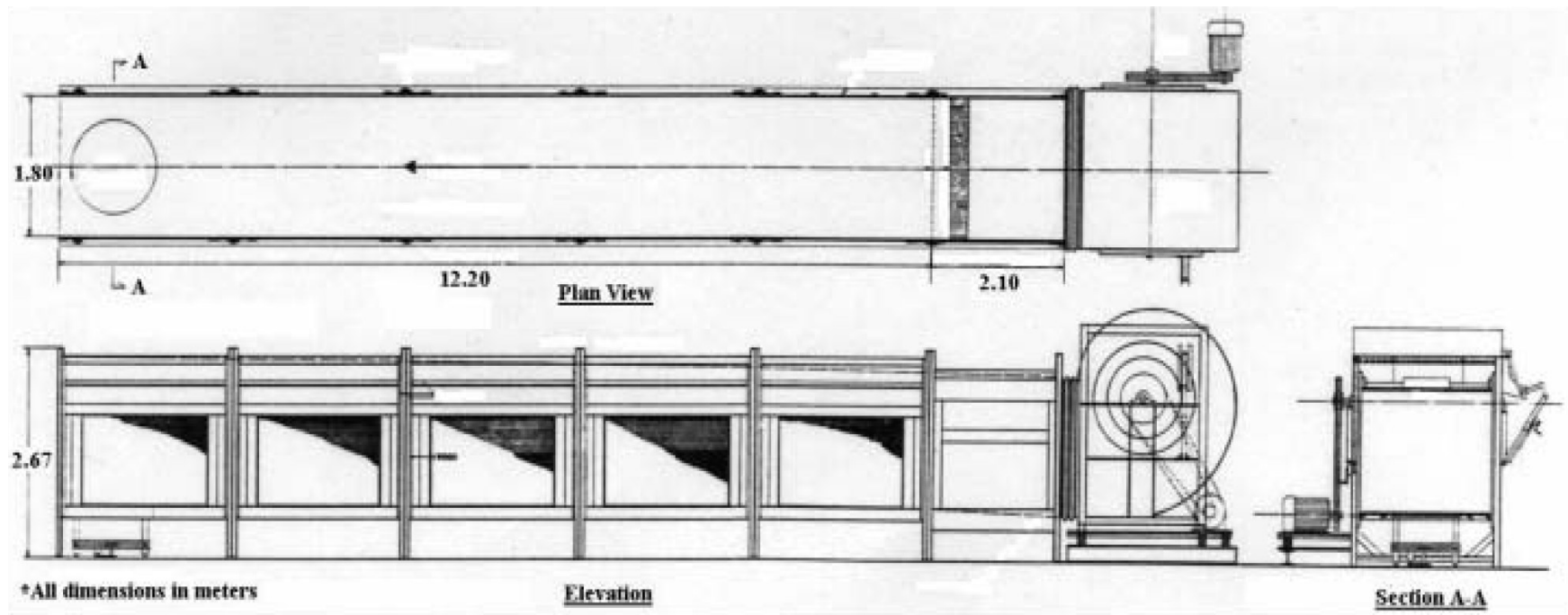


Figure A.1 – Concordia University's atmospheric boundary layer wind tunnel (from Stathopoulos 1984).

Table A.2 – Repeatability test for the wind profile velocities measured above the mechanical room roof in the wind tunnel.

Height from ground (mm)	U (m/s)		Percent Difference (%)
	Test 1	Test 2	
67	10.13	10.27	1
70	10.07	10.01	1
75	9.82	9.90	1
80	9.76	9.80	0
85	9.69	9.65	0
90	9.72	9.59	1
95	9.57	9.58	0
100	9.61	9.59	0
105	9.65	9.58	1
110	9.63	9.50	1
115	9.71	9.49	2
120	9.77	9.60	2

Table A.3 – Repeatability test for the velocities measured near the east facade in the wind tunnel.

Point	U (m/s)		Percent Difference (%)
	Test 1	Test 2	
1	5.74	6.02	5
2	5.36	5.55	3
3	5.21	5.35	3
4	5.79	5.67	2
5	6.63	6.54	1
6	4.80	5.38	11
7	3.79	4.00	5
8	3.46	3.40	2
9	4.72	5.55	15
11	2.67	2.76	3
12	2.73	2.59	6
13	2.99	2.97	1
14	4.75	5.44	13
15	2.69	3.07	12
16	4.85	5.55	13
17	3.81	4.06	6
18	3.51	3.41	3
19	5.88	5.81	1
20	5.41	5.23	4
21	5.29	4.99	6
22	5.73	5.37	7
23	6.67	6.53	2

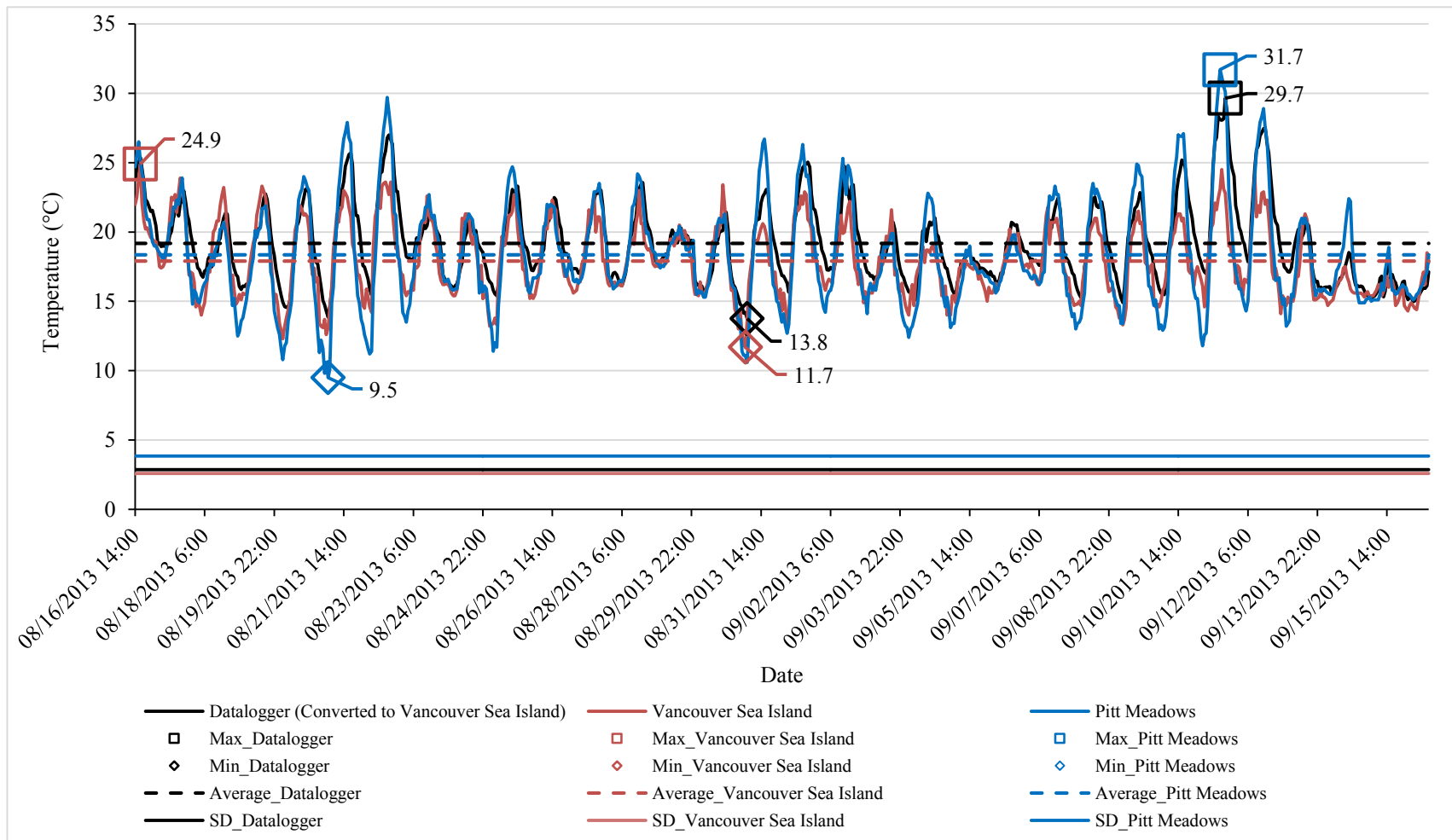


Figure A.2 – Hourly values of temperature between the test building, Vancouver Sea Island and Pitt Meadows.

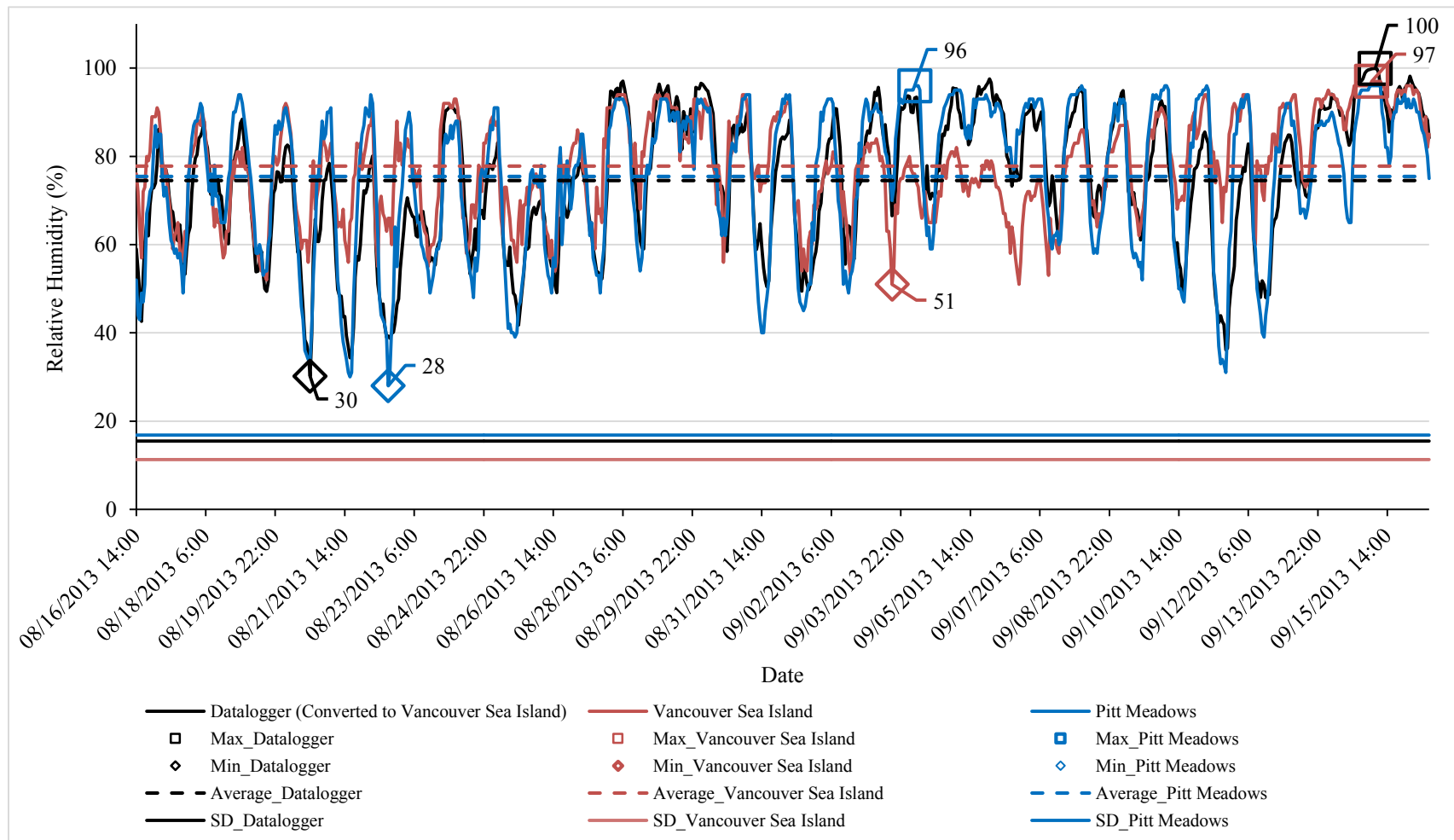


Figure A.3 – Hourly values of relative humidity between the test building, Vancouver Sea Island and Pitt Meadows.

Table A.4 – Rain events.

	Rain Event	Date	No. Rain Hours	Mean Wind Speed, U_{ref} (m/s)*	Prevailing Wind Direction*	Mean Rainfall Intensity (mm/hr)	Total R_h (mm)
No Overhang	RE 1	August 23 to September 16, 2013	67	2.07	E, ESE	1.2	83.5
	RE 2	September 20 to October 2, 2013	120	3.21	E, ESE	1.1	83.5
	RE 3	October 27 to November 19, 2013	126	2.21	E, ESE, ENE	1.2	145.8
	RE 4	November 29 to December 1, 2013	36	1.96	E, ENE	1.4	50.4
	RE 5	December 10, 2013 to January 2, 2014	162	1.46	E	0.7	111.5
	RE 6	January 7 to January 12, 2014	86	2.91	E	1.5	129.8
	RE 7	February 10 to February 25, 2014	145	2.36	E, ESE	1.1	162.8
	RE 8	March 2 to March 9, 2014	90	2.31	E, ESE	1.4	121.7
	RE 9	March 13 to April 8, 2014	164.7	2.75	E, ENE	0.9	164.7
	RE 10	April 15 to April 27, 2014	92	2.78	E, ESE, ENE	1.2	107.8
	RE 11	May 2 to May 9, 2014	56	2.73	E, ENE	1.0	55.9
	RE 12	May 19 to May 29, 2014	49	1.94	E, ESE	1.1	52.1
	RE 13	September 17 to October 4, 2014	83	2.17	ESE, E	1.0	83.5
	RE 14	October 10 to November 9, 2014	261	2.85	E, ESE	1.3	342.1
	RE 15	November 20 to December 1, 2014	105	2.75	E, ESE	1.3	140
1.2 m Overhang	RE 16	December 4, 2014 to December 11, 2014	90	3.05	ESE, E	1.5	132
	RE 17	December 16 to December 29, 2014	85	2.42	E	0.9	77.7
	RE 18	January 2 to January 29, 2015	159	2.13	E	1.5	231.3
	RE 19	January 31 to February 13, 2015	151	2.48	ESE, E	0.9	138.5
0.6 m Overhang	RE 20	March 11 to April 4, 2015	170	2.52	E	1.4	236.1
	RE 21	April 21 to May 5, 2015	72	2.57	E, ENE	0.7	53.4
	RE 22	September 17, 2015 to September 25, 2015	47	2.38	E, ENE	0.9	47.0
	RE 23	October 7, 2015 to October 12, 2015	43	2.32	E	1.0	44.9

*During rain hours.

Table A.5 – Relative error (e_{tot}) associated with the WDR measured by the gauges on the east facade.

		WDR Gauge																	
	Rain Event	EN1	EN2	EN3	EN4	EN5	EN6	EN7	EN8	EN9	EC1	EC2	ES1	ES2	ES3	ES4	ES5	ES6	ES7
No Overhang	RE 1	6.6	9.2	14.2	19.0	9.6	12.0	19.7	8.7	19.4	6.6	16.2	5.5	8.4	n/a	16.3	7.3	11.5	11.4
	RE 2	3.0	6.7	8.3	10.6	5.0	7.2	13.9	5.0	14.9	3.7	19.4	2.6	5.6	n/a	11.6	3.5	6.2	9.4
	RE 3	5.4	10.8	13.3	19.3	6.0	11.3	19.6	6.7	16.7	5.6	27.6	5.3	11.5	n/a	21.7	6.2	10.5	16.1
	RE 4	4.8	4.5	11.8	23.2	5.6	9.9	19.4	5.0	13.1	5.2	36.0	3.2	10.2	n/a	19.9	6.8	7.9	14.6
	RE 5	7.2	9.3	14.8	23.3	9.0	15.6	27.6	9.7	19.0	6.8	43.8	9.3	16.2	n/a	40.9	10.6	15.8	23.9
	RE 6	1.7	2.7	3.9	7.2	2.5	4.7	7.7	2.7	6.4	1.5	12.6	1.9	5.0	n/a	13.1	2.6	4.1	7.0
	RE 7	2.7	6.0	5.3	7.7	3.1	4.6	7.1	3.5	11.4	3.1	9.6	2.7	4.8	n/a	9.2	4.1	5.0	5.3
	RE 8	2.0	4.4	6.3	13.4	2.3	6.6	12.2	3.7	10.1	2.9	17.3	1.7	3.9	n/a	10.3	2.8	4.8	6.8
	RE 9	3.8	6.4	10.1	16.5	5.2	10.1	16.8	6.0	13.7	5.6	27.7	4.4	10.9	n/a	26.7	6.7	11.9	18.1
	RE 10	2.5	6.2	9.5	13.2	3.4	10.3	14.4	5.3	13.7	3.3	20.1	2.8	6.8	n/a	18.4	4.4	7.9	9.8
	RE 11	4.1	5.8	6.6	8.8	5.2	6.6	12.6	5.0	11.4	6.5	15.4	5.8	8.3	n/a	19.0	6.3	9.9	12.6
	RE 12	7.2	10.4	26.7	29.2	7.6	16.3	35.4	11.3	23.6	7.5	40.2	5.2	8.8	13.1	31.9	9.1	12.4	23.9
	RE 13	4.0	6.1	13.1	12.4	5.3	14.1	21.9	6.3	11.2	5.1	23.7	2.9	7.7	9.0	24.8	6.3	8.8	13.6
	RE 14	2.6	3.6	6.6	10.8	3.4	7.2	12.2	3.3	10.3	3.4	12.4	2.1	4.9	5.8	13.1	3.8	5.6	8.3
	RE 15	2.6	3.5	5.3	n/a	2.6	4.1	7.7	3.1	6.4	2.8	8.0	2.2	4.1	4.3	8.8	2.0	3.7	5.4
1.2 m Overhang	RE 16	11.7	9.1	8.8	n/a	43.8	24.2	23.4	53.3	25.6	2.7	9.6	1.6	3.5	5.2	9.9	3.0	4.9	6.3
	RE 17	29.7	18.1	14.7	n/a	-	57.4	44.7	-	54.8	6.8	22.9	5.4	9.8	14.8	28.7	8.4	11.2	19.9
	RE 18	11.0	5.3	5.5	n/a	-	17.1	10.4	-	12.6	2.5	8.2	2.3	3.8	5.0	11.1	3.1	4.3	6.5
	RE 19	66.7	47.9	38.6	n/a	-	108.3	70.8	-	86.1	5.7	27.0	4.6	9.3	12.9	24.9	6.0	10.7	16.3
0.6 m Overhang	RE 20	5.5	5.2	6.9	n/a	9.6	9.8	n/a	10.8	14.9	2.8	13.1	2.1	3.5	6.8	14.4	2.8	5.0	8.8
	RE 21	15.6	15.0	16.4	16.7	23.1	15.2	22.5	25.0	23.6	7.8	20.7	6.6	10.0	15.9	23.6	7.5	10.1	17.4
	RE 22	28.9	18.1	21.7	36.9	53.3	42.9	47.0	66.7	43.3	11.1	28.7	8.6	12.0	10.0	22.8	10.6	14.6	24.0
	RE 23	31.0	27.3	24.1	47.0	88.9	33.3	47.0	108.3	61.9	6.8	33.3	8.3	15.5	22.8	47.2	10.0	25.3	34.0

* Shaded rows contain gauges which are located under the extended overhang (0.6 m and 1.2 m).

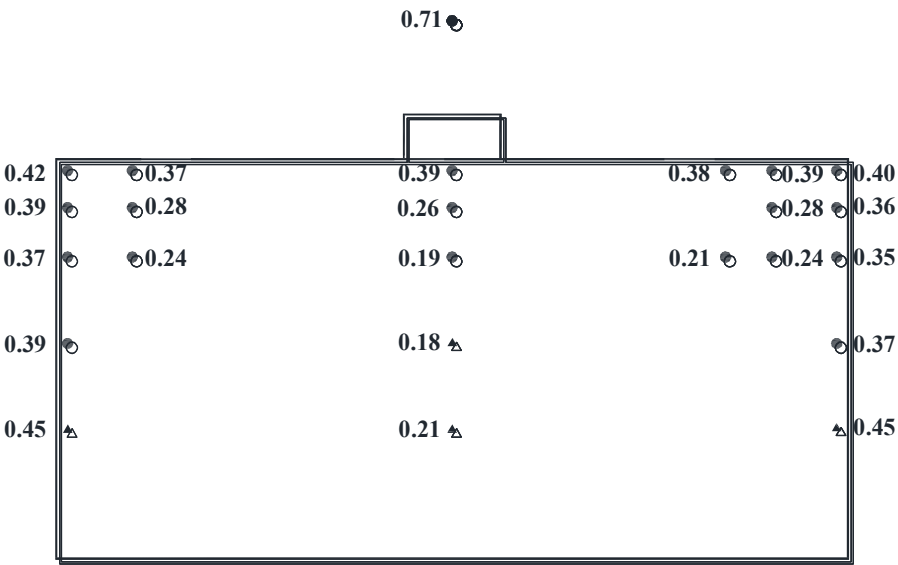
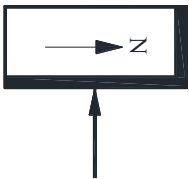
Table A.6 – Relative error (e_{tot}) associated with the WDR measured by the gauges on the north facade.

		WDR Gauge										
	Rain Event	NW1	NW2	NW3	NC1	NC2	NC3	NE1	NE2	NE3	NE4	NE5
No Overhang	RE 1	34.4	46.2	59.0	31.4	48.4	46.7	27.2	46.2	37.3	38.6	50.0
	RE 2	27.6	48.7	93.3	23.9	33.8	48.5	54.2	51.7	26.4	37.3	56.7
	RE 3	13.7	32.3	61.1	13.0	17.5	27.3	23.9	25.9	11.5	21.6	27.0
	RE 4	40.4	94.4	116.7	32.5	53.1	56.7	116.7	87.5	38.3	64.6	100.0
	RE 5	19.9	45.0	62.1	17.1	19.7	30.0	40.4	36.0	19.2	37.3	44.2
	RE 6	8.4	19.4	76.7	7.2	10.9	18.8	44.7	49.1	10.1	18.9	31.5
	RE 7	19.5	46.8	84.8	23.7	24.8	38.9	66.7	66.7	32.9	46.9	71.1
	RE 8	55.2	84.4	108.3	58.9	67.3	70.7	108.3	100.0	63.1	84.7	94.4
	RE 9	15.0	29.8	61.1	13.8	14.9	24.9	34.6	35.5	15.3	23.2	31.4
	RE 10	31.8	52.8	100.0	28.1	36.8	57.1	50.0	52.6	32.7	44.2	62.2
	RE 11	10.5	20.7	73.8	8.0	12.0	21.4	46.2	54.5	10.3	29.5	40.0
	RE 12	56.9	85.4	133.3	54.8	85.2	75.9	116.7	108.3	65.4	103.3	108.3
	RE 13	36.7	42.4	87.5	23.6	37.0	69.7	86.7	85.7	42.3	43.1	66.7
	RE 14	16.3	27.5	45.5	17.1	23.5	30.7	22.9	26.1	20.0	25.7	32.2
	RE 15	10.6	17.8	56.7	10.8	23.3	27.5	24.3	31.1	13.7	18.8	26.8
1.2 m Overhang	RE 16	31.4	42.2	103.3	-	133.3	45.8	54.5	54.8	183.3	61.1	53.3
	RE 17	18.1	28.2	86.1	-	133.3	86.1	47.9	40.5	-	103.3	75.9
	RE 18	13.3	17.3	46.7	-	183.3	39.7	25.4	21.1	-	19.0	15.9
	RE 19	43.3	60.1	87.5	-	-	-	66.7	71.8	-	-	183.3
0.6 m Overhang	RE 20	9.0	15.3	48.2	91.7	35.9	25.5	30.1	22.2	34.0	26.7	31.0
	RE 21	20.0	26.7	51.7	-	64.6	39.7	46.2	52.6	88.9	36.9	36.9
	RE 22	28.3	30.7	63.9	-	116.7	116.7	75.0	95.8	-	86.7	108.3
	RE 23	14.6	25.5	38.9	-	91.7	88.9	43.8	38.9	91.7	45.8	66.7

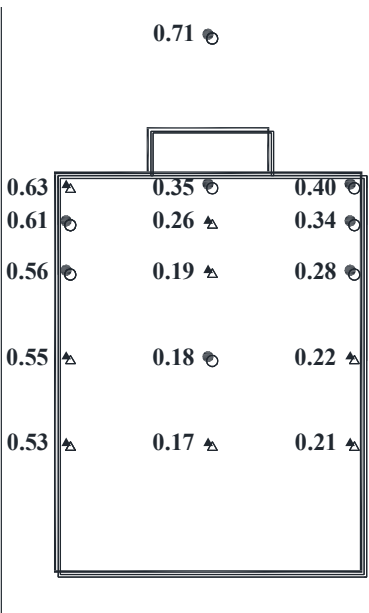
* Shaded rows contain gauges which are located under the extended overhang (0.6 m and 1.2 m).

APPENDIX B

Stand-Alone Building, $\theta = 0^\circ$



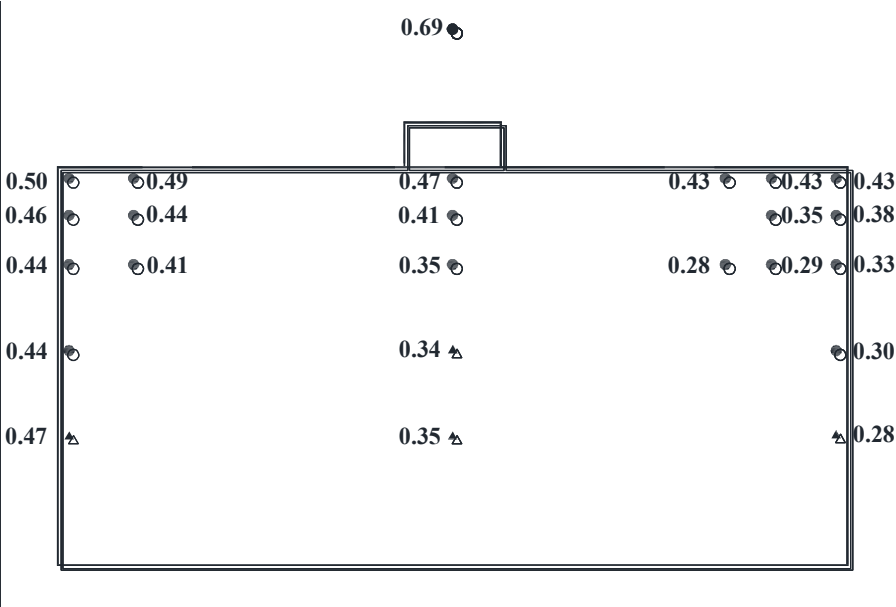
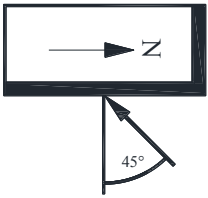
(a)



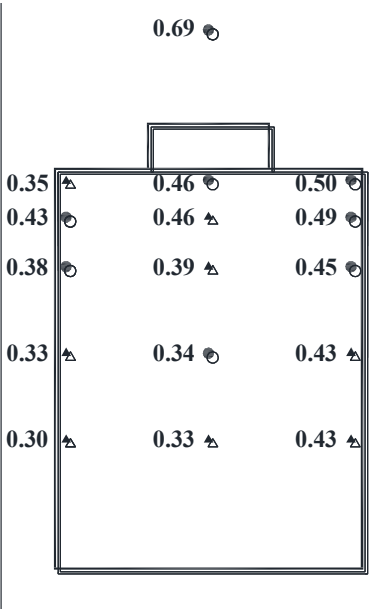
(b)

Figure B.1 – Normalized velocities on the (a) East facade, (b) North facade
Stand-alone test building, $\theta = 0^\circ$.

Stand-Alone Building, $\theta = 45^\circ$ (From North-East) $^\circ$



(a)



(b)

Figure B.2 – Normalized velocities on the (a) East facade, (b) North facade
Stand-alone test building, $\theta = 45^\circ$ (from north-east).

A diagram showing a rectangular box. Inside the box, there is a horizontal arrow pointing to the right, followed by the letter 'Z'. Below the box, there is a vertical arrow pointing upwards towards the bottom center of the box.



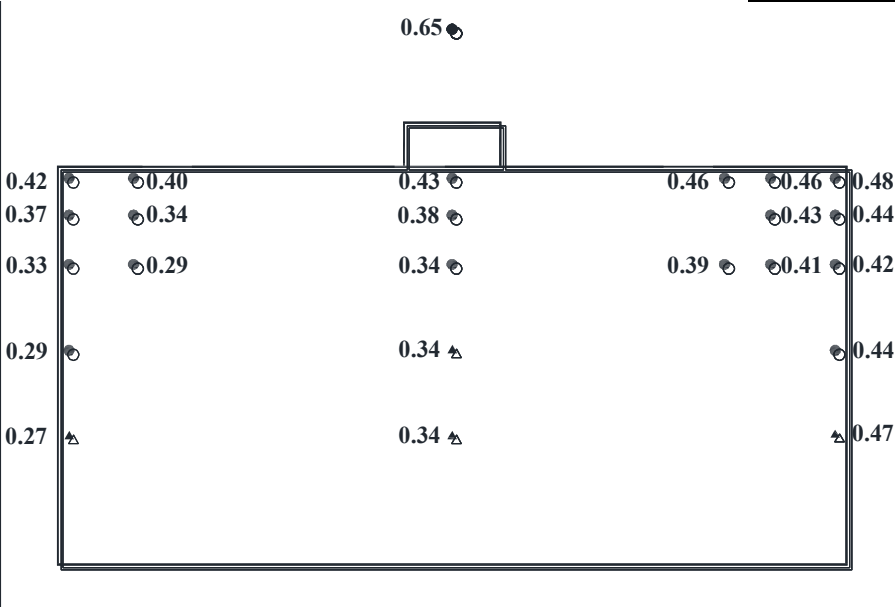
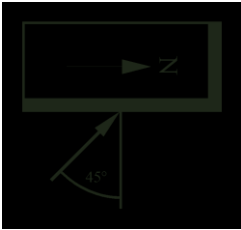
B-3

A diagram of a horizontal beam. At its right end, there is a vertical reaction force represented by an arrow pointing upwards, labeled 45° .

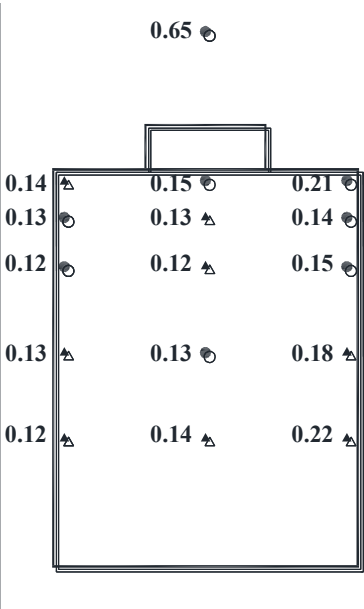


B-4

Building with Surroundings, $\theta = 45^\circ$ (From South-East)



(a)



(b)

Figure B.5 – Normalized velocities on the (a) East facade, (b) North facade
Test building with surrounding buildings, $\theta = 45^\circ$ (from south-east).

Table B.1 – Summary of On-Site Weather Conditions for the Different Monitoring Periods.

		Entire Monitoring Period	No Overhang	0.6 m Overhang	1.2 m Overhang
Wind Direction Frequency (%)	All Hours	East-North-East	6	7	5
		East	17	21	14
		East-South-East	16	20	15
	Rain Hours	East-North-East	12	13	15
		East	29	34	30
		East-South-East	19	23	15
Wind Speed Frequency (%)	All Hours	> 0-2 m/s	64	63	61
		> 2-4 m/s	31	31	33
		> 4-6 m/s	4	5	4
		> 6 m/s	1	1	1
	Rain Hours	> 0-2 m/s	42	43	40
		> 2-4 m/s	47	46	50
		> 4-6 m/s	8	8	6
		> 6 m/s	3	2	3
Rainfall Intensity Frequency (%)		> 0-2 mm/hr	84	84	78
		> 2-4 mm/hr	14	13	18
		> 4-6 mm/hr	3	3	3
		> 6 mm/hr	1	1	1

Table B.2 – Catch ratios for each monitoring period.

Catch Ratios				
	WDR Gauge	No Overhang	0.6 m Overhang	1.2 m Overhang
East Facade	EN1	0.199	0.079	0.015
	EN2	0.141	0.096	0.035
	EN3	0.085	0.075	0.049
	EN4	0.055	0.048	
	EN5	0.167	0.045	0.001
	EN6	0.091	0.057	0.012
	EN7	0.055	0.045	0.019
	EN8	0.157	0.037	0.001
	EN9	0.066	0.038	0.014
	EC1	0.173	0.174	0.186
	EC2	0.042	0.051	0.049
	ES1	0.213	0.208	0.213
	ES2	0.119	0.125	0.131
	ES3	0.093	0.095	0.097
	ES4	0.049	0.047	0.049
	ES5	0.158	0.178	0.173
	ES6	0.106	0.088	0.110
	ES7	0.074	0.070	0.074
North Facade	NW1	0.042	0.059	0.039
	NW2	0.023	0.041	0.027
	NW3	0.008	0.022	0.006
	NC1	0.045	0.004	0.000
	NC2	0.032	0.011	0.001
	NC3	0.026	0.016	0.002
	NE1	0.012	0.018	0.011
	NE2	0.013	0.021	0.014
	NE3	0.042	0.013	0.000
	NE4	0.020	0.017	0.003
	NE5	0.015	0.017	0.005

* Shaded rows contain gauges which are located under the retractable overhang.

Table B.3 – Comparison of measured wall factors with ISO suggested wall factors

	Distance from Roofline (m)	WDR Gauge	ISO Suggested Wall Factors	Measured Wall Factors			Percent Difference (%)		
				No OH	0.6 m OH	1.2 m OH	No OH	0.6 m OH	1.2 m OH
East Facade	0.6 m	EN1	0.50	0.49	0.19	0.04	2	62	93
		EN5	0.50	0.41	0.11	0.00	18	78	99
		EN8	0.50	0.39	0.09	0.00	23	82	100
		EC1	0.50	0.43	0.42	0.45	15	17	11
		ES5	0.50	0.39	0.42	0.41	23	15	17
		ES1	0.50	0.52	0.49	0.51	-5	1	-2
	2.4 m	EN2	0.50	0.36	0.23	0.09	29	53	83
		EN6	0.50	0.23	0.14	0.03	54	72	94
		ES6	0.50	0.27	0.21	0.27	46	57	46
		ES2	0.50	0.30	0.31	0.32	40	39	35
	4.9 m	EN3	0.20	0.22	0.19	0.12	-11	5	38
		EN7	0.20	0.14	0.12	0.05	28	42	76
		EN9	0.20	0.17	0.10	0.04	13	52	82
		EC2	0.20	0.11	0.13	0.12	45	36	38
		ES7	0.20	0.19	0.18	0.19	3	11	5
		ES3	0.20	0.23	0.24	0.25	-15	-20	-24
	9.1 m	EN4	0.20	0.16	0.13		22	34	
		ES4	0.20	0.14	0.13	0.14	30	35	32
North Facade	0.6 m	NW1	0.5	0.67	0.80	0.74	-34	-60	-48
		NC1	0.5	0.75	0.05	0.00	-51	89	99
		NE3	0.5	0.67	0.17	0.01	-35	67	97
	2.4 m	NW2	0.5	0.33	0.50	0.48	33	-1	4
		NE4	0.5	0.35	0.25	0.08	31	51	84
		NE1	0.5	0.21	0.24	0.21	59	53	58
	3.7 m	NC2	0.2	0.52	0.17	0.02	-160	13	92
	4.9 m	NW3	0.2	0.11	0.26	0.10	43	-32	50
		NE5	0.2	0.25	0.26	0.13	-26	-31	34
		NE2	0.2	0.22	0.28	0.26	-11	-38	-31
	9.1 m	NC3	0.2	0.43	0.25	0.09	-113	-26	55

* Shaded rows contain gauges which are located under the retractable overhang.

Table B.4 – Catch ratios for rain events used to assess the effectiveness of overhang.

	No Overhang								1.2 m Overhang					0.6 m Overhang			
	E7	E9	E11	E12	E13	E14	E15		E16	E17	E18	E19		E20	E21	RE22	RE23
W1	0.002	0.003	0.001	0.008	0.003	0.010	0.008		0.008	0.004	0.003	0.004		0.006	0.011	0.001	0.001
NW1	0.036	0.066	0.068	0.022	0.029	0.042	0.056		0.025	0.064	0.050	0.022		0.067	0.074	0.053	0.037
NW2	0.019	0.029	0.032	0.017	0.025	0.027	0.036		0.019	0.036	0.034	0.019		0.042	0.050	0.045	0.029
NW3	0.007	0.011	0.013	0.005	0.005	0.007	0.010		0.005	0.009	0.008	0.003		0.011	0.017	0.027	0.017
NC1	0.039	0.075	0.087	0.025	0.032	0.044	0.059		0.000	0.001	0.000	0.000		0.001	0.001	0.001	0.001
NC2	0.031	0.052	0.060	0.019	0.023	0.029	0.021		0.002	0.004	0.001	0.000		0.011	0.015	0.009	0.005
NC3	0.028	0.037	0.036	0.018	0.013	0.023	0.025		0.002	0.009	0.005	0.000		0.017	0.020	0.009	0.008
NE1	0.009	0.019	0.020	0.007	0.007	0.013	0.019		0.007	0.018	0.013	0.006		0.019	0.021	0.019	0.015
NE2	0.009	0.019	0.018	0.010	0.009	0.016	0.021		0.009	0.023	0.018	0.010		0.022	0.022	0.022	0.017
NE3	0.036	0.067	0.069	0.025	0.029	0.040	0.051		0.001	0.001	0.001	0.000		0.018	0.006	0.001	0.005
NE4	0.015	0.031	0.036	0.012	0.012	0.022	0.028		0.002	0.008	0.004	0.000		0.020	0.022	0.013	0.008
NE5	0.012	0.021	0.023	0.010	0.011	0.017	0.021		0.003	0.012	0.007	0.001		0.019	0.022	0.011	0.009
EN1	0.281	0.233	0.303	0.132	0.158	0.197	0.213		0.019	0.023	0.018	0.003		0.082	0.084	0.027	0.024
EN2	0.169	0.158	0.184	0.104	0.127	0.164	0.151		0.051	0.043	0.039	0.010		0.092	0.088	0.039	0.037
EN3	0.118	0.100	0.118	0.051	0.068	0.086	0.100		0.056	0.061	0.059	0.021		0.080	0.088	0.033	0.030
EN4	0.074	0.073	0.091	0.048	0.061	0.060	0.000		n/a	n/a	n/a	n/a		n/a	0.060	0.026	0.022
EN5	0.228	0.202	0.240	0.112	0.146	0.172	0.200		0.005	0.001	0.000	0.000		0.039	0.036	0.011	0.008
EN6	0.121	0.100	0.118	0.056	0.074	0.098	0.101		0.024	0.011	0.012	0.004		0.057	0.058	0.027	0.023
EN7	0.070	0.066	0.074	0.037	0.047	0.055	0.056		0.026	0.021	0.021	0.009		n/a	0.047	0.022	0.022
EN8	0.210	0.168	0.192	0.096	0.134	0.172	0.178		0.003	0.001	0.000	0.000		0.033	0.034	0.009	0.011
EN9	0.073	0.071	0.080	0.051	0.073	0.071	0.066		0.017	0.017	0.018	0.005		0.043	0.040	0.020	0.015
EC1	0.217	0.184	0.207	0.126	0.152	0.185	0.199		0.202	0.174	0.195	0.168		0.170	0.145	0.128	0.126
EC2	0.050	0.045	0.048	0.027	0.044	0.055	0.054		0.057	0.046	0.049	0.045		0.052	0.045	0.032	0.032
ES1	0.284	0.196	0.232	0.160	0.220	0.245	0.252		0.266	0.216	0.204	0.182		0.200	0.183	0.148	0.119
ES2	0.162	0.112	0.130	0.098	0.118	0.136	0.130		0.168	0.124	0.127	0.112		0.133	0.115	0.077	0.068
ES3	n/a	n/a	n/a	0.068	0.089	0.105	0.105		0.117	0.086	0.096	0.092		0.091	0.083	0.053	0.049
ES4	0.066	0.041	0.046	0.036	0.046	0.057	0.054		0.059	0.047	0.046	0.049		0.046	0.040	0.032	0.035
ES5	0.210	0.155	0.168	0.117	0.144	0.161	0.170		0.186	0.151	0.174	0.174		0.180	0.150	0.134	0.125
ES6	0.143	0.098	0.111	0.071	0.091	0.121	0.121		0.132	0.104	0.107	0.101		0.104	0.094	0.065	0.045
ES7	0.104	0.062	0.074	0.056	0.066	0.085	0.086		0.091	0.067	0.071	0.070		0.066	0.058	0.043	0.045
S1	0.096	0.074	0.057	0.068	0.098	0.129	0.095		0.173	0.054	0.063	0.170		0.083	0.046	0.101	0.198

* Shaded rows contain gauges which are located under the retractable overhang.

APPENDIX C

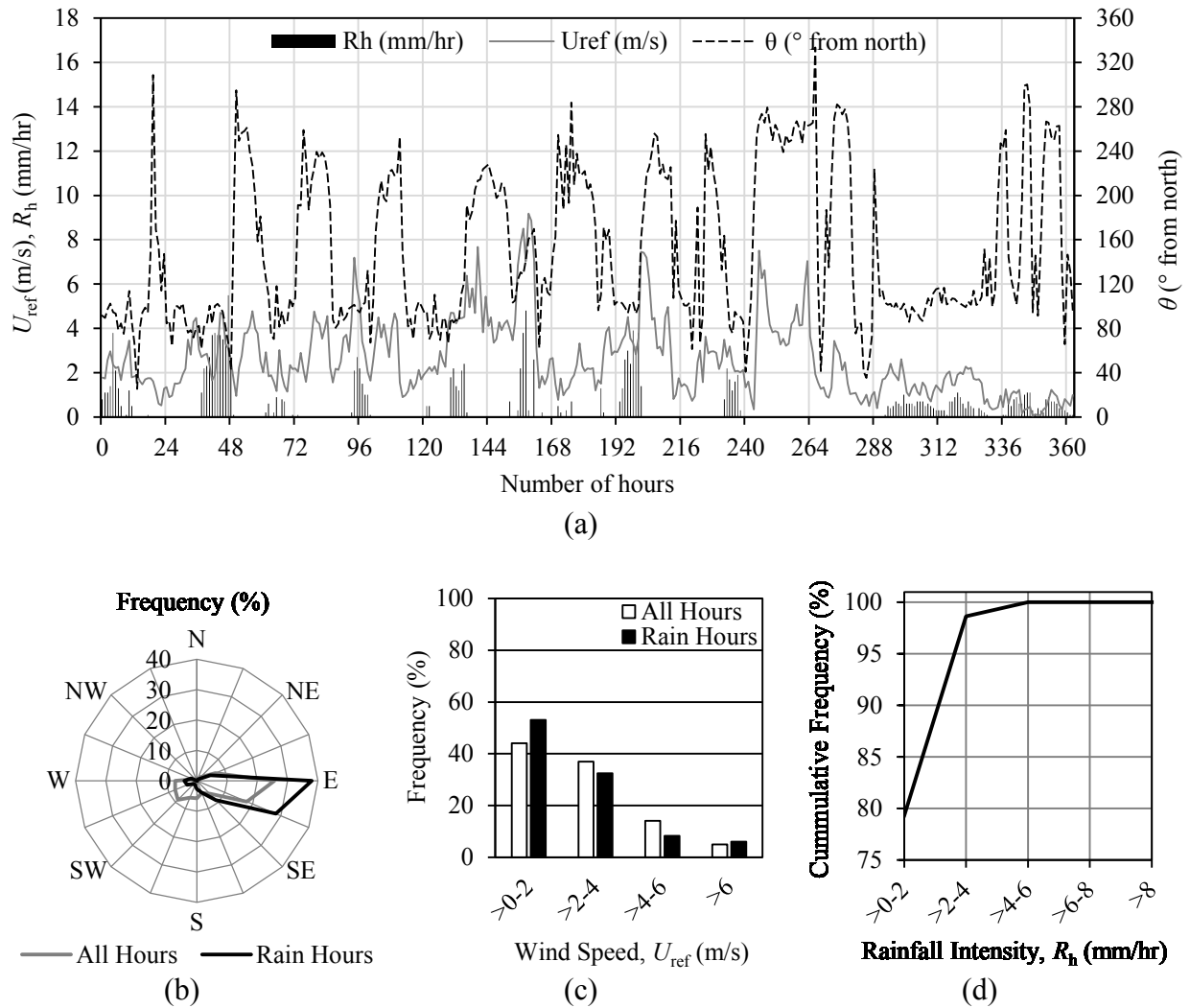


Figure C.1 – Rain event 7.

(a) Hourly horizontal rainfall intensity (R_h), wind speed (U_{ref}), and wind direction (θ); (b) Wind direction frequency; (c) Wind speed frequency; and (d) Rainfall intensity cumulative frequency.

Table C.1 – Rain event 7 summary.

No. Rain Hours	145
Total Horizontal Rainfall, R_h (mm)	162.8
Average Horizontal Rainfall Intensity (mm/hr)	1.1
Average Wind Speed (Rain Hours), U_{ref} (m/s)	2.36
Prevailing Wind Direction (Rain Hours)	East

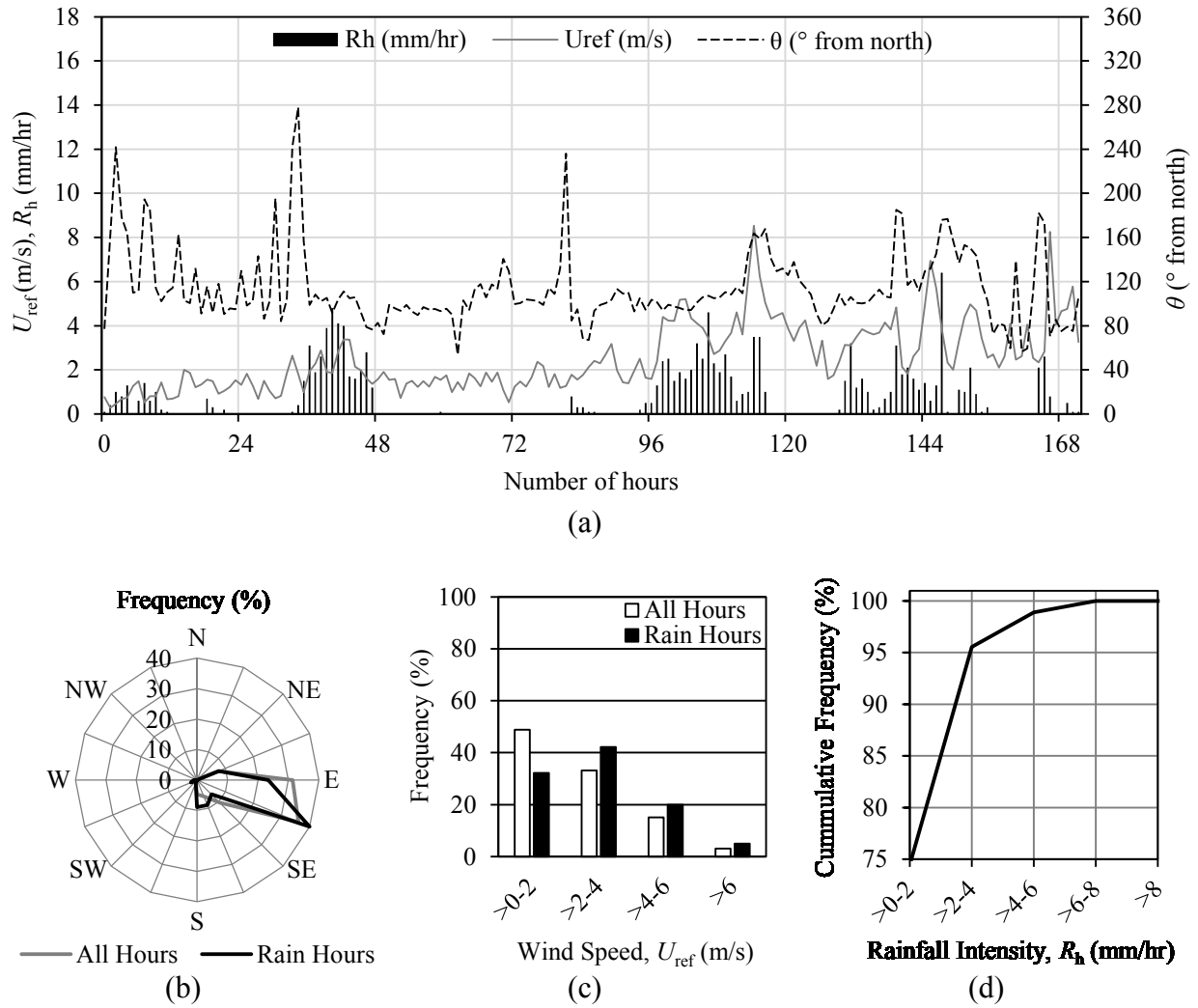


Figure C.2 - Rain event 16.

(a) Hourly horizontal rainfall intensity (R_h), wind speed (U_{ref}), and wind direction (θ); (b) Wind direction frequency; (c) Wind speed frequency; and (d) Rainfall intensity cumulative frequency.

Table C.2 – Rain event 16 summary.

No. Rain Hours	90
Total Horizontal Rainfall, R_h (mm)	132
Average Horizontal Rainfall Intensity (mm/hr)	1.5
Average Wind Speed (Rain Hours), U_{ref} (m/s)	3.05
Prevailing Wind Direction (Rain Hours)	East-south-east

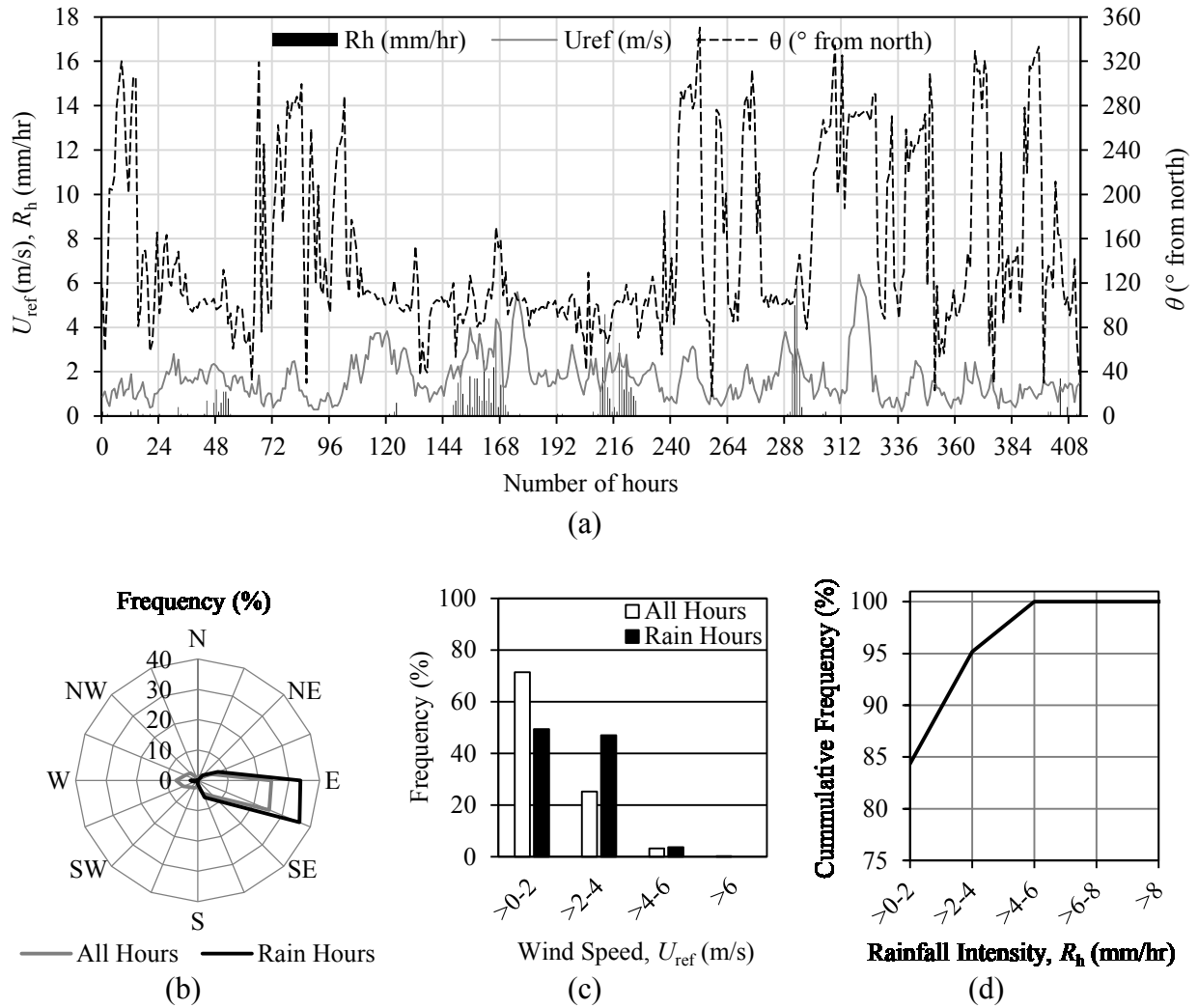


Figure C.3 - Rain event 13.

(a) Hourly horizontal rainfall intensity (R_h), wind speed (U_{ref}), and wind direction (θ); (b) Wind direction frequency; (c) Wind speed frequency; and (d) Rainfall intensity cumulative frequency.

Table C.3 – Rain event 13 summary

No. Rain Hours	83
Total Horizontal Rainfall, R_h (mm)	83.5
Average Horizontal Rainfall Intensity (mm/hr)	1.0
Average Wind Speed (Rain Hours), U_{ref} (m/s)	2.17
Prevailing Wind Direction (Rain Hours)	East-south-east

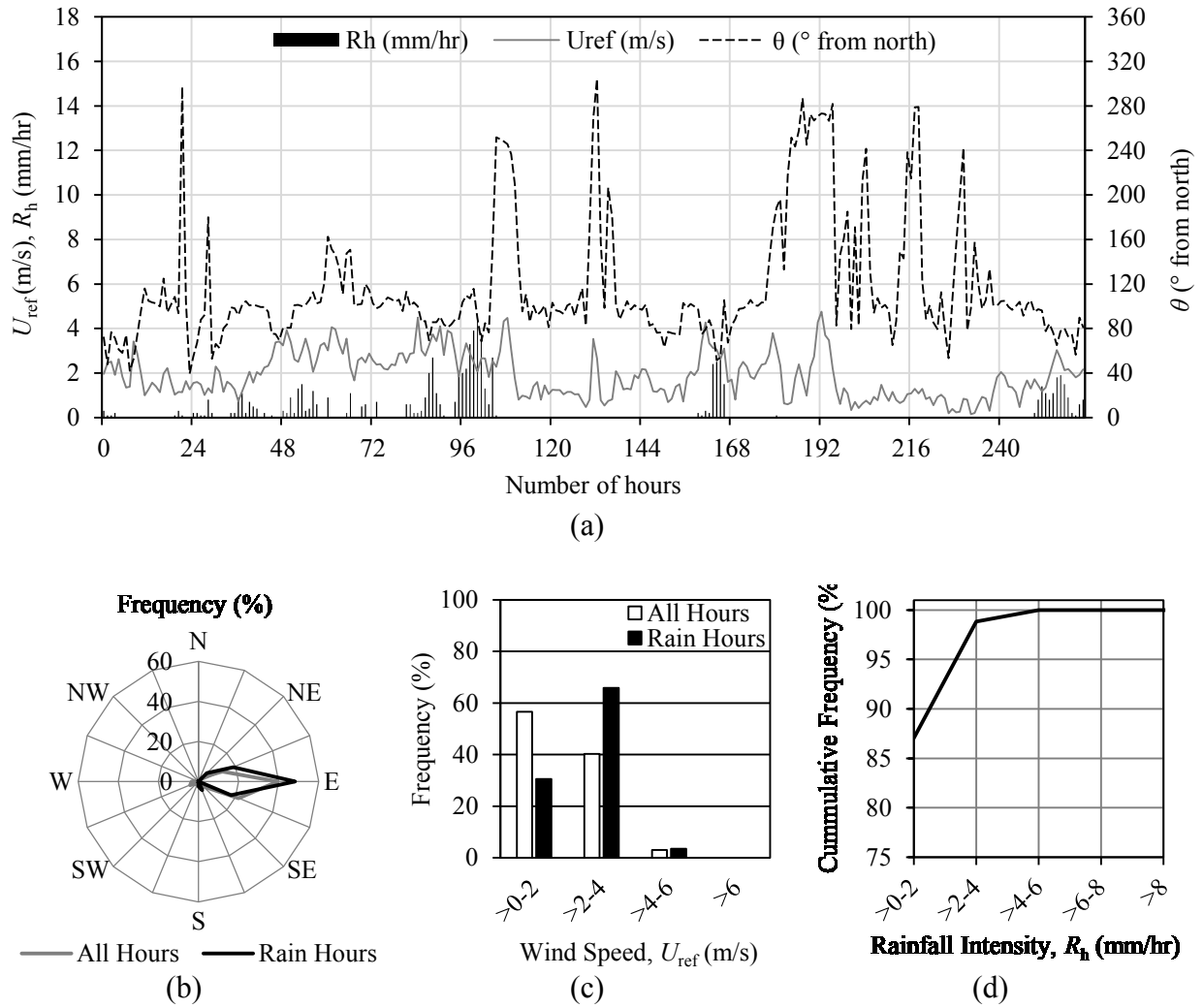


Figure C.4 - Rain event 17.

(a) Hourly horizontal rainfall intensity (R_h), wind speed (U_{ref}), and wind direction (θ); (b) Wind direction frequency; (c) Wind speed frequency; and (d) Rainfall intensity cumulative frequency.

Table C.4 – Rain event 17 summary

No. Rain Hours	85
Total Horizontal Rainfall, R_h (mm)	77.7
Average Horizontal Rainfall Intensity (mm/hr)	0.9
Average Wind Speed (Rain Hours), U_{ref} (m/s)	2.42
Prevailing Wind Direction (Rain Hours)	East

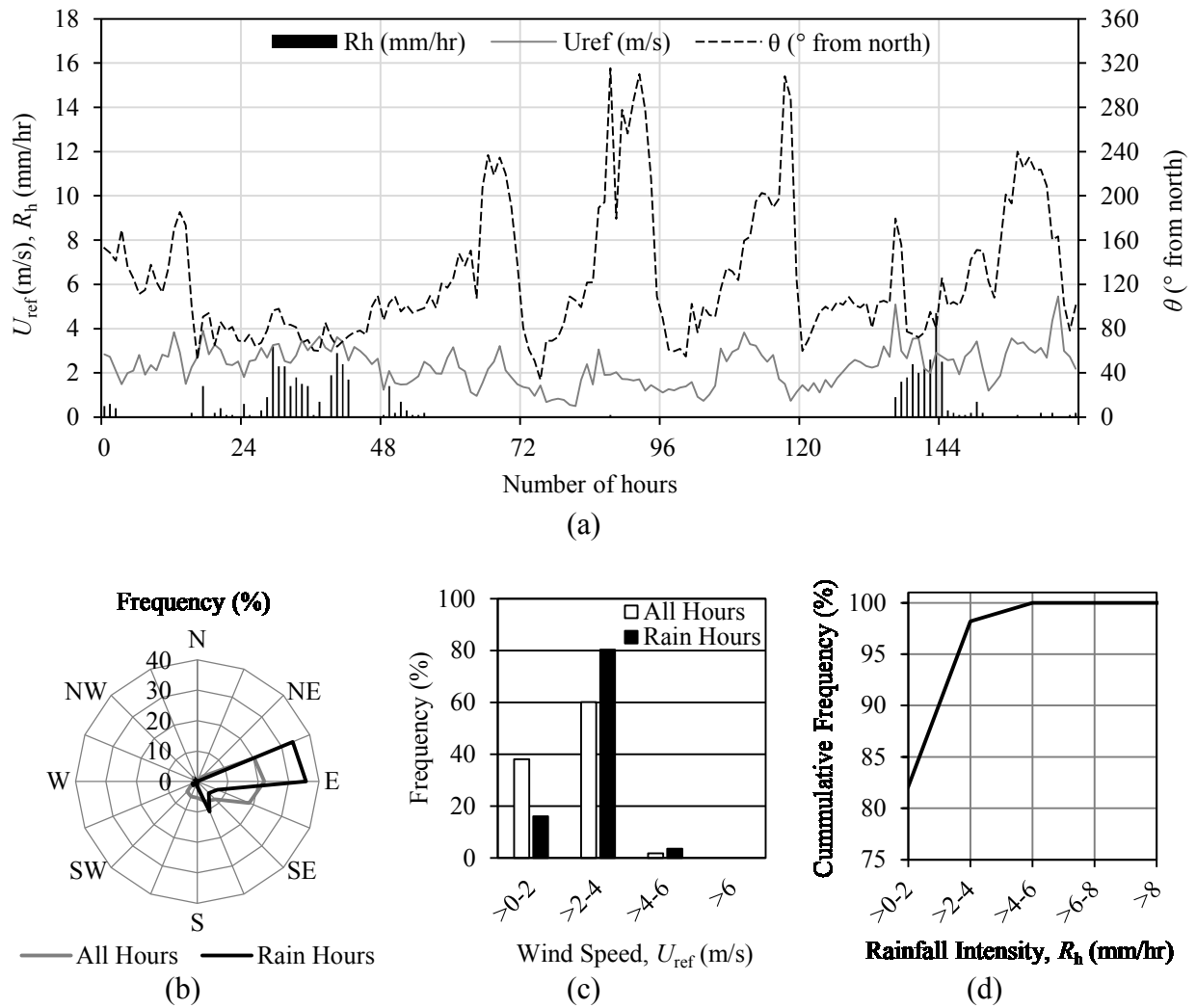


Figure C.5 - Rain event 11.

(a) Hourly horizontal rainfall intensity (R_h), wind speed (U_{ref}), and wind direction (θ); (b) Wind direction frequency; (c) Wind speed frequency; and (d) Rainfall intensity cumulative frequency.

Table C.5 – Rain event 11 summary.

No. Rain Hours	56
Total Horizontal Rainfall, R_h (mm)	55.9
Average Horizontal Rainfall Intensity (mm/hr)	1.0
Average Wind Speed (Rain Hours), U_{ref} (m/s)	2.73
Prevailing Wind Direction (Rain Hours)	East

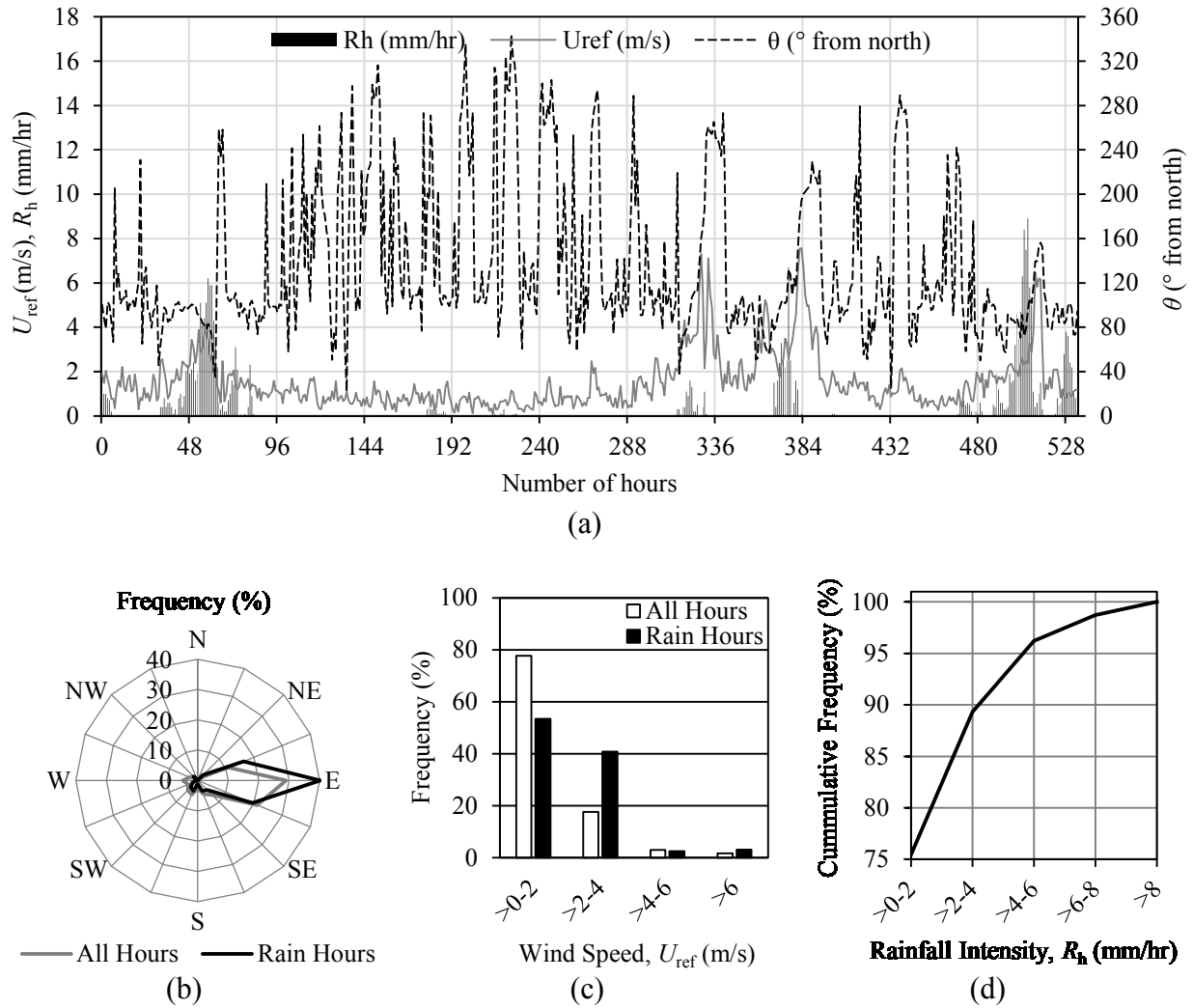


Figure C.6 - Rain event 18.

(a) Hourly horizontal rainfall intensity (R_h), wind speed (U_{ref}), and wind direction (θ); (b) Wind direction frequency; (c) Wind speed frequency; and (d) Rainfall intensity cumulative frequency.

Table C.6 – Rain event 18 summary.

No. Rain Hours	159
Total Horizontal Rainfall, R_h (mm)	231.3
Average Horizontal Rainfall Intensity (mm/hr)	1.5
Average Wind Speed (Rain Hours), U_{ref} (m/s)	2.13
Prevailing Wind Direction (Rain Hours)	East

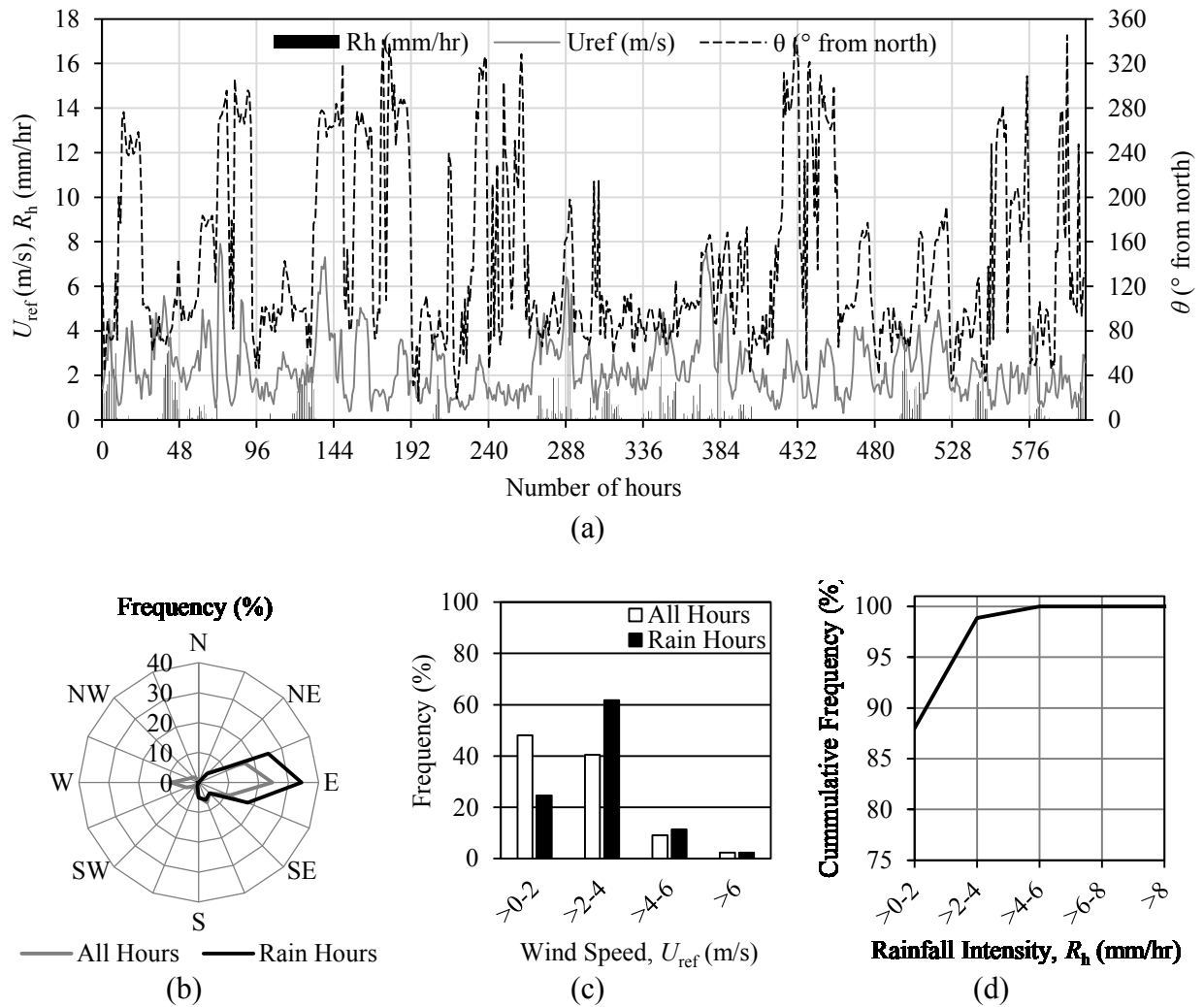


Figure C.7 - Rain event 9.

(a) Hourly horizontal rainfall intensity (R_h), wind speed (U_{ref}), and wind direction (θ); (b) Wind direction frequency; (c) Wind speed frequency; and (d) Rainfall intensity cumulative frequency.

Table C.7 – Rain event 9 summary.

No. Rain Hours	175
Total Horizontal Rainfall, R_h (mm)	164.7
Average Horizontal Rainfall Intensity (mm/hr)	0.9
Average Wind Speed (Rain Hours), U_{ref} (m/s)	2.75
Prevailing Wind Direction (Rain Hours)	East

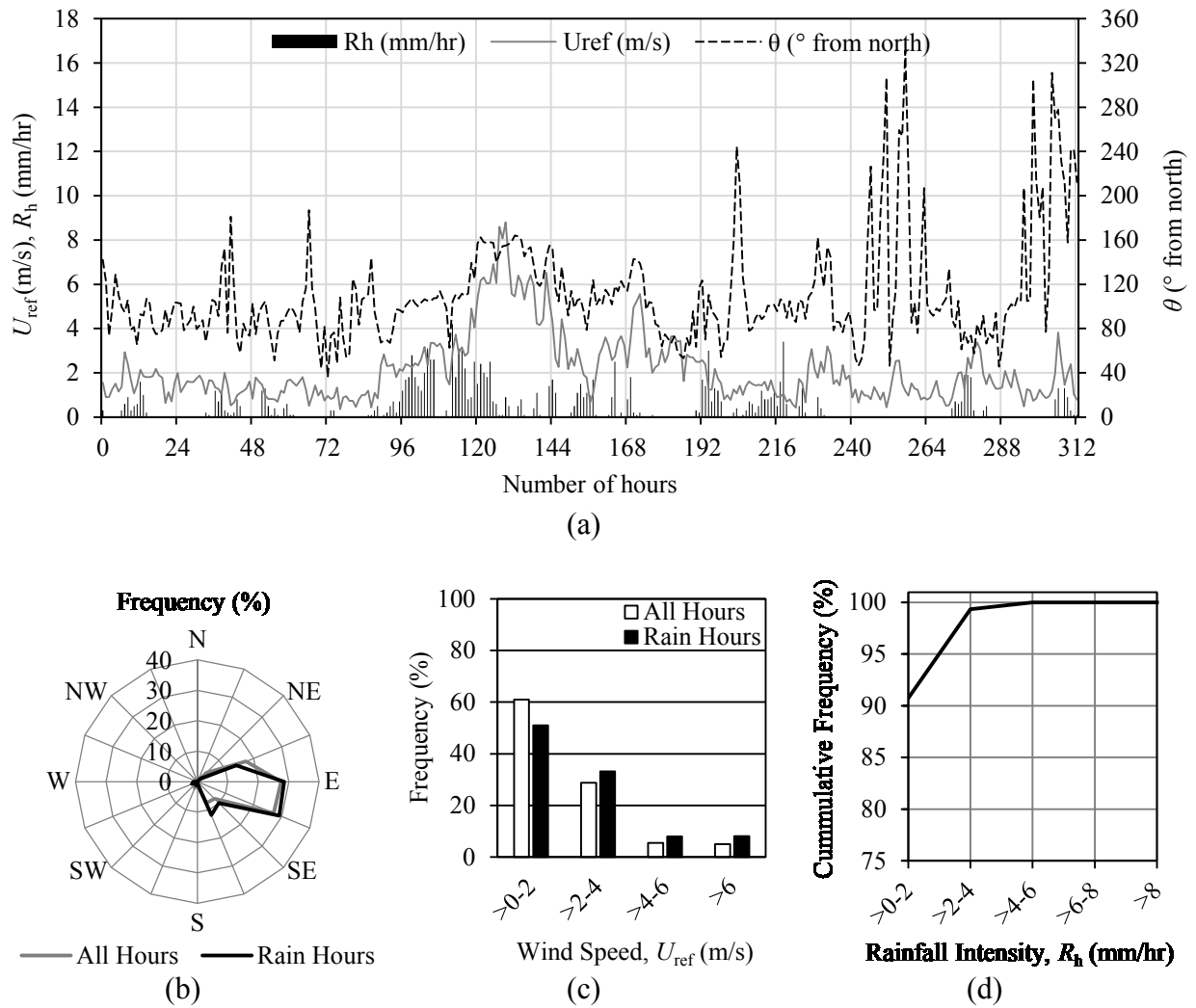


Figure C.8 - Rain event 19.

(a) Hourly horizontal rainfall intensity (R_h), wind speed (U_{ref}), and wind direction (θ); (b) Wind direction frequency; (c) Wind speed frequency; and (d) Rainfall intensity cumulative frequency.

Table C.8 – Rain event 19 summary.

No. Rain Hours	151
Total Horizontal Rainfall, R_h (mm)	138.5
Average Horizontal Rainfall Intensity (mm/hr)	0.9
Average Wind Speed (Rain Hours), U_{ref} (m/s)	2.48
Prevailing Wind Direction (Rain Hours)	East-south-east

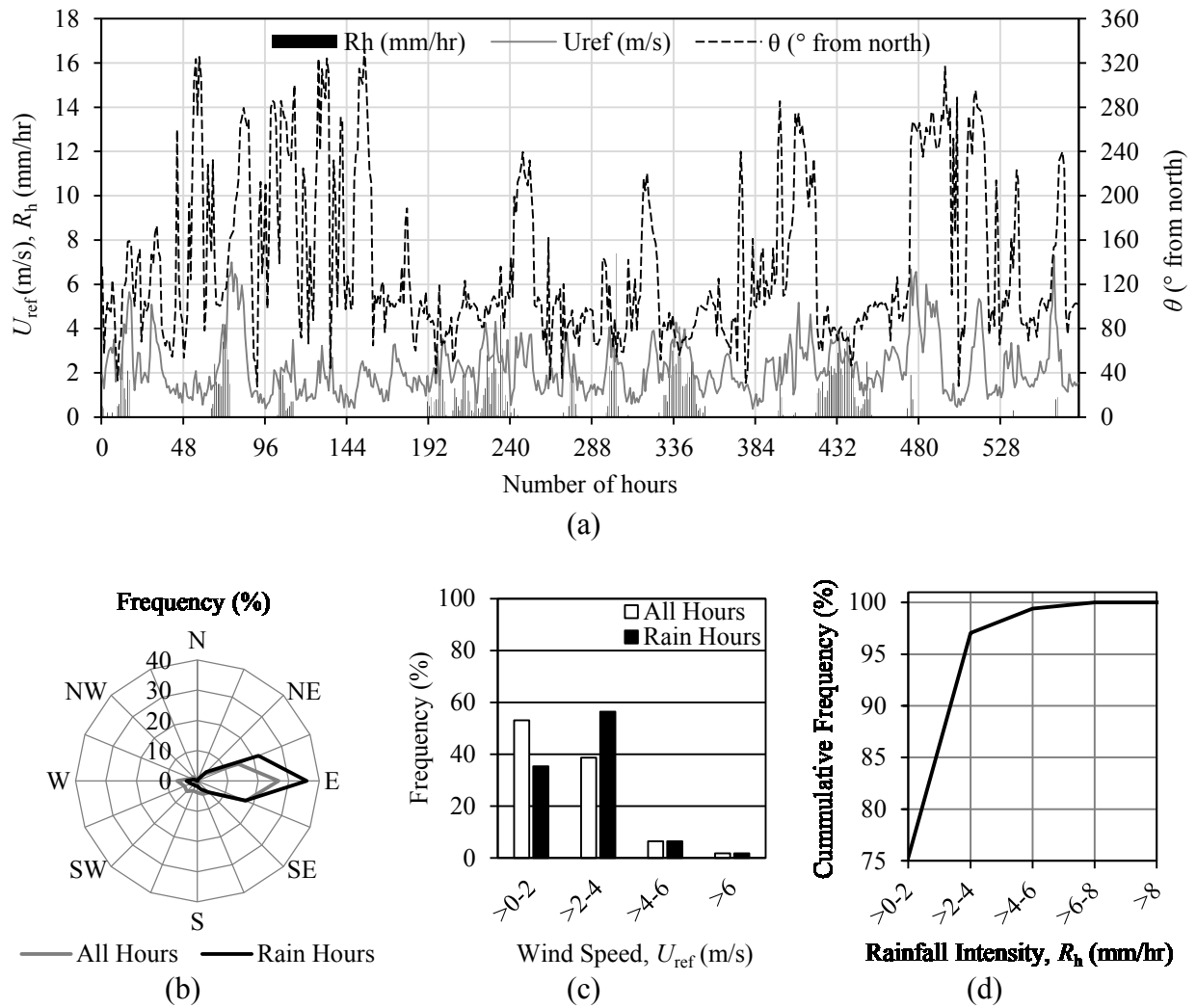


Figure C.9 - Rain event 20.

(a) Hourly horizontal rainfall intensity (R_h), wind speed (U_{ref}), and wind direction (θ); (b) Wind direction frequency; (c) Wind speed frequency; and (d) Rainfall intensity cumulative frequency.

Table C.9 – Rain event 20 summary.

No. Rain Hours	170
Total Horizontal Rainfall, R_h (mm)	236.1
Average Horizontal Rainfall Intensity (mm/hr)	1.4
Average Wind Speed (Rain Hours), U_{ref} (m/s)	2.52
Prevailing Wind Direction (Rain Hours)	East

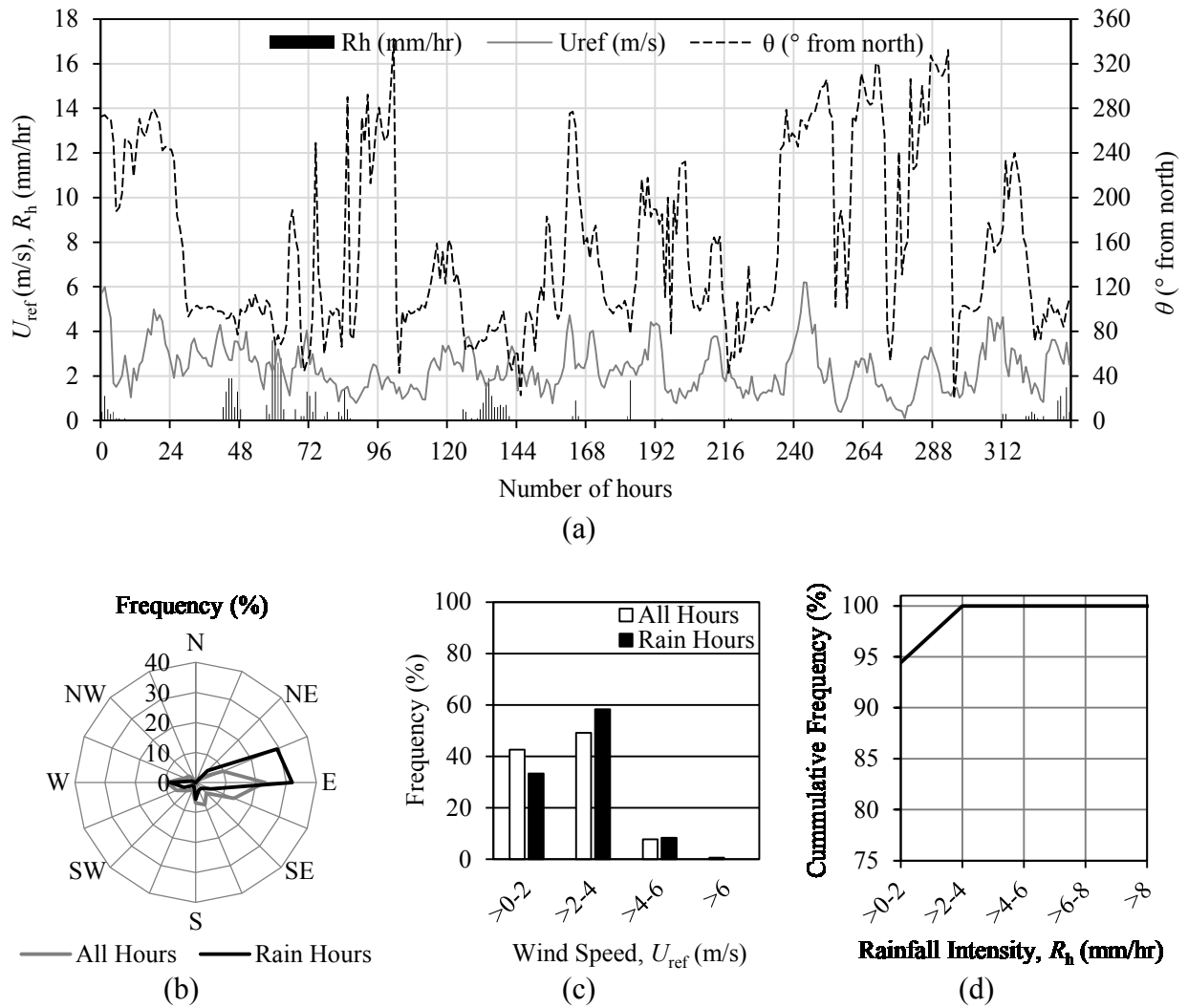


Figure C.10 - Rain event 21.

(a) Hourly horizontal rainfall intensity (R_h), wind speed (U_{ref}), and wind direction (θ); (b) Wind direction frequency; (c) Wind speed frequency; and (d) Rainfall intensity cumulative frequency.

Table C.10 – Rain event 21 summary.

No. Rain Hours	175
Total Horizontal Rainfall, R_h (mm)	164.7
Average Horizontal Rainfall Intensity (mm/hr)	0.9
Average Wind Speed (Rain Hours), U_{ref} (m/s)	2.75
Prevailing Wind Direction (Rain Hours)	East